A FLOW BIREFRINGENCE STUDY OF POLYMER CONFORMATION

J. W. M. NOORDERMEER

A FLOW BIREFRINGENCE STUDY OF POLYMER CONFORMATION

A FLOW BIREFRINGENCE STUDY OF POLYMER CONFORMATION

PROEFSCHRIFT

TER VERKRIJGING VAN DE GRAAD VAN DOCTOR IN DE TECHNISCHE WETENSCHAPPEN AAN DE TECHNISCHE HOGESCHOOL DELFT, OP GEZAG VAN DE RECTOR MAGNIFICUS Ir. H. B. BOEREMA, HOOGLERAAR IN DE AFDELING DER ELEKTROTECHNIEK, VOOR EEN COMMISSIE AANGEWEZEN DOOR HET COLLEGE VAN DEKANEN, TE VERDEDIGEN OP WOENSDAG 20 FEBRUARI 1974 TE 16.00 UUR

DOOR

JACOBUS
WILHELMUS MARIA NOORDERMEER
SCHEIKUNDIG INGENIEUR
GEBOREN TE PIJNACKER

1974

DRUKKERIJ J. H. PASMANS, 'S-GRAVENHAGE

DIT PROEFSCHRIFT IS GOEDGEKEURD DOOR DE PROMOTOR
PROF. DR. H.R.K.N. JANESCHITZ-KRIEGL

Aan Betty en Minke

Aan allen, die hebben bijgedragen aan de totstandkoming van dit werk, betuig ik mijn oprechte dank, in het bijzonder aan ir. R. Daryanani, door wiens energieke inbreng een groot gedeelte van het onderzoek aanzienlijk werd versneld.

Verder gaat mijn dank uit naar Prof. Dr. W. Burchard en Dr. A. Horvath voor het ter beschikking stellen van de monsters en voor vele waardevolle discussies. Ik dank drs. U. Daum van het Centraal Laboratorium TNO te Delft, die mij in de gelegenheid heeft gesteld niet-Newtonse viscositeiten te meten, en ir. A. Ghijsels voor de bereiding van enkele monsters.

Tot slot dank ik de heer A.J. Dekker voor het vervaardigen van de tekeningen en de foto's.

CONTENTS

CHAPTER 1

GENERAL INTRODUCTION

1.1 Disposition

Since the discovery of the double helix of DNA and RNA[1] and the α-helix of polypeptides[2] it is well known that biopolymers and their synthetic analogs can retain a well ordered conformation, not only in the crystalline state but under certain conditions also in solution. This ordered conformation is stabilized by intramolecular hydrogen bonds. These conformations are extremely stable in the sense, that breaking of one hydrogen bond is not advantageous. This does not lead to the realization of a noticeable number of additional degrees of freedom; only with the simultaneous breaking of a large number of adjacent hydrogen bonds the ordered conformation collapses. This explains the sharp changes in the conformational state of these polymers with small changes of the external parameters. The transition from a well ordered (helical) conformation to a disordered (coiled) state usually takes place in a rather narrow interval of temperature or solvent composition.

At the present time conformational transitions in biological macromolecules are the subject of very intensive study, both experimental and theoretical. This is quite obvious, since such transitions are directly related to a number of extremely important life processes, such as the transfer of hereditary properties and the enzymatic activity of proteins. While within the living organism the study of these phenomena encounters great difficulties, an investigation of conformational transitions can be performed quite easily outside the organism. Under varying conditions the complete arsenal of modern physical methods can be applied, as for example O.R.D., small angle x-ray scattering, light scattering, I.R.-spectroscopy, N.M.R., viscosity measurements, etc.

Surprisingly the technique of flow birefringence has been applied to the study of conformational transitions only in a few cases. As an example the experiments can be mentioned, which were done by Tsvetkov et al.[3,4], on the helix-coil transition of poly(γ-benzyl-L-glutamate) (PBLG) in mixtures of dichloro-ethane and dichloroacetic acid. In the rather apolar solvent dichloro-ethane PBLG is present as an α-helix, while in the strongly polar solvent dichloroacetic acid the intramolecular hydrogen bonds are broken and the molecule assumes a coil-conformation. At this transition the specific viscosity of the PBLG-solution decreases by a moderate factor of 2.5 only. However, the intrinsic anisotropy of the molecules, a quantity which can be determined with the

aid of flow birefringence, appears to decrease by a factor of 40-50. This transition is thus accompanied by a tremendous change of the optical properties of the molecule.

The theoretical background of flow birefringence as well as the technique of measurement are rather complicated. Flow birefringence is characterized by two quantities which are measured separately, viz. the extinction angle and the birefringence, both as functions of shear rate. In addition, the viscosity of the solution must be known for an interpretation of these measurements. The measured birefringence is mainly determined by the optical properties, the intrinsic anisotropy, of the macromolecules, while the extinction angle depends on the hydrodynamic properties of the particles. The viscosity of a polymer solution also depends on the hydrodynamic properties of the macromolecules. The example, given above, therefore clearly illustrates the great advantage of the combined hydrodynamic-optical measuring technique over a purely hydrodynamic one for the investigation of conformational transitions of polymers. The aim of this thesis is to investigate the importance of flow birefringence as a technique for the study of conformational transitions.

As is well known, most biopolymers not only are stabilized by hydrogen bonds. They also possess a great number of ionizable groups, arranged along the molecular chain. These groups are responsible for a pronounced polyelectrolyte character of these macromolecules. As a consequence, the molecular conformation of these polymers is also influenced by the degree of ionization of the molecules. From these facts it becomes obvious that the conformational transitions of these polymers usually have a quite complicated character. For this reason two separate synthetic polymers were chosen for this investigation, each possessing one of the characteristic properties of biopolymers: a polyelectrolyte without intramolecular hydrogen bonds and an uncharged polymer, which is capable of forming intramolecular hydrogen bonds.

1.2 A Poly(amide carboxylic acid)

Only a few investigations of the flow birefringence of polyelectrolyte solutions have been published until now. The investigations of Fuoss and Signer[5] and of Jordan and coworkers[6,7] on poly(4-vinyl-N-butyl pyridinium bromide) and poly(4-vinyl pyridinium chloride) have shown that extinction angle and birefringence considerably change with an increasing degree of ionization of the macromolecules. The investigations of Kuhn et al.[8] and of Tsvetkov and coworkers[9] on poly(acrylic acid) and poly(methacrylic acid) in aqueous solutions give similar results. The interpretation of these results, however, is complicated by a considerable contribution of the form-birefringence. This birefringence be-

comes considerable if too large a difference exists between the refractive indices of polymer and solvent. In such a case the coil-molecule as a whole contrasts too much with the solvent.

Vollmert and Horvath[10-12] recently performed viscosity and light-scattering measurements on a poly(amide carboxylic acid) (PACA) from pyromellitic anhydride and benzidine:

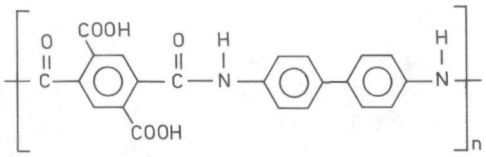

Fig. 1.1. Structure of poly(amide carboxylic acid).

As a solvent N,N-dimethyl acetamide (DMA) was used. On ionization of this polyacid with the organic base triethylamine (TEA) the viscosity of the solution sharply increases. For the ionized PACA the dependence of the reduced viscosity η_{sp}/c on concentration is characterized by a typical increase which is always observed with polyelectrolytes when the concentration is lowered. On the other hand, for the unionized PACA the dependence of η_{sp}/c on concentration corresponds to that for uncharged macromolecules.

The degree of ionization and, with it, the coil expansion of the PACA are determined by the equilibrium constant of the acid-base reaction, the concentration of the dissolved PACA and the concentration of TEA. As an excess of unreacted TEA remains non-ionic, it does not contribute to the ionic strength of the solution.

In this thesis the flow birefringence of this polyelectrolyte system will be described. Because of the great number of aromatic rings in the PACA-chain this polyelectrolyte has a very high intrinsic anisotropy even in the uncharged state. As will be shown later, the intrinsic anisotropy of this uncharged PACA is about ten times as large as that of polystyrene, for example. Therefore the influence of the form-birefringence is relatively small, in spite of the rather high refractive index increment ($dn/dc = 0.375$ ml/g [10]). In such a case also the ionic atmosphere of the protonated TEA-molecules around the charged PACA-molecules may have only a minor influence on the anisotropy of the macromolecule. Another advantage of the high optical anisotropy of the PACA-molecules is that the flow birefringence of its solutions can be measured at very low concentrations of the PACA, where the polyelectrolyte-effects are most pronounced.

It may be concluded that the described system should be extremely suitable for the investigation and interpretation of changes of properties as caused by ionization. For a preliminary presentation of this part of the work see ref. 13.

1.3 Cellulose tricarbanilate

Cellulose and its derivatives are reckoned among the stiff macromolecules. Very flexible macromolecules assume an unordered coil conformation in solution. This conformation is characterized by a Gaussian distribution of the end-to-end distance of the molecular chain. Cellulose, occurring in nature, and its derivatives have too low a degree of polymerization to furnish such a Gaussian distribution. Most molecular theories, however, describing the behaviour of macromolecules in solution, are based on such a Gaussian distribution. Hence cellulose-derivatives are extremely suitable for a study of the influence of deviations from these Gaussian statistics on optical and hydrodynamic properties.

For this investigation Cellulose tricarbanilate (CC) was used:

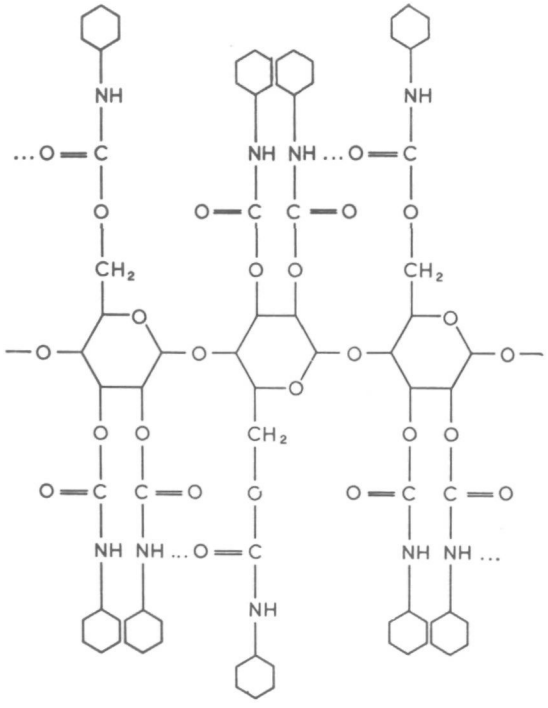

Fig. 1.2. Structure of cellulose tricarbanilate. The hydrogen bonds are given by dotted lines.

obtained by formation of a urethane from cellulose and phenyl isocyanate in hot pyridine, according to Burchard and Husemann[14]. These authors have shown with the aid of light-scattering and viscosity-measurements, that the coil-dimensions of the CC-chain are strongly dependent on the choice of the solvent. This polymer is soluble in organic esters, ethers and ketones. However, in general the molecular coil appears to have larger dimensions in ethers than in esters and ketones. Especially in mixtures of ketones and water or methanol very peculiar changes of the mean square radius of gyration of the CC-chains could be observed[15].

An explanation of this difference in stiffness, resp. coil-dimensions, was sought in the formation of intramolecular hydrogen bonds[16]. Their occurrence can be deduced from the structure of the chain, as given above. With the aid of macroscopic Stuart-models it was checked that the given hydrogen bonds can occur from a sterical point of view. These hydrogen bonds form a sort of ladder-conformation which, as a matter of fact, causes a greater stiffness, than if the monomers are coupled only by single bonds. In fact, in the absence of hydrogen bonds the stiffness of CC is only determined by the sterical hindrance of rotations around the β-glycosidic bonds.

Janeschitz-Kriegl and Burchard[17] measured the flow birefringence of a number of sharp fractions of CC with different molecular weights. As a solvent benzophenone was used. In the present work the flow birefringence of CC is studied in ethers and esters and mixtures of both kinds of solvents. The aim was to check whether phenomena could be found with flow birefringence, which point to pronounced changes of the stiffness of the molecular chain.

Also CC appears to have a high intrinsic optical anisotropy, which simplifies the choice of the solvents. In most cases, however, solvents were preferred, for which the refractive index increments were small. In cases, where this was impossible, the influence of the form-birefringence was estimated. It appeared that also in those cases the influence of the form-birefringence was relatively small.

Literature

1. J.D. Watson, F.H.C. Crick, Nature *171*, 737 (1953).
2. L. Pauling, R.B. Corey, H.R. Branson, Proc. Natl. Acad. Sci. *37*, 205 (1951).
3. V.N. Tsvetkov, I.N. Shtennikova, Ye.I. Ryumtsev, G.F. Pirogova, Vysokomolekul. Soedin. *A9*, 1583 (1967).
4. V.N. Tsvetkov, I.H. Shtennikova, V.S. Skazka, Ye.I. Ryumtsev, J. Polymer Sci. C, *16*, 3205 (1968).
5. R.M. Fuoss, R. Signer, J. Am. Chem. Soc. *73*, 5872 (1951).
6. D.O. Jordan, A.R. Mathieson, M.R. Porter, J. Polymer Sci. *21*, 463 (1956).
7. D.O. Jordan, T. Kurucsev, Polymer *1*, 202 (1960).
8. W. Kuhn, O. Künzle, A. Katchalski, Helv. Chim. Acta *31*, 1994 (1948).
9. V.N. Tsvetkov, Newer Methods of Polymer Characterization, B. Ke Ed., Interscience, New York (1964) p. 563.
10. A. Horvath, Thesis Karlsruhe (1970).
11. B. Vollmert, A. Horvath, Angew. Makromol. Chem. *23*, 117 (1972).
12. A. Horvath, B. Vollmert, Angew. Makromol. Chem. *23*, 141 (1972).
13. J.W.M. Noordermeer, H. Janeschitz-Kriegl, A. Horvath, Polymer *14*, 178 (1973).
14. W. Burchard, E. Husemann, Makromol. Chem. *44-46*, 358 (1961).
15. W. Burchard, Z. Physik. Chem. *42*, 293 (1964).
16. W. Burchard, Makromol. Chem. *88*, 11 (1965).
17. H. Janeschitz-Kriegl, W. Burchard, J. Polymer Sci. A2, *6*, 1965 (1968).

CHAPTER 2

PRINCIPLES AND BACKGROUND OF EXPERIMENTAL TECHNIQUES

2.1 Introduction

An important field of research on polymers is the study of their hydrodynamic properties in dilute solution. These properties determine the motion of the polymer molecules through a viscous medium under influence of external fields of force and of Brownian motion.

In this chapter the general principles of viscosity and flow birefringence measurements will be discussed. For both techniques the field of forces is exclusively caused by a laminar shear flow of the solution. Any external forces, as for example electric or magnetic forces, are disregarded. Gravitational and inertial forces will be neglected and left out of consideration henceforth. This is a rather good approximation because of the small dimensions of the molecules and the existence of Brownian motion.

2.2 The stress tensor

The flow field, used for both techniques, is a laminar shear flow. If one imagines that this flow takes place between two infinite parallel plates, which are moving with respect to each other at constant speed, one can define a coordinate system, such that the 1- (or x-) direction is chosen parallel with the stream lines, the 2- (or y-) direction perpendicular to the shearing planes, resp. to the plates. The 3- (or z-) direction completes a right-handed Cartesian coordinate system.

In that case the velocity of the fluid between the plates will be given by:

$$v_x = v_1 = qy \qquad v_y = v_z = 0 \tag{2.1}$$

where

$$q = \frac{dv_x}{dy} \tag{2.2}$$

is the shear rate.

Besides the normal energy dissipation in the solvent itself, an extra energy dissipation takes place in a polymer solution because of the work, done on the flowing fluid by the polymer molecules. The polymer molecules undergo a simultaneous orientation and deformation in the flow. To maintain steady shear flow a set of forces has to be applied on the plates. The force in the 1-direction, taken per unit-area of the plate,

is called the shear stress and appears to be one of the components of the stress tensor. If the deformation in the fluid is uniform, this stress tensor describes the state of stress for each point within the flowing solution.

The form of the stress tensor[1,2] is illustrated in Fig. 2.1:

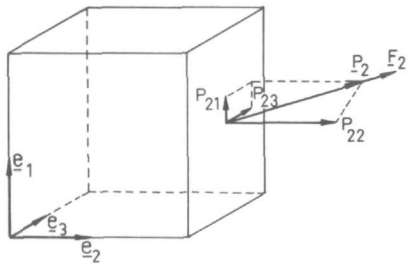

Fig. 2.1. Definition of the components of the stress tensor.

To maintain an arbitrary flow field a force $\underline{F}_i$ has to be exerted on a surface perpendicular to the i-direction (i = 1,2,3). After dividing this force by the area of the surface, on which it acts, a stress $\underline{P}_i$ is obtained. Its components in the 1-, 2- and 3-direction are: P_{i1}, P_{i2} and P_{i3}. This can be done for all three directions i. In this way nine components are obtained, which define the stress tensor for the flowing solution:

$$P_{ij} = \begin{pmatrix} P_{11} & P_{12} & P_{13} \\ P_{21} & P_{22} & P_{23} \\ P_{31} & P_{32} & P_{33} \end{pmatrix} \tag{2.3}$$

The components P_{11}, P_{22} and P_{33} are called normal stresses, the components P_{12}, P_{13}, P_{21}, P_{23}, P_{31} and P_{32} are shear stresses, because they try to change the shape of the cube. If there are no preferential directions in the solution at rest, i.e. the fluid is isotropic, it can be proved that the stress tensor is symmetric[1,2]:

$$P_{ij} = P_{ji} \tag{2.4}$$

Under this condition no resultant couple is acting on the fluid. Such a couple would cause an accelerating rotation. For the shear flow, as defined above, the components P_{13}, P_{23} and consequently P_{31} and P_{32} vanish for symmetry reasons[1].

For all theoretical and experimental considerations it will be supposed henceforth that the solution is incompressible. This is a necessary simplification, because otherwise considerable mathematical difficulties

arise. However, this is a reasonable approximation for dilute solutions, as the bulk modulus of fluids is always very large compared with the (time dependent) shear modulus.

A further simplification is obtained by assuming that the stress tensor for a streaming solution of macromolecules can be given as the sum of a spherically symmetric hydrostatic pressure, a contribution of the solvent and a separate contribution of the polymer molecules[3,4]. The contribution of the solvent is usually considered to be independent of the polymer concentration. As is obvious, this assumption becomes more and more incorrect, when the polymer concentration is increased. However, with increasing concentration the relative solvent contribution decreases rapidly, so that it becomes completely negligible, anyway.

Low molecular weight fluids, like the solvents used in this work, cannot build up normal stresses[1]. So these solvents contribute only to the shear stress. Moreover, this contribution appears to be proportional to the shear rate. The proportionality-constant η_s is called the Newtonian solvent viscosity. It is independent of the shear rate.

The stress tensor for a polymer solution, which is submitted to steady shear flow, now assumes the following simple form:

$$P_{ij} = -p_o \begin{pmatrix} 1 & 0 & 0 \\ 0 & 1 & 0 \\ 0 & 0 & 1 \end{pmatrix} + \eta_s \begin{pmatrix} 0 & q & 0 \\ q & 0 & 0 \\ 0 & 0 & 0 \end{pmatrix} + \begin{pmatrix} p_{11} & p_{12} & 0 \\ p_{21} & p_{22} & 0 \\ 0 & 0 & p_{33} \end{pmatrix} \tag{2.5}$$

where p_o = the hydrostatic pressure,

p_{ij} = the contribution of the polymer molecules to the stress tensor P_{ij}.

It is quite irrelevant to include the hydrostatic pressure into the definition of the stress tensor for incompressible liquids. This component is therefore usually disregarded in theoretical considerations.

For the study of the hydrodynamic behaviour of polymers we are only interested in the contribution of the macromolecules to the stress tensor, i.e. the last term of eq. (2.5). This tensor can be represented by a stress ellipsoid. In the Cartesian coordinate system, formed by the three principal axes of this ellipsoid, this tensor only has components on the diagonal. All components with mixed indices are equal to zero. Because of the simple form of the chosen flow pattern it can easily be seen that one of the principal axes (the III-axis) of this ellipsoid coincides with the 3-direction. As a consequence, both other principal axes (the I- and II-axis) must lie in the plane of flow, i.e. the 1-2 plane. If the first principal axis is defined as the one making an angle χ', smaller than 45 degrees, with the direction of the stream lines (see

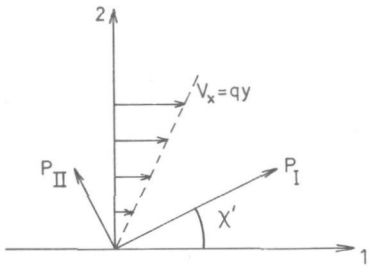

Fig. 2.2. Laboratory coordinate system: 1 direction of flow, 2 direction of the velocity gradient. p_I, p_{II} principal stresses, χ' orientation angle of the stress tensor.

Fig. 2.2), one obtains the following equations for the transformation of tensor components:

$$\Delta p \sin 2\chi' = 2\, p_{21} \tag{2.6}$$

$$\Delta p \cos 2\chi' = p_{11} - p_{22} \tag{2.7}$$

$$p_{III} = p_{33} \tag{2.8}$$

where $\Delta p = p_I - p_{II}$, the difference between the two principal stresses in the plane of flow,

$p_{11} - p_{22}$ = the so-called first normal stress difference.

A combination of eqs. (2.6) and (2.7) gives the following relation for the orientation angle χ':

$$\cot 2\chi' = \frac{p_{11} - p_{22}}{2\, p_{21}} \tag{2.9}$$

For the technical processing of polymers a detailed knowledge of the mechanical behaviour of these polymers is quite important. In view of this a lot of research is done nowadays in order to measure the different components of the stress tensor. In fact, the relations between stresses and flow pattern characterize the mechanical behaviour of the fluids. A great variety of techniques have been developed, which can be quoted under the head "rheology".

An extensive discussion of all these techniques falls far outside the scope of this work. Mention will be made only of a few aspects, which are related to the work described in this thesis.

2.3 Viscosity measurements

Since a long time the contribution of the macromolecules to the shear stress P_{21} of a solution in laminar shear flow has been found

with the aid of various viscometric methods. The most common method is the one using the flow of the fluid through a cylindrical capillary, i.e. Poiseuille flow. All viscosity measurements in this work were performed by this method. For a detailed description of the apparatus reference is made to chapter 4.

As is well known, the relation between shear stress and shear rate is normally given by:

$$P_{21} = \eta q \tag{2.10}$$

where the proportionality constant η is called the viscosity. For a polymer solution, however, this viscosity normally shows non-Newtonian behaviour, i.e. η decreases with increasing shear rate.

According to eq. (2.5) P_{21} is composed of a solvent and a polymer contribution, so that the latter can be found by subtracting the solvent contribution, as obtained at the same shear rate, from the total shear stress P_{21}:

$$p_{21} = q(\eta - \eta_s) \tag{2.11}$$

The hydrodynamic behaviour of a macromolecule and, consequently, its contribution to the stress tensor are partly the result of the movements of the separated molecule and partly of mutual interactions between neighbouring macromolecules. In studying dilute solutions one is mainly interested in the behaviour of the isolated molecules and tries to eliminate the mutual interactions. Thus, in the limit of zero concentration, the contribution of the individual molecules to the viscosity can be determined in the following way:

$$[\eta] = \lim_{c \to 0} \frac{\eta - \eta_s}{\eta_s c} = \lim_{c \to 0} \frac{\eta_{sp}}{c} \tag{2.12a}$$

where c = the polymer concentration in g/cm^3,

$[\eta]$ = the intrinsic viscosity in cm^3/g,

η_{sp} = the specific viscosity.

When only the zero shear behaviour of a polymer is of interest, the value of the intrinsic viscosity, extrapolated to zero shear rate, is used:

$$[\eta]_o = \lim_{q \to 0} [\eta] \tag{2.12b}$$

The intrinsic viscosity of a polymer in a certain solvent is a quantity, which is determined exclusively by the hydrodynamic properties of the individual macromolecules in that solvent and therefore is of special importance for the investigation of these properties.

2.4 Flow birefringence measurements

Flow birefringence was discovered in 1870 by Maxwell[5]. He observed that Canada balsam becomes birefringent when sheared. This birefringence disappears rapidly, when the flow ceases. When a fluid consists of geometrically anisotropic molecules, a co-operative mechanism of flow and Brownian motion causes a slight average orientation of these molecules. This induces an overall optical anisotropy within the fluid, which can be observed as a birefringence. Macromolecules are in general built up of optically anisotropic units. As a consequence, orientation and deformation of those molecules, as caused by flow, also result in a birefringence effect.

As is well known, a birefringent medium can be characterized by a refractive index ellipsoid[6], resp. refractive index tensor, with three principal refractive indices n_I, n_{II} and n_{III}. For the same reasons, as in the case of the stress tensor, the n_{III}-direction coincides for a laminar shear flow with the neutral 3-direction. The other two principal directions lie in the 1-2 plane. One of them forms an acute angle χ with the 1-direction, analogous to the orientation angle χ' of the stress tensor. The thus defined orientation angle of the index ellipsoid is called the extinction angle. The extinction angle and the birefringence can both be measured separately as functions of shear rate. The apparatus, used for these measurements, is described in chapter 4.

For pure low molecular weight liquids the birefringence is found to be simply proportional to the shear rate. The extinction angle remains 45 degrees within the accessible range of shear rates. However, for polymer solutions the extinction angle has a value of 45 degrees only in the limit of zero shear rate. With increasing shear rate it decreases gradually: the refractive index ellipsoid of the streaming solution rotates around the neutral direction, finally aligning itself in the direction of the 1-axis. The birefringence initially increases linearly with the shear rate. At higher shear rates there are two alternatives: it either continues to increase more than linearly, viz. in the case of very flexible, sufficiently long macromolecules, or it shows a saturation effect for stiff unflexible molecules. A great number of examples of both types of effects can be found in review articles on flow birefringence[3,7-16].

It is usually assumed that the birefringence, which is observed in streaming polymer solutions, can be interpreted as composed of two independent refractive index ellipsoids: the solvent ellipsoid and the polymer ellipsoid, and that both contributions are simply additive, the solvent contribution being independent of the polymer concentration. To obtain the pure polymer contribution to the flow birefringence the measured extinction angle and the birefringence have to be corrected for

the solvent contribution. The pertinent correction formulas were derived by Sadron[17]:

$$\Delta n_c \sin 2\chi_c = \Delta n \sin 2\chi - \Delta n_s \tag{2.13}$$

$$\Delta n_c \cos 2\chi_c = \Delta n \cos 2\chi \tag{2.14}$$

By a combination of eqs. (2.13) and (2.14) one obtains:

$$\cot 2\chi_c = \frac{\cos 2\chi}{\sin 2\chi - (\Delta n_s/\Delta n)} \tag{2.15}$$

where the following parameters are used:

Δn, χ = the flow birefringence of the solution in the 1-2 plane, at shear rate q,

Δn_s, $\pi/4$ = the flow birefringence of the pure solvent, at shear rate q,

Δn_c, χ_c = the flow birefringence as caused by the dissolved macromolecules after the correction for the solvent contribution.

For solutions of very flexible coiled macromolecules there appears to be a simple relation between their contributions to the stress tensor and to the refractive index ellipsoid of the streaming solution, the well known "stress-optical law". According to this law both ellipsoids are coaxial and the flow birefringence is proportional to the principal stress difference in the plane of flow:

$$\chi_c = \chi' \quad \text{and} \quad \Delta n_c = C\,\Delta p \tag{2.16}$$

where C = the stress-optical coefficient.
Inserting eq. (2.16) into eqs. (2.6) and (2.7) one obtains:

$$\Delta n_c \sin 2\chi_c = 2\,C\,p_{21} \tag{2.17}$$

$$\Delta n_c \cos 2\chi_c = C\,(p_{11} - p_{22}) \tag{2.18}$$

As a matter of fact these equations enable us to obtain the first normal stress difference $p_{11} - p_{22}$ for a flowing solution from birefringence measurements. As we are only interested in the polymer contribution to the flow birefringence, the index c will not be used henceforth. If not explicitely stated otherwise or mentioned in the text, it is assumed that the measurements are automatically corrected for the solvent contribution.

The eqs. (2.16), (2.17) and (2.18) are only valid, if the refractive index of the solvent is more or less equal to that of the polymer ("matching solvent"). The refractive index increment dn/dc must be as small as possible. Otherwise the birefringence, caused by the shape of

the molecular coil (form birefringence), gives a complicated contribution to the stress-optical coefficient[19].

For many polymers the stress-optical coefficient appears to be independent of the shear rate and, in the absence of the form birefringence effect, also independent of molecular weight[15] and concentration[18]. However, solutions of relatively stiff or very short macromolecules show deviations from this rule: a decrease of the measured value of the stress-optical coefficient is found with increasing shear rate. Moreover, on theoretical grounds it can no longer be expected that the principal axes of the stress- and refractive index ellipsoids will coincide. The stress-optical coefficient becomes dependent on the molecular weight: it decreases with decreasing molecular weight[20].

From a theoretical point of view the stress-optical coefficient appears to be independent of the hydrodynamic properties of the macromolecules. It is only determined by the microstructure, resp. the conformation of the macromolecules. A detailed discussion of this fact will be given in the next chapter. It will be shown that very valuable information about the structure of macromolecules can be obtained from the stress-optical coefficient data. Conformational transitions of polymers will appear to be quite well observable from pronounced changes of the value of the stress-optical coefficient.

For flexible coil molecules, the extinction angle coincides with the orientation angle of the stress tensor. In those cases the extinction angle is a quantity, which, just as the intrinsic viscosity, is determined only by the hydrodynamic properties of the macromolecules. As these two angles do not coincide for stiff macromolecules, the orientation angle cannot be derived from a measurement of the extinction angle. The investigation of the influence of chain stiffness on the extinction angle is one of the subjects of this thesis. This point will therefore be discussed more extensively in the following chapters.

Literature

1. A.S. Lodge, Elastic Liquids, Academic Press, London (1964).
2. H.J. Merk, Macroreologie A, Principes van de continuums mechanica, Collegedictaat, Delft.
3. H. Janeschitz-Kriegl, Adv. Polymer Sci. *6*, 170 (1969).
4. A.S. Lodge, Yeen-jing Wu, Rheol. Acta *10*, 539 (1971).
5. J.C. Maxwell, Collected Papers, Cambridge Univ. Press, Vol. II, 379 (1890); Proc. Roy. Soc. (London) *A22*, 46 (1873).
6. A.C.S. van Heel, Inleiding in de Optica, M. Nijhoff, 5e druk, 's-Gravenhage (1964).
7. G. Boehm, Abderhalden's Handbuch Biol. Arbeitsmethoden, Abt. II-3, Urban und Scharzenberg, Berlin/Wien (1939) p. 3939.
8. J.T. Edsall, Adv. Colloid Sci. *1*, 269 (1942).
9. A. Peterlin, H.A. Stuart, Hand- und Jahrbuch der Chemischen Physik, A. Eucken and K.L. Wolf Eds., Vol. 8, Ib, Akadem. Verlagsgesellschaft, Leipzig (1943) p. 1.
10. R. Cerf, H.A. Scheraga, Chem. Rev. *51*, 185 (1952).
11. A. Peterlin, H.A. Stuart, Das Makromolekul in Lösungen (Vol. II of Die Physik der Hochpolymeren), H.A. Stuart Ed., Springer, Berlin (1953) p. 569.
12. A. Peterlin, Rheology, F.R. Eirich Ed., Vol. I, Academic Press, New York (1956) p. 615.
13. R. Cerf, Adv. Polymer Sci. *1*, 383 (1959).
14. H.A. Scheraga, R. Signer, Technique of Organic Chemistry, 3rd ed., A. Weissberger Ed., Vol. I, part 3, Interscience, New York (1960) p. 2387.
15. V.N. Tsvetkov, Newer Methods of Polymer Characterization, B. Ke Ed., Interscience, New York (1964) p. 563.
16. A. Peterlin, P. Munk, Physical Methods of Chemistry, Vol. I, part 3c, A. Weissberger and B. Rossiter Eds., Wiley, New York (1972) p. 271.
17. C. Sadron, J. phys. radium *9*, 381 (1938).
18. H. Janeschitz-Kriegl, Makromol. Chem. *40*, 140 (1960).
19. M. Čopič, J. Chem. Phys. *26*, 1382 (1957).
20. Yu.Ya. Gotlib, Yu.E. Svetlov, Dokl. Akad. Nauk SSSR *168*, 621 (1966).

CHAPTER 3

THEORY

3.1 Introduction

The orientation and deformation of macromolecules in a flowing solution are determined by the form and deformability of the particles. Very stiff particles, as Tobacco Mozaic Virus, poly(α-amino acids) in the α-helix conformation, globular proteins with a well defined secondary and tertiary structure, etc. cannot be deformed, so that flow only causes an orientation of these particles. Very flexible macromolecules, as the synthetic polymers polyethylene, polystyrene and many others, are statistically coiled up in the stationary solution. These coils possess on the average only a slight anisotropy of form. They undergo a combined deformation and orientation in flow.

These combined effects determine the viscoelastic and optical properties of polymer solutions in laminar shear flow. In the past several theories have been proposed which are able to describe these properties with reasonable success. It will be impossible to describe all these theories here. It should suffice to describe the general lines on a few models which have shown to give particularly simple or useful results.

Before starting with an outline of viscoelastic theories and of the influence of chain stiffness on them, first clear criteria have to be established with regard to the chain stiffness of a certain macromolecule.

3.2 Definition of chain stiffness

A definition of the stiffness, resp. the flexibility, of a macromolecular chain must be derived from conformational statistics. These conformational statistics have been subject of very intensive studies in recent years[1-3]. The flexibility of a macromolecule originates from the large number of internal degrees of freedom, determined by rotations around single bonds. The contributions from other degrees of freedom, such as deformations of chemical bonds and valence angles, are usually quite small and can therefore be neglected. During such a rotation around a certain single bond the internal energy of the molecule appears to be a function of the rotation angle and passes through a number of minima and maxima. The minima correspond with the most stable conformations: the rotational isomers. The levels of the energy minima, however, can differ from each other; this implies that not all possible conformations are equally probable in an absolute sense. The maxima, usually called energy barriers, determine the rate, with which the different conforma-

tions can interchange. If no strong external forces are applied and the energy barriers are not too high, the macromolecule will pass through a large number of conformations in a short time, due to Brownian motion. However, if the energy barriers are high, the macromolecule will show a certain chain stiffness.

In connection with this problem usually a distinction is made between thermodynamic chain stiffness and kinetic chain stiffness[4,5]. The former depends on the relative levels of the energy minima and thus on the probability of certain conformations. The thermodynamic stiffness is an equilibrium quantity, depending merely on temperature. The kinetic chain stiffness, also called "internal viscosity"[4,5], originates from the fact that, during deformation of a macromolecule, a certain number of energy barriers have to be passed to change conformation. This should cause a force, by which the macromolecule opposes the deformation process and which disappears as soon as the macromolecule is not further deformed. At this point, however, it should be emphasized that special techniques are necessary to separate effects stemming from this force and the one which is caused by friction of the parts of the macromolecule with the surrounding solvent molecules. As a consequence, a lot of controversy exists in literature about the theoretical and practical implications of the internal viscosity. Therefore the internal viscosity will be left out of consideration in this work. By chain stiffness only the thermodynamic stiffness will be meant.

As the interactions just described occur between neighbouring atoms of the chain molecule, these effects are usually called "short-range" interactions. Apart from these interactions also "long-range" interactions or "excluded volume" effects are known to occur for macromolecules in solution. These interactions take place between atoms of the same chain molecule, which are at large distance along the contour of the chain, but approach each other in the process of random fluctuations in the coil.

The usefulness of this classification of intramolecular forces is based on the fact that the influence of the long-range interactions on the coil dimensions can be approximately eliminated, if measurements are done in the so-called θ-point or "Flory-point"[6]. For a certain binary system of polymer and solvent, the θ-temperature can be determined by light scattering as the temperature, where the second virial coefficient becomes equal to zero. At that point the effect of exclusion is compensated in the average by the formation of a few intramolecular contacts. As a consequence, there is no longer any deviation from the coil dimensions as derived from simple random walk statistics (see below).

An exact determination of the total number of possible conformations of a flexible macromolecule on basis of all possible effects is an in-

tractable task. Already for a macromolecule, built up of only a few monomers, one meets with serious mathematical problems. Therefore usually simplified statistical approaches are used. One of them, which has proven to be the most fruitful, is the "random walk" model of a polymeric chain, introduced by Kuhn[7], Guth and Mark[8]. As the reader is expected to be quite familiar with this statistical theory no extensive discussion will be given. In a stationary solution without external force fields the mean square end-to-end distance of the model chain can be given by the simple relation:

$$\langle h_o^2 \rangle = Z\, A^2 \tag{3.1}$$

where $\langle h_o^2 \rangle$ = the mean square end-to-end distance of the chain,
Z = the number of so-called random links or Kuhn elements,
A = the length of the random links.

The fully extended length or contour length L is the length of the stretched conformation with the lowest energy. In the Kuhn-statistics the following relation applies:

$$L = Z\, A \tag{3.2}$$

The derivation of eq. (3.1) is based on certain approximations, which are valid only when the end-to-end distance of the chain is considerably smaller than its contour length. Therefore Z must be sufficiently large and the chain far from completely extended. In that case one obtains a Gaussian distribution of the endpoints. Zimm[9] and Nagai[10] have shown that a Gaussian distribution of the end-to-end distance is always obtained for sufficiently high molecular weights ($Z \to \infty$), not only for hypothetical, freely jointed chains, but also for macromolecules with fixed valence angles and restricted internal rotations (as long as no long-range interactions occur = θ-conditions).

When for the Kuhn model the number of random links is small, the range of end-to-end distances for which the Gaussian statistics approximately applies, becomes very limited. For very short chains, with $Z = 5$ or smaller, the exact distribution of the end-to-end distance of the Kuhn model does neither agree with a Gaussian distribution nor with that of any realistic chain molecule[11].

Equations (3.1) and (3.2) represent two relations for the two unknown quantities Z and A. For a given L a thermodynamically stiffer chain has a larger $\langle h_o^2 \rangle$ than a more flexible chain. It follows that A increases, while Z decreases with increasing stiffness. In the case of $Z \to \infty$, the chain takes the form of a Gaussian coil; in the case of $Z \to 0$ it seems that the chain can better be approximated by a stiff rod. The total length of the chain is not large enough to form even one random link. Unfortunate-

ly, the random walk problem yields rather unrealistic distributions of the end-to-end distances for $Z < 5$. This was the historical reason for the search for another sort chain statistics which is described below.

While the Kuhn-statistics derives its great value from the good description of Gaussian coils, for the description of stiff macromolecules another sort of statistics is often used for the just mentioned reasons, i.e. the statistics of the "wormlike chain", according to Kratky and Porod[12]. The macromolecule is considered to be a continuously bent thread with a negligibly small diameter.

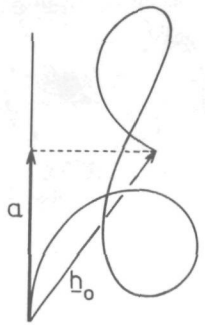

Fig. 3.1. Projection of a wormlike chain with end-to-end vector $\underline{h}_o$ on its initial tangent. For infinite length the average of this projection becomes equal to the persistence length a.

If one takes the tangent to this thread at one endpoint and considers the mean projection of the other endpoint on this tangent, one finds that for $L \to \infty$ the distance between the first endpoint and the projection converges to a finite length. This length, denoted by a in Fig. 3.1, is called the persistence length. According to Kratky and Porod the mean square end-to-end distance of the thread for any arbitrary value of L is given by:

$$\langle h_o^2 \rangle = 2\, a^2\, [x - 1 + \exp(-x)] \qquad (3.3)$$

where $x = L/a$, the reduced contour length.
In the limit of a stiff rod, i.e. for $x \to 0$, one obtains an obvious result, viz.:

$$\langle h_o^2 \rangle = L^2 \qquad (3.4)$$

With increasing contour length also this thread passes into a Gaussian coil, where the Kuhn- and the persistence-statistics have to be equivalent.

For $x \to \infty$ eq. (3.3) takes the form:

$$\langle h_o^2 \rangle = 2\, a\, L \tag{3.5}$$

A combination of eqs. (3.1) and (3.2), however, gives for $\langle h_o^2 \rangle$ the product of AL. From this it appears that, for sufficiently long chains, both statistical approaches are identical if:

$$A = 2\, a \tag{3.6}$$

Once again it must be stressed that the chain statistics, as described above, are valid only if the excluded volume effects can be neglected. This applies also to the calculations of hydrodynamic quantities with the aid of these statistics. For strongly coiled macromolecules the excluded volume has quite an influence on the hydrodynamic properties. However, when the chain becomes stiffer and more extended, this influence will diminish. For strongly coiled macromolecules therefore one must keep in mind that differences between theoretical and experimental results can be due to an omission of the theoretical treatment with regard to the excluded volume.

3.3 Formulation of the hydrodynamic problem

The irreversible processes in solutions of macromolecules are determined by hydrodynamic forces, which the polymer molecules exert on the solvent, and by Brownian motion. The perturbation of the flow pattern of the solvent by the macromolecules determines the viscoelastic properties of these solutions. The stochastic process of chain movement under influence of Brownian motion can be described by a distribution function[13,14], which satisfies a generalized equation of diffusion in the molecular configuration space*.

* The term "configuration space" requires some explanation. In statistical physics the space, in which the mutual positions of atoms, that fluctuate as a result of thermal motion, are described, is usually called the "configuration space". In stereochemistry, however, the term "configuration" refers to the structure of a molecule which changes only if chemical bonds are broken. On the other hand, a molecular shape which fluctuates as a result of thermal motion is called "conformation". The usage of the term configuration may at times violate conventions of organic chemists. Therefore, Birshtein and Ptitsyn[15] proposed to use the stereochemical term conformation in all cases in which it is customary to talk ot configurations in statistical mechanics. However, the latter term was well established in statistical mechanics, independently of its appropriation for special stereochemical purposes. We may, for example, conceive of a configuration of a macromolecular model as being specified by a point in configuration space, without any reference to the stereochem-

For the purpose, a macromolecule is supposed to be built up of N+1 structurally identical elements, usually called beads, connected by N bonds of arbitrary length. Interactions of the macromolecules with the solvent take place at the beads, elastic deformation of the macromolecules occurs within the bonds, usually represented by springs. If there exists no mutual connection between the orientations and lengths of the N springs in space, such a macromolecule possesses 3N+3 degrees of freedom which describe the positions of the N+1 beads in space. If, however, restrictions are imposed, such as a fixed bond length, the number of degrees of freedom is lowered considerably.

Each configuration of this model is completely described by the N+1 vectors $\underline{r}_n$ (n = 0,1,...,N), specifying the positions of the beads in space. The 3-dimensional space, where the position vectors are defined in, is assumed to be Cartesian. Now we can define a (3N+3)-dimensional

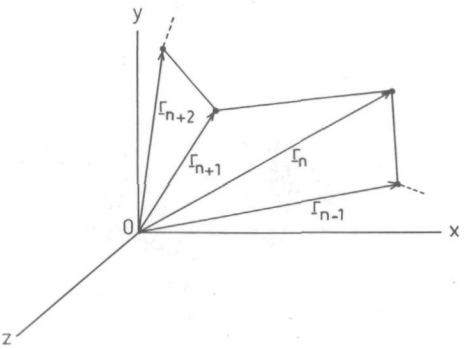

Fig. 3.2. General model of a macromolecule: N+1 beads connected by N bonds of arbitrary length. $\underline{r}_n$ indicates the position of the n^{th} bead in space.

space, in which the total configuration of the model chain is given by a single vector $\bar{R}$. This vector $\bar{R}$ is a (3N+3)-dimensional column vector, composed of the position vectors $\underline{r}_n$:

$$\bar{R} = (\bar{X},\bar{Y},\bar{Z}) = \begin{bmatrix} \underline{r}_0 \\ \underline{r}_1 \\ \cdot \\ \cdot \\ \cdot \\ \underline{r}_N \end{bmatrix} \quad \text{with } \underline{r}_n = (x_n, y_n, z_n) \tag{3.7}$$

ical conformation of the real macromolecule. In this sense the term configuration space will be used throughout this work, as long as only statistical mechanical problems are involved. When the real chemical structure of a chain is concerned, the appropriate stereochemical terms will be used.

(Bars above the symbols indicate vectors in the configuration space, those below the symbols vectors in the 3-dimensional space).

The description of macromolecular diffusion in this multidimensional configuration space was worked out in its most general form by Kramers[16], Kirkwood and Fuoss[17-19]. Their work was based on certain assumptions, which can be summarized as follows[20]:

(i) The polymer solution contains ν identical polymer molecules per unit of volume and is dilute enough, so that no mutual interactions occur between separate macromolecules.

(ii) The dimensions of the macromolecules are large, compared with the solvent molecules. The solvent is considered as a continuum.

(iii) The solution is incompressible (compare section 2.2). The overall shear rate is identical with the shear rate of the solvent, undisturbed by the polymer molecules.

(iv) The Brownian motion can be described by a stochastic Markoff process.

(v) The equations of motion of the particles are linear in the accelerations and velocities of the particles. This means that all deformations, rates of deformation, linear velocities of the mass centers and angular velocities of the macromolecules must be infinitesimal.

(vi) Inertia of the macromolecules is neglected.

(vii) The macromolecules are apolar.

(viii) The deformations of the macromolecules are purely elastic.

On the basis of these assumptions the diffusion equation in the configuration space can be derived in its most general form[20]:

$$\frac{\partial \Psi}{\partial t} = \left(\frac{\partial}{\partial \bar{R}} \right)^{T} \cdot \left(-\bar{\bar{V}}\Psi + \frac{\Psi}{\rho} \frac{\partial}{\partial \bar{R}} W + \frac{kT}{\rho} \frac{\partial}{\partial \bar{R}} \Psi \right) \tag{3.8}$$

where

$$\frac{\partial}{\partial \bar{R}} = \begin{bmatrix} \partial/\partial \underline{r}_0 \\ \partial/\partial \underline{r}_1 \\ \cdot \\ \cdot \\ \cdot \\ \partial/\partial \underline{r}_N \end{bmatrix} \qquad \bar{\bar{V}} = \begin{bmatrix} \underline{v}_0 \\ \underline{v}_1 \\ \cdot \\ \cdot \\ \cdot \\ \underline{v}_N \end{bmatrix} \tag{3.9}$$

Ψ = the probability density of the beads in the configuration space,

W = the internal energy of the macromolecule, as caused by elastic deformation,

ρ = the hydrodynamic friction factor of a bead,

$\underline{v}_n$ = the velocity which the fluid would have at the position $\underline{r}_n$, if bead n were absent,

k = the Boltzmann's constant,

T = the absolute temperature. (T as superfix means transpose).

Ψ is normalized over the whole configuration space V:

$$\int\cdot\cdot\cdot\int_V \Psi d^3\underline{r}_0\cdots d^3\underline{r}_N = 1 \tag{3.10}$$

This general diffusion equation is obtained from a more general Fokker-Planck equation, defined in the combined momentum-configuration space of the macromolecule. Integration of the Fokker-Planck equation over the momentum space leads to the diffusion (Smoluchowski) equation which, as a consequence of this integration, holds in the sub-space of configuration. However, the mentioned integration can only be performed if several linearizations in the momentum space are permitted. These linearizations are summed up in assumption (v). This means that the diffusion equation is a linear equation, which is valid for systems departing only slightly from equilibrium. An explanation of non-linear effects, such as a non-Newtonian viscosity, can probably not be based on this equation[21,22]. In fact, as it will become obvious below, all theories, based on this equation, naturally yield only linear effects. Non-linear effects in general emerged from modifications, rather arbitrarily introduced into the second term between the brackets in eq. (3.8). As a matter of fact this means that the theory in its genuine state can only be used for the interpretation of experimental results, which are extrapolated to zero shear rate. Only in that case the system can be considered as departing slightly from equilibrium. A discussion, however, on the range of shear rates for which these theories remain valid, will be postponed until chapter 7, where non-linear theories are discussed more extensively.

The right hand side of eq. (3.8) contains three terms, which describe the different kinds of processes, which take place on a macromolecule. The first term describes the transport of beads by the flow. Since there is a velocity gradient in the flowing solution, the fluid velocity will vary with the positions of the different beads of the macromolecule. As a consequence, the macromolecule will be deformed. A deformation is also caused by a diffusion process, which causes the beads to move apart in configuration space. This diffusion process is described by the last term of eq. (3.8). The factor kT/ρ can be written as the diffusion coefficient for a bead according to the first relation of Einstein for Brownian motion:

$$\mathbb{D} = kT/\rho \tag{3.11}$$

Because of the deformation of the macromolecule its internal energy is increased, which gives rise to a reverse flow of beads in opposite direction, described by the second term in eq. (3.8).

As the solution is macroscopically considered as a continuum, the macroscopic fluid velocity in shear flow at the position $\underline{r}_n$ can simply be given by:

$$v^o_{x,n} = q\, y_n \qquad v^o_{y,n} = v^o_{z,n} = 0 \tag{3.12}$$

This equation is identical with eq. (2.1). We call this the "undisturbed fluid velocity" as, on a microscopic scale, the fluid velocity $\underline{v}_n$ at $\underline{r}_n$ differs from the undisturbed velocity $\underline{v}^o_n$. The beads, which are in the vicinity of position $\underline{r}_n$, disturb the flow pattern at that point. This disturbance is generally described by the Burgers[23], Kirkwood-Riseman[24] approximation of the Oseen[25]-equation for hydrodynamic interaction:

$$\underline{v}_n = \underline{v}^o_n + \sum_{\substack{m=0 \\ m\neq n}}^{N} T_{mn}\, \underline{f}_m \tag{3.13}$$

where

$$T_{mn} = T_{nm} = (1/6\pi\eta_s)\langle 1/(\underline{r}_n - \underline{r}_m)\rangle \qquad n\neq m \tag{3.14}$$

T_{mn} = the elements of a symmetric matrix of order N+1,

$\underline{f}_m$ = the total force on bead m, as exerted by the connectivity in the chain and by Brownian motion. This force is in equilibrium with the force exerted by the solvent flow,

$\langle 1/(\underline{r}_n - \underline{r}_m)\rangle$ = the mean value of the reciprocal distance between the beads n and m.

As a matter of fact, $\underline{f}_m$ contains the forces due to diffusion and the elastic deformation. Both kinds of forces on bead m can be obtained from the second and third terms of the right hand side of eq. (3.8) by multiplying them by ρ/Ψ. This transforms both current densities into the corresponding forces. Taking that component of the corresponding (3N+3)-dimensional force, which applies to bead m, one obtains:

$$\underline{f}_m = -\frac{\partial}{\partial \underline{r}_m} W - kT \frac{\partial}{\partial \underline{r}_m} \ln\Psi \tag{3.15}$$

If eqs. (3.13) and (3.15) are combined and a new symmetric matrix $\bar{\bar{H}}$ of order N+1 is defined with the elements:

$$H_{mn} = \begin{cases} 1 & m = n \\ T_{mn} & m \neq n \end{cases} \tag{3.16}$$

than eq. (3.8) becomes:

$$\frac{\partial\Psi}{\partial t} = \left(\frac{\partial}{\partial \bar{R}}\right)^T \cdot \left(-\bar{V}^o\Psi + \frac{\Psi}{\rho}\bar{\bar{H}} \cdot \frac{\partial}{\partial \bar{R}} W + \frac{kT}{\rho}\bar{\bar{H}} \cdot \frac{\partial}{\partial \bar{R}}\Psi\right) \tag{3.17}$$

where for $\bar{V}^o$ an analog definition is given as for $\bar{V}$ (see eq. (3.9)). (Double bars above the symbols indicate matrices in the configuration space).

The matrix $\bar{\bar{H}}$ describes the mutual hydrodynamic interactions between the beads. If these interactions are neglected, $\bar{\bar{H}}$ becomes equal to the unity matrix. Now the hydrodynamic behaviour of the model chain is in principle determined. The knowledge of Ψ enables us to average over all possible configurations, which the macromolecule can assume in flow. In this way we are led to the calculation of hydrodynamic properties. As a matter of fact, an exact solution of Ψ from eq. (3.17) is not always necessary. Certain averages over Ψ can often be determined straightforwardly by a partial integration of eq. (3.17).

3.4 Description of the elastic effects

Much theoretical work has been done based on the general model described in section 3.3. However, many contributions differ from each other in the way the internal elastic energy of the model is described. For this purpose both bonds around the n^{th} bead are considered:

Fig. 3.3. Definition of the elastic forces within the model chain.

Two sorts of elastic deformations can be introduced:

(i) First, the bonds can be taken as Hookean springs. The longitudinal (directed along the chain) elastic force $\underline{f}^{e}_{n,L}$, which arises in the n^{th} spring, is proportional to the distance between the beads n and n-1. The proportionality- or spring force-constant will be given by σ:

$$\underline{f}^{e}_{n,L} = \sigma(\underline{r}_n - \underline{r}_{n-1}) \tag{3.18a}$$

The internal potential energy of the model chain due to these forces is given by:

$$W_L = \sum_{n=1}^{N} \frac{\sigma}{2} (\underline{r}_n - \underline{r}_{n-1})^2 \tag{3.18b}$$

(ii) Besides, another elastic force can be introduced. We can define a transverse (directed perpendicular to the chain) elastic force $\underline{f}^{e}_{n,Tr}$, which is proportional to the angle θ_n between both bonds connected with the n^{th} bead. According to Harris and Hearst[26] this force reads:

$$\underline{f}^{e}_{n,Tr} = \alpha(-\underline{r}_{n-1} + 2\underline{r}_{n} - \underline{r}_{n+1}) \tag{3.19a}$$

where α = a bending force constant.

The internal potential energy due to these forces reads:

$$W_{Tr} = \sum_{n=1}^{N-1} \frac{\alpha}{2} (-\underline{r}_{n-1} + 2\underline{r}_{n} - \underline{r}_{n+1})^2 \tag{3.19b}$$

The total elastic energy stored in the molecule is given by the sum of both. This can be inserted in the diffusion equation (3.17).

In the past, most authors have restricted themselves to only one of both elastic effects[24,27-30]. So Rouse[28] and Zimm[30] only confine themselves to longitudinal elastic forces. Particularly their results concerning flow birefringence of flexible polymers can readily be confirmed experimentally[31]. However, their model fails to describe the behaviour of stiffer macromolecules. For those cases the model of Harris and Hearst[26] seems to give better results. The latter authors take both elastic forces into account.

There appears to be an obvious correspondence between the Rouse-Zimm (RZ)- and the Harris-Hearst (HH)-treatment of the elastic energy[32,33]. In the RZ-treatment only the longitudinal elastic energy is inserted into the diffusion equation:

$$\frac{\partial}{\partial \bar{R}} W = \frac{\partial}{\partial \bar{R}} W_L = \frac{\partial}{\partial \bar{R}} \{ \frac{\sigma}{2} \sum_{n=1}^{N} (\underline{r}_{n} - \underline{r}_{n-1})^2 \} = \sigma \bar{\bar{A}} \cdot \bar{R} \tag{3.20}$$

where $\bar{\bar{A}}$ = a positive definite symmetric matrix of order N+1, given by Rouse[28]:

$$\bar{\bar{A}} = \begin{pmatrix} 1 & -1 & 0 & \cdot & \cdot & \cdot \\ -1 & 2 & -1 & \cdot & \cdot & \cdot \\ 0 & -1 & 2 & \cdot & \cdot & \cdot \\ \cdot & \cdot & \cdot & \cdot & \cdot & \cdot \\ \cdot & \cdot & \cdot & \cdot & 2 & -1 \\ \cdot & \cdot & \cdot & \cdot & -1 & 1 \end{pmatrix} \tag{3.21}$$

However, Harris and Hearst introduce also the transverse elastic energy, so that in their treatment the elastic energy term in the diffusion equation reads:

$$\begin{aligned} \frac{\partial}{\partial \bar{R}} W &= \frac{\partial}{\partial \bar{R}} W_L + \frac{\partial}{\partial \bar{R}} W_{Tr} \\ &= \sigma \bar{\bar{A}} \cdot \bar{R} + \frac{\partial}{\partial \bar{R}} \{ \frac{\alpha}{2} \sum_{n=1}^{N-1} (-\underline{r}_{n-1} + 2\underline{r}_{n} - \underline{r}_{n+1})^2 \} \\ &= \sigma \bar{\bar{A}} \cdot \bar{R} + \alpha \bar{\bar{B}} \cdot \bar{R} \end{aligned} \tag{3.22}$$

where $\bar{\bar{B}}$ = also a positive definite symmetric matrix or order N+1, given by Harris and Hearst[26]:

$$\bar{\bar{B}} = \begin{pmatrix} 1 & -2 & 1 & 0 & 0 & 0 & \cdot & \cdot & \cdot & \cdot & \cdot & \cdot \\ -2 & 5 & -4 & 1 & 0 & 0 & \cdot & \cdot & \cdot & \cdot & \cdot & \cdot \\ 1 & -4 & 6 & -4 & 1 & 0 & \cdot & \cdot & \cdot & \cdot & \cdot & \cdot \\ 0 & 1 & -4 & 6 & -4 & 1 & \cdot & \cdot & \cdot & \cdot & \cdot & \cdot \\ \cdot & \cdot & \cdot & \cdot & \cdot & \cdot & \cdot & \cdot & \cdot & \cdot & \cdot & \cdot \\ \cdot & \cdot & \cdot & \cdot & \cdot & \cdot & \cdot & 1 & -4 & 6 & -4 & 1 \\ \cdot & \cdot & \cdot & \cdot & \cdot & \cdot & \cdot & 0 & 1 & -4 & 5 & -2 \\ \cdot & \cdot & \cdot & \cdot & \cdot & \cdot & \cdot & 0 & 0 & 1 & -2 & 1 \end{pmatrix} \tag{3.23}$$

If one defines:

$$\frac{\sigma}{\alpha} = \Lambda \tag{3.24}$$

where Λ is a parameter dependent on the relative contributions of both elastic effects to the total elastic energy, eq. (3.22) becomes:

$$\frac{\partial}{\partial \bar{R}} W = \alpha \bar{\bar{A}}_{HH} \cdot \bar{R} \tag{3.25a}$$

where

$$\bar{\bar{A}}_{HH} = \bar{\bar{B}} + \Lambda \bar{\bar{A}} \ . \tag{3.25b}$$

So, if the diffusion equation for the RZ-model is given by a combination of eq. (3.20) and (3.17), viz.:

$$\frac{\partial \Psi}{\partial t} = \left(\frac{\partial}{\partial \bar{R}} \right)^T \cdot \left(-\bar{V}^o \Psi + \frac{\Psi}{\rho} \sigma \bar{\bar{H}} \cdot \bar{\bar{A}} \cdot \bar{R} + \frac{kT}{\rho} \bar{\bar{H}} \cdot \frac{\partial}{\partial \bar{R}} \Psi \right) , \tag{3.26}$$

the diffusion equation for the HH-model is simply obtained by replacing $\sigma \bar{\bar{A}}$ by $\alpha \bar{\bar{A}}_{HH}$.

Equation (3.26) can be solved by using a linear normal coordinate transformation[28-30] of the type:

$$\bar{R} = \bar{\bar{Q}} \cdot \bar{\Xi} \tag{3.27a}$$

$$\frac{\partial}{\partial \bar{R}} = \bar{\bar{Q}}^{-1^T} \cdot \frac{\partial}{\partial \bar{\Xi}} \tag{3.27b}$$

where

$$\bar{\Xi} = \begin{bmatrix} \xi_0 \\ \xi_1 \\ \cdot \\ \cdot \\ \cdot \\ \xi_N \end{bmatrix} \quad \text{with } \xi_n = (\zeta_n, \eta_n, \vartheta_n) \ . \tag{3.27c}$$

The vectors $\underline{\xi}_n$ are linear functions of $\underline{r}_n$ and represent normalized configurations (normal modes) with variable amplitudes in the configuration space, from which all possible configurations can be derived by summation. The transformation matrix $\bar{\bar{Q}}$, of order N+1, diagonalizes the matrix product $\bar{\bar{H}}\cdot\bar{\bar{A}}$:

$$\bar{\bar{Q}}^{-1}\cdot\bar{\bar{H}}\cdot\bar{\bar{A}}\cdot\bar{\bar{Q}} = \bar{\bar{G}} \tag{3.28a}$$

where $\bar{\bar{G}}$ = a diagonal matrix, built up of the eigenvalues $\gamma_0,\gamma_1,\ldots,\gamma_N$ of the matrix product, which are the (real) roots of the equation:

$$\det\,|\bar{\bar{H}}\cdot\bar{\bar{A}} - \gamma\,\bar{\bar{I}}\,| = 0 \tag{3.29}$$

where $\bar{\bar{I}}$ = the unity matrix.
The columns of the matrix $\bar{\bar{Q}}$ are the eigenvectors of the above mentioned matrix product. The same matrix $\bar{\bar{Q}}$ can be used to diagonalize matrix $\bar{\bar{A}}$ separately[30]:

$$\bar{\bar{Q}}^{T}\cdot\bar{\bar{A}}\cdot\bar{\bar{Q}} = \bar{\bar{M}} \tag{3.28b}$$

where $\bar{\bar{M}}$ = also a diagonal matrix with elements μ_n.

If hydrodynamic interaction is neglected, which is the case considered by Rouse, the matrix $\bar{\bar{H}}$ turns into the unity matrix. In that case it follows that:

$$\bar{\bar{Q}}^{-1} = \bar{\bar{Q}}^{T} \quad\text{and}\quad \gamma_n = \mu_n \tag{3.30}$$

After inserting eq. (3.12) into eqs. (3.10) and (3.26) one obtains the following results for the RZ-case:

$$\int\cdots\int_V \Psi\, d^3\xi_0\cdots d^3\xi_N = J^{-1} \tag{3.31}$$

where J = the Jacobian of the coordinate transformation, and

$$\frac{\partial\Psi}{\partial t} = -q\sum_{n=0}^{N}\eta_n\frac{\partial\Psi}{\partial\zeta_n} + \sum_{n=0}^{N}\left(\frac{\partial}{\partial\underline{\xi}_n}\right)^{T}\cdot\left(\frac{kT}{\rho}\frac{\gamma_n}{\mu_n}\frac{\partial\Psi}{\partial\underline{\xi}_n} + \frac{\sigma}{\rho}\gamma_n\underline{\xi}_n\Psi\right) \tag{3.32}$$

As a matter of fact, similar results are obtained for the HH-model[33], with σ replaced by α and γ_n, resp. μ_n replaced by $\gamma_{n,HH}$, resp. $\mu_{n,HH}$, corresponding to the diagonalization of the matrices $\bar{\bar{H}}\cdot\bar{\bar{A}}_{HH}$ and $\bar{\bar{A}}_{HH}$ with the aid of a transformation matrix $\bar{\bar{Q}}_{HH}$.

3.5 General form of results

3.5.1 Separation of the diffusion equation

With the aid of the transformed diffusion equation (3.32) the hydrodynamic properties of the macromolecules can be calculated, such as their

contributions to the stress tensor of the streaming solution. However, at first it has to be pointed out that the diffusion equation can be separated.

Formally one of the eigenvalues of the matrix product $\overline{\overline{H}}\cdot\overline{\overline{A}}$, say γ_0, appears to be equal to zero. This is recognized by the fact that the determinant of matrix $\overline{\overline{A}}$ vanishes. According to Zimm[30] the advantage of this choice of coordinates is that one position vector $\underline{\xi}_0$ remains for the description of the location of the center of resistance in the configuration space. It is just this vector $\underline{\xi}_0$, which corresponds to the eigenvalue γ_0. $\underline{\xi}_0$ is only of importance for the translation diffusion of the center of resistance of the polymer molecule, but does not influence the hydrodynamic properties of the solution. Therefore we are free to give $\underline{\xi}_0$ any arbitrary value. If we put $\underline{\xi}_0$ equal to the $\underline{0}$-vector, the center of resistance coincides with the origin of the coordinate system.

The center of resistance usually does not coincide with the mass center of a macromolecule. The two centers do coincide only when no hydrodynamic interaction takes place within the macromolecule. As was mentioned before this means that the matrix $\overline{\overline{H}}$ becomes equal to the unity matrix.

Now the diffusion equation can be separated into a part, which describes the movements of the center of resistance, and a second part, which contains the equations of motion of the N springs. Zimm[30] proved the separability only in the absence of external forces, i.e. for the case q = 0. However, Lodge and Wu[34] have shown that the separability generally holds, independent of the shear rate. They introduce an extra transformation, which first separates the equation for the center of resistance from the diffusion equation. The normal coordinate transformation is then only applied to the equations of motion of the springs. This greatly simplifies the calculations in the RZ-case. However, the HH-case appears to become more complicated. Since the eigenvalues $\gamma_1,\ldots,\gamma_N$ remain unaltered yet, it seems reasonable to follow the description of Zimm without separation of the diffusion equation.

3.5.2 The stress tensor

The calculation of the polymer contribution to the stress tensor, p_{ij}, has been given in a clear way by Lodge and Wu[34]. Let us consider a macroscopic plane, of area A, with unit normal $\underline{e}$ within the volume V of the solution. That volume V contains νV identical independent polymer molecules, each of them built up of N+1 beads. According to the definition of the stress tensor the material on the "+$\underline{e}$"-side of the plane "(A,$\underline{e}$)" must exert a force on the material on the "-$\underline{e}$"-side. This force is exerted on the beads, which are just in the plane (A,$\underline{e}$).

Therefore we must determine the probability density $\Phi_n(\underline{u})$, to find the n^{th} bead of a certain macromolecule at the position $\underline{u}$, situated in

the plane $(A,\underline{e})$. In terms of Dirac δ-functions we have:

$$\Phi_n(\underline{u}) = \int_V \delta(\underline{u} - \underline{r}_n)\Psi(\underline{r}_0,\ldots,\underline{r}_N)\,d^3\underline{r}_0 \ldots d^3\underline{r}_N$$

$$= V^{-1}\int_V \Psi(\underline{r}_0,\ldots,\underline{r}_{n-1},\underline{u},\underline{r}_{n+1},\ldots,\underline{r}_N)\,d^3\underline{r}_0 \ldots d^3\underline{r}_{n-1} \times$$

$$d^3\underline{r}_{n+1} \ldots d^3\underline{r}_N \qquad (3.33)$$

because of the normalization of Ψ over the configuration space, eq. (3.10). The beads labelled n are uniformly distributed within the volume V, so that the number of beads labelled n within a specified volume ΔV is equal to:

$$\nu V \int_V \Phi_n(\underline{u})\,d^3\underline{u} = \nu\Delta V \int_V \Psi(\underline{r}_0,\ldots,\underline{r}_N)\,d^3\underline{r}_0 \ldots d^3\underline{r}_{n-1}d^3\underline{r}_{n+1}\ldots d^3\underline{r}_N \qquad (3.34)$$

For any given value of n in the range $0,1,\ldots,N$, let us consider the contribution to the stress tensor from all beads labelled n and situated in the plane $(A,\underline{e})$. On each bead in that plane a force $\underline{f}_n$ is exerted by the "$+\underline{e}$"-material. The number of beads n is given by eq. (3.34) with:

$$\Delta V = A\ \underline{u} \cdot \underline{e} \qquad (3.35)$$

On adding such contributions for all values of n and for all possible orientations of $\underline{u}$, dividing by A and using the fact that $\underline{e}$ is an arbitrary unity vector, we obtain the required equation:

$$p_{ij} = -\nu \int_V \Psi(\underline{r}_0,\ldots,\underline{r}_N) \sum_{n=0}^{N} f_{n,i}\, r_{n,j}\, d^3\underline{r}_0 \ldots d^3\underline{r}_N \qquad (3.36)$$

where $r_{n,j}$, resp. $f_{n,j}$ = the projection of the vector $\underline{r}_n$, resp. $\underline{f}_n$, on the j-axis.

We will write eq. (3.36) as:

$$p_{11} = -\nu \left\langle \sum_{n=0}^{N} f_{n,x}\, x_n \right\rangle = -\nu \langle \bar{F}_X \cdot \bar{X} \rangle \qquad (3.37a)$$

$$p_{22} = -\nu \left\langle \sum_{n=0}^{N} f_{n,y}\, y_n \right\rangle = -\nu \langle \bar{F}_Y \cdot Y \rangle \qquad (3.37b)$$

$$p_{33} = -\nu \left\langle \sum_{n=0}^{N} f_{n,z}\, z_n \right\rangle = -\nu \langle \bar{F}_Z \cdot \bar{Z} \rangle \qquad (3.37c)$$

$$p_{12} = p_{21} = -\nu \left\langle \sum_{n=0}^{N} f_{n,x}\, y_n \right\rangle = -\nu \langle \bar{F}_X \cdot \bar{Y} \rangle \qquad (3.37d)$$

where $\langle\ \rangle$ indicates the averaging procedure using Ψ according to eq. (3.36) and $\bar{F}_X$, $\bar{F}_Y$, $\bar{F}_Z$, resp. $\bar{X}$, $\bar{Y}$, $\bar{Z}$, are defined in the configuration space, see eq. (3.7).

The force $\underline{f}_n$ is given by eq. (3.15). After inserting eq. (3.15) into the eqs. (3.37 a-d) and transforming to normal coordinates we obtain the

following results for the RZ-model:

$$p_{11} = \nu kT \sum_{n=1}^{N} [-1 + \frac{\sigma}{kT} \mu_n J\langle\zeta_n^2\rangle] \tag{3.38a}$$

$$p_{22} = \nu kT \sum_{n=1}^{N} [-1 + \frac{\sigma}{kT} \mu_n J\langle\eta_n^2\rangle] \tag{3.38b}$$

$$p_{33} = \nu kT \sum_{n=1}^{N} [-1 + \frac{\sigma}{kT} \mu_n J\langle\vartheta_n^2\rangle] \tag{3.38c}$$

$$p_{12} = p_{21} = \nu kT \sum_{n=1}^{N} [\frac{\sigma}{kT} \mu_n J\langle\zeta_n\eta_n\rangle] \tag{3.38d}$$

The first terms in eqs. (3.38 a-c) are obtained from the diffusion term in eq. (3.15) by partial integration over the whole configuration space, making use of the fact that Ψ and all derivatives of Ψ vanish at infinity.

The averages in eqs. (3.38 a-d) have been calculated by Zimm[30]. For shear flow, as given by eq. (3.12), they read:

$$J\langle\zeta_n^2\rangle = \frac{kT}{\mu_n\sigma} [1 + \rho^2q^2/2\sigma^2\gamma_n^2] \tag{3.39a}$$

$$J\langle\eta_n^2\rangle = J\langle\vartheta_n^2\rangle = \frac{kT}{\mu_n\sigma} \tag{3.39b}$$

$$J\langle\zeta_n\eta_n\rangle = \frac{kT}{\mu_n\sigma} [\rho q/2\sigma\gamma_n] \tag{3.39c}$$

Inserting these eqs. into the eqs. (3.38a-d) finally gives the required polymer contributions to the stress tensor of the streaming solution:

$$p_{11} = \nu kT \frac{\rho^2q^2}{2\sigma^2} \sum_{n=1}^{N} \gamma_n^{-2} \tag{3.40a}$$

$$p_{22} = p_{33} = 0 \tag{3.40b}$$

$$p_{21} = p_{12} = \nu kT \frac{\rho q}{2\sigma} \sum_{n=1}^{N} \gamma_n^{-1} \tag{3.40c}$$

The corresponding equations for the HH-model are obtained by replacing σ, resp. γ_n, by α, resp. $\gamma_{n,HH}$.

The number of polymer molecules ν per cm^3 can be expressed in the concentration of the solution:

$$\nu = \frac{cM}{N_A} \tag{3.41}$$

where c = the polymer concentration in g/cm^3,
M = the molecular weight of a polymer molecule,
N_A = Avogadro's constant.

Finally this results in the following equations for the intrinsic viscosity and the orientation angle of the stress tensor:

$$[\eta]_o = p_{21}/q\ \eta_s\ c = \frac{N_A\ k\ T\ \rho}{2\sigma\ \eta_s\ M} \sum_{n=1}^{N} \gamma_n^{-1} \tag{3.42}$$

and

$$\cot 2\chi' = \frac{p_{11} - p_{22}}{2\, p_{21}} = \left\{ \frac{\sum_{n=1}^{N} \gamma_n^{-2}}{\left(\sum_{n=1}^{N} \gamma_n^{-1} \right)^2} \right\} \nu kT\, p_{21}$$

$$= J_{eR}\, \beta_N \tag{3.43}$$

where

$$J_{eR} = \frac{\sum_{n=1}^{N} \gamma_n^{-2}}{\left(\sum_{n=1}^{N} \gamma_n^{-1} \right)^2} \tag{3.44}$$

the reduced steady state shear compliance, as defined by Tschoegl[35]. The reduced shear rate β_N is defined by[36]:

$$\beta_N = \nu kT\, p_{21} = \frac{q\, (\eta - \eta_s)\, M}{c\, R\, T} \tag{3.45a}$$

where R = the gas constant.
The subscript N means, that the Newtonian solution viscosity has to be used for a calculation of β_N. When the parameter β_N is used one aims at a reduction of experimental data with respect to temperature, molecular weight and concentration. In theoretical expressions, which are valid only for infinite dilution, β_N can be given by:

$$\beta_N = \frac{q\, [\eta]_o\, \eta_s\, M}{R\, T} \tag{3.45b}$$

The corresponding formulas for the HH-case are obtained by the above mentioned substitutions.

Since according to section 3.3 the validity of this theory is restricted to very small shear rates, it can be expected that eqs. (3.42) and (3.43) are valid only for sufficiently small values of β_N.

3.6 Specification of the eigenvalues

3.6.1 The Rouse-Zimm model

As was pointed out in section 3.4 Rouse and Zimm are only concerned with longitudinal elastic effects. They identify the mean square length of the springs with the mean square end-to-end distance of a Gaussian chain molecule. Their model can be considered to be built up of a great number of Gaussian "submolecules" and is therefore usually referred to as the "subchain model". The elastic forces which arise in the subchains equal the elastic forces in a Gaussian macromolecule, as given by Kuhn and Kuhn[37]. This implies that the spring force constant σ for the RZ-model is given by:

$$\sigma = 3kT/b_o^2 \tag{3.46}$$

where b_o^2 = the mean square end-to-end distance of the Gaussian subchain in the absence of external forces.

As to the choice of the number of beads we are free to give N any arbitrary value starting from 1 up to infinity. The value N=1, however, represents a special case. This model, two beads connected by a single elastic spring, is identical with the elastic dumbbell model of Kuhn[37]. From a historical point of view this model is of great importance, as a great deal of pioneering work was done on this model with regard to the hydrodynamic properties of macromolecules.

A third point of discussion is the hydrodynamic interaction. For the present purpose it suffices to state that one cannot à priori say how great the hydrodynamic interaction within a real macromolecule will be. So we can only approximately guess between which extrema it must lie.

Only small deviations from equilibrium conditions will be regarded. Further, in the state of rest, the separate springs in the RZ-model are oriented in space in an arbitrary way with regard to each other. This will result in a Gaussian distribution of all springs. This distribution will hardly be disturbed by the small deviations from equilibrium. Therefore, the hydrodynamic interaction matrix T_{mn}, eq. (3.14), is usually averaged over this Gaussian distribution in an early stage of the calculations[24,30], which gives for T_{mn}:

$$T_{mn} = 1/(6\pi^3)^{\frac{1}{2}}\ \eta_s\ b_o\ (|m - n|)^{\frac{1}{2}} \tag{3.47}$$

This expression is incorporated in the calculations. As to the errors introduced by this preaveraging procedure very little is known. However, there exist some indications[38,39] that they are comparatively small. Svetlov[40] has recently given a solution of the diffusion equation without preaveraging the hydrodynamic interaction. The degree of hydrodynamic interaction is determined by the values ascribed to the non-diagonal elements of the matrix $\bar{\bar{H}}$, eq. (3.16), i.e. to ρT_{mn}, where the hydrodynamic friction factor ρ and the magnitude of b_o act as adjustable parameters. With respect to the latter adjustment, a choice has to be made first with respect to the value of N, in accordance with the molecular weight.

For the calculations of the intrinsic viscosity and the value of the reduced steady state shear compliance only the determination of the eigenvalues $\gamma_1,\ldots,\gamma_N$ remains. The most simple case is the one in which, according to Rouse[28], the hydrodynamic interaction is completely absent. The model is considered to be fully drained by the solvent: the free-draining case. The matrix $\bar{\bar{H}}$ becomes equal to the unity matrix and the eigenvalues of $\bar{\bar{A}}$ can be determined for any value of N [28]:

$$\mu_n = \gamma_n = 4 \sin^2 \left(\frac{n\pi}{2(N+1)} \right) \qquad n = 1,\ldots,N \tag{3.48a}$$

which for sufficiently large N and n<<N can be approximated by:

$$\mu_n = \gamma_n = \frac{n^2\pi^2}{N^2} \tag{3.48b}$$

For sufficiently large N the elements of the n^{th} column of the transformation matrix $\bar{\bar{Q}}$, corresponding to the n^{th} eigenvalue, are given by:

$$Q_{mn} = \left(\frac{2}{N}\right)^{\frac{1}{2}} \alpha(r) \tag{3.49a}$$

with

$$\alpha(r) = \cos \left(\frac{n\pi}{2} r \right), \qquad n \text{ - even} \tag{3.49b}$$

$$\alpha(r) = \sin \left(\frac{n\pi}{2} r \right), \qquad n \text{ - odd} \tag{3.49c}$$

where r = a new numbering parameter for the beads, given by:

$$r = \frac{2m}{N} - 1 \tag{3.49d}$$

For large N the elements Q_{mn} vary slowly with the index m, so that they may be considered to be continuous eigenfunctions of the matrix product $\bar{\bar{H}} \cdot \bar{\bar{A}}$.

After inserting the eqs. (3.46) and (3.48b) into eq. (3.42) and carrying out the summation using Riemann zeta functions the following equation is obtained for $N \to \infty$:

$$[\eta]_o = \frac{N_A \, b_o^2 \, \rho \, N^2}{36 \, M \, \eta_s} \tag{3.50}$$

The peculiarity of this relation is that it does not make much physical sense: if the hydrodynamic interaction is neglected one assumes that the hydrodynamic friction factor ρ of the beads practically vanishes: $\rho T_{mn} \cong 0$. This means that also the contributions of the chain molecules to the viscosity should be extremely small.

However, more important in this context are the values, obtained for the reduced steady state shear compliance J_{eR}. For N=1, the elastic dumbbell, only one eigenvalue is found which, according to eq. (3.44), gives a value for J_{eR}:

$$\text{(Free-draining)} \quad N = 1 \qquad J_{eR} = 1 \tag{3.51a}$$

This result has already been derived by Hermans[41]. An increase of N causes a decrease of the value of J_{eR}, which becomes for N approaching infinity:

$$\text{(Free-draining)} \quad N \to \infty \qquad J_{eR} = 0.4 \tag{3.51b}$$

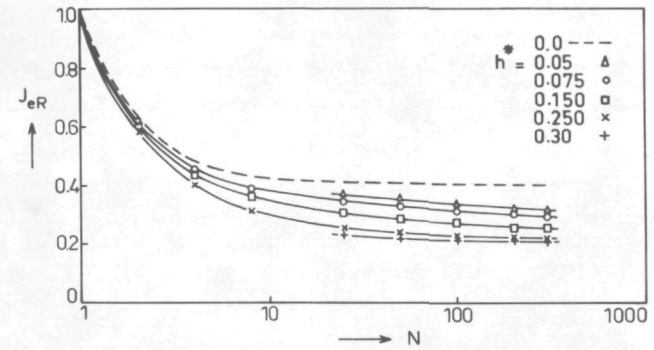

Fig. 3.4. Values of J_{eR} against N obtained for the RZ-model. Values of h* are given in the figure. h* = 0.0: free-draining, according to Rouse.

The values of J_{eR} for the free-draining case are given in Fig. 3.4 as a function of N by a dashed line.

If one takes the hydrodynamic interaction into account, for large N eq. (3.29) can be approximated by an integro-differential equation, originally derived by Zimm[30], but recently improved by Osaki[42]:

$$\alpha''(r)\ (1 - 4h^*) + h \int_{-1}^{1} \alpha''(s)\ |r - s|^{-\frac{1}{2}}\ ds = -\frac{N^2}{4}\ \gamma\ \alpha(r) \qquad (3.52)$$

with the boundary condition $\alpha'(\pm 1) = 0$. (Prime and double prime at function $\alpha(r)$ mean the first and second derivatives with respect to r). The variable s is defined in exactly the same way as r, eq. (3.49d). h and h* are measures for the hydrodynamic interaction[43]:

$$h^* = h\ N^{-\frac{1}{2}} = \rho/(12\ \pi^3)^{\frac{1}{2}}\ b_o \eta_s \qquad (3.53)$$

A minor advantage in using h*, rather than h, is given by the fact that, for infinite N and finite hydrodynamic interaction h becomes infinite while h* remains finite as well.

According to Lodge and Wu[44] a useful range for h* is $0 < h^* \leqslant 0.26$. Thurston and Morrison[43] even quote a value of 0.471 for the upper bound of h*. However, Osaki[42] shows that for $h^* > 0.25$ negative eigenvalues γ can be found for large N. This is in contradiction to the principles of thermodynamics of irreversible processes. So as an upper limit of h* a value of 0.25 seems the most acceptable.

The notation $h \gg 1$ used by Zimm actually corresponds to $h^* = 0.25$, as in that case only the integral term in the left hand side of eq. (3.52) remains. For that case and $N \to \infty$ Zimm et al.[45] have calculated the eigenvalues in a numerical way. One of their most satisfactory results becomes obvious if one looks at the overall dimensions of the molecular model. These dimensions are proportional to:

$$b_o^3 N^{3/2} = \langle h_o^2 \rangle^{3/2} \tag{3.54}$$

where $\langle h_o^2 \rangle$ = the mean square end-to-end distance of the chain in rest, according to the definition given in eq. (3.1).

The Zimm case gives the following relation for the intrinsic viscosity:

$$[\eta]_o = 2.84 \times 10^{23} \langle h_o^2 \rangle^{3/2}/M \tag{3.55a}$$

Equation (3.55a) has just the form of the well-known Flory-Fox equation[46]. This equation holds for sufficiently high molecular weights. Apparently, the Flory-Fox parameter of eq. (3.55a) reads:

$$\Phi_o = 2.84 \times 10^{23} \tag{3.55b}$$

Experimentally, a value between 2.5 - 2.9 x 10^{23} is found, when measurements are done on solutions of high molecular weight polymers in θ-solvents. The conclusion can be drawn that the treatment in terms of the non-draining case is quite adequate for sufficiently long molecules that form Gaussian chains. Tschoegl[47], Hearst[48] and Osaki[42] calculated Φ_o for the intermediate values of h* and N → ∞. They found values for Φ_o from 0 for h* = 0 up to 2.84 x 10^{23} for h* = 0.25.

The value of J_{eR}, found by Zimm, reads:

$$\text{(Non-draining)} \quad N \to \infty \qquad J_{eR} = 0.205 \tag{3.56}$$

For finite values of N the eigenvalue equation (3.29) has to be solved by use of a computer. This was done by Thurston and Morrison[43] for N from 1 to 15 and values of h* from 0.01 to 0.4. Lodge and Wu[44] have recently extended these computations up to N = 300. The values of J_{eR} calculated by Lodge and Wu are given in Fig. 3.4 as functions of N and h*. Again, a decrease of J_{eR} is found when N is increased, while all curves converge to J_{eR} = 1 for N = 1. This is a logical consequence of the definition of J_{eR}. Because N = 1 always results in only one eigenvalue, J_{eR} should always be equal to unity, independent of the magnitude of that eigenvalue.

3.6.2 The Harris-Hearst model

A much more complicated situation is encountered, when the HH-model is considered. As yet only the free-draining- and the non-draining-case were studied for N ≫ 1. For the free-draining case the eigenvalue equation for the HH-model can be solved. The following equation:

$$\mu_{n,HH} = \gamma_{n,HH} = \nu_{1,n}^4 + \Lambda\nu_{1,n}^2 \equiv \nu_{2,n}^4 - \Lambda\nu_{2,n}^2 \tag{3.57a}$$

must hold simultaneously with one of the following two equations:

$$\nu_{1,n}^3 \cot (\tfrac{1}{2} \nu_{1,n} N) = -\nu_{2,n}^3 \coth (\tfrac{1}{2} \nu_{2,n} N), \quad n \text{ - even} \tag{3.57b}$$

$$\nu_{1,n}^3 \tan (\tfrac{1}{2} \nu_{1,n} N) = -\nu_{2,n}^3 \tanh (\tfrac{1}{2} \nu_{2,n} N), \quad n \text{ - odd} \tag{3.57c}$$

which are derived from two free end boundary conditions, related to the special position of the last bead with respect to restoring and bending forces. In these equations the $\nu_{1,n}$'s and the $\nu_{2,n}$'s are auxiliary quantities. As a matter of fact, for a solution of the eqs. (3.57 a-c) only a value for ΛN^2 is needed.

For this model two limiting cases can easily be discerned: the Gaussian coil limit and the limit of a straight elastic necklace, where all beads are arranged along a straight line and the deformability is preserved only in the direction of that line. No bending of the necklace is allowed. The Gaussian coil limit is characterized by the absence of any resistance against bending, which results in a very large value of Λ. On the other hand, the straight elastic necklace is characterized by an overwhelming influence of forces resisting bending, which means a very small value of Λ.

For the free-draining Gaussian coil limit it can be derived from the eqs. (3.57 a-c) that $\nu_{1,n}N$ becomes equal to $n\pi$, which gives for the eigenvalues:

$$\text{(Free-draining coil)} \quad \mu_{n,HH} = \gamma_{n,HH} = \Lambda \left(\frac{n^2\pi^2}{N^2} \right) \tag{3.58}$$

$$n = 1,\ldots,N$$

The approximate eigenfunctions for the free-draining coil are identical with the Rouse eigenfunctions, given in eqs. (3.49 a-c). The HH-eigenvalues appear to be equal to the Rouse eigenvalues multiplied by Λ. It appears from an inspection of eq. (3.42), where σ must be replaced by α, that both the Rouse model and the free-draining HH-model for the coil give the same results. The extra factor Λ^{-1} in front of the sum of the reciprocal eigenvalues transforms α back in σ, according to eq. (3.24). This results in exactly the same equation (3.50) as for the Rouse model. Also the value of J_{eR} becomes 0.4. The conclusion can be drawn that both models are identical.

The other limiting case, the straight pearl necklace, is characterized by a very small value of Λ. In that case it can be derived from eq. (3.57a) that $\nu_{1,n}$ and $\nu_{2,n}$ must be nearly equal to each other. This results in the following equations for the free-draining eigenvalues:

(Free-draining straight necklace)

$$\mu_{1,HH} = \gamma_{1,HH} = 12\ \Lambda/N^2 + \Lambda(12\ \Lambda/N^2)^{\frac{1}{2}} \tag{3.59a}$$

$$\mu_{n,HH} = \gamma_{n,HH} = (n - \tfrac{1}{2})^4 \pi^4/N^4 \quad n = 2,\ldots,N \tag{3.59b}$$

However, the first eigenvalue appears to be extremely small compared with all higher eigenvalues, which means that the contributions of these higher eigenvalues to the intrinsic viscosity and the value of J_{eR} practically vanish. This means that in this case a value of J_{eR} equal to unity is found, as in the case of the elastic dumbbell.

For a certain number of intermediate values of ΛN^2 the eqs. (3.57a-c) were solved by a computer with the aid of an iterative procedure, which furnished a solution for $\nu_1 N$ in each quadrant. Since the contributions of higher eigenvalues to the value of J_{eR} steadily decrease, the values of J_{eR} were calculated with the first fifty eigenvalues. The results obtained for the free-draining case are given in Table 3.1, column 2.

Table 3.1

Values of J_{eR} and $[\cot 2\chi/\beta_N]_{opt}$ for the HH-model with ΛN^2 varying over a wide range

ΛN^2	J_{eR}		$[\cot 2\chi/\beta_N]_{opt}$	
	Free-draining	Non-draining	Non-draining	
4×10^{-3}	1.0	1.0	1.0	straight necklace
7.05	0.80	0.75	0.81	
421	0.50	0.45	0.47	
9.7×10^3	0.43	0.33	0.34	
4×10^4	0.42	0.30	0.30	
4×10^6	0.41	0.24	0.24	
4×10^8	0.41	0.22	0.22	coil

The non-draining case is a lot more complicated. For lower values of ΛN^2 a more detailed description of the dimensions of the model is required, before an averaging of the hydrodynamic interaction can be carried out. For this purpose Harris and Hearst[26] and Fixman and Kovac[49] derived a correlation between the present model and the statistical chain model of the wormlike chain. According to these authors there exists a relation between the bending force constant α and the persistence length a, given by:

$$\alpha = (3/2)kT\, a \tag{3.60}$$

From this equation a direct relation can be derived between Λ and the persistence length. However, the derivation of eq. (3.60) is not clearly understood, so that for the time being it is quite premature to found conclusions on it.

In the case of very high ΛN^2 the Gaussian distribution of the springs remains. For that case Hearst et al.[32] find an intrinsic viscosity identical with the result of Zimm, eqs. (3.55 a-b). For very small ΛN^2 also an exact calculation can be carried out. The results are in agreement with both Kirkwood and Auer[27] for the rod and Simha[50] for the prolate ellipsoid of large axial ratio, when for the length of these stiff models the finite mean length, caused by axial diffusion, of the straight pearl necklace is inserted.

Using eq. (3.60) Noda and Hearst[33] have calculated J_{eR} for several values of ΛN^2 for the model with hydrodynamic interaction. Their results are given in Table 3.1, column 3. The result for the coil limit agrees with the Zimm-result, eq. (3.56), while for the straight necklace again a value equal to unity is found. It seems that for the straight pearl necklace the hydrodynamic interaction has no influence on the results.

One remark remains to be made. This procedure, valid only for the straight elastic pearl necklace, does not give a value for the J_{eR} of a straight rigid pearl necklace. This will be discussed in more detail in the next paragraph.

3.7 A comparison with other model theories

In conclusion of the discussion of the hydrodynamic properties of the general model it is quite illustrative to compare the obtained results with other model theories. For the single elastic dumbbell a J_{eR}-value equal to unity has been obtained. Another model, which also is very well known, is the rigid dumbbell model: two beads connected by a rigid bond of fixed length. Recently Bird et al.[51] have shown that for the latter model the value of J_{eR} equals 3/5. From this difference of J_{eR}-values it may be concluded, that these two models show differences in hydrodynamic behaviour.

A discussion of this fact was given by Janeschitz-Kriegl[31,52] in another context. In a well-known paper Kuhn and Kuhn[53] have shown that the extra energy dissipation per unit of time due to the presence of a rigid particle in a flowing solution always consists of two parts: a contribution due to angular movements of the particle relative to the solvent and a so-called hydrodynamic contribution. The former is caused by diffusion forces corresponding to the state of orientation of the particle, the latter is due to radial flow of solvent along the particle. The radial force, as exerted by the flowing solvent, is balanced by the rigidity of the particle and has no influences on its orientation. For a rigid dumbbell it can be derived that the contribution by rotary diffusion to the intrinsic viscosity reads:

(Rigid dumbbell) $\quad [\eta]_d = (3/5)[\eta]_o \qquad (3.61a)$

For elastic dumbbells another result is obtained. If no diffusion were present both beads of an elastic dumbbell would be contracted into one point, in a resting solution. Just due to diffusion both beads are on the average at a certain distance from each other. When the length of the rigid dumbbell is adjusted to this average distance for the elastic dumbbell both models give the same $[\eta]_o$. Moreover, in both cases the contributions by rotary diffusion to the intrinsic viscosity are the same. However, the remaining part of $2/5[\eta]_o$, which is due to the radial "hydrodynamic" forces for the rigid dumbbell, must be ascribed to a disturbance of the equilibrium between diffusion and restoring forces in the case of the elastic dumbbell. Since, according to this description, the hydrodynamic properties of elastic dumbbells are completely determined by diffusion, one finds:

$$\text{(Elastic dumbbell)} \quad [\eta]_d = [\eta]_o \tag{3.61b}$$

The eqs. (3.61 a-b) show exactly the same factor 3/5 as the different J_{eR}-values for both models. The reduced steady state shear compliance for an elastic dumbbell is a quantity, determined only by the diffusion of its endpoints, while for a rigid dumbbell the J_{eR} must be smaller for physical reasons: the "hydrodynamic" forces give a contribution to the shear stress, which does not lead to a reversible change of the structure of the fluid.

As was mentioned before, in the limit of $\Lambda N^2 \to 0$ the HH-model consists of a straight necklace, built up of N elastic dumbbells. Apparently, the hydrodynamic behaviour of this model does not differ from that of a single elastic dumbbell, if hydrodynamic interaction is disregarded. In both cases a value of J_{eR} equal to unity was found. A similar remark applies to a comparison of the models of the straight rigid necklace and the single rigid dumbbell. For the straight rigid necklace Kotaka[54] already reported a value of J_{eR} equal to 3/5. The same value was found for the rigid dumbbell, as mentioned before. The correspondences between both pairs of models can easily be accounted for. Since for a straight pearl necklace all dumbbells have the same spatial orientation and on the average the same deformation, they all give the same sort of contribution to the hydrodynamic properties of the solutions as one single dumbbell of the same orientation and deformation.

The question arises whether the general HH-model (with ΛN^2 varying over a wide range) describes essentially the same effects as the RZ-model with a variable finite number of beads. In fact, the basic concept of the RZ-model, comprising an infinite number of beads was the existence of an infinite number of overall motions within the molecule: "normal modes". This resulted in the value of J_{eR} calculated by Rouse. However, the introduction of a bending force implies that the connected elastic dumbbells

are restricted in their mutual orientations in space. This restricts the number of degrees of freedom for this model and so decreases the number of effective normal modes. For the completely straight elastic necklace ($\Lambda N^2 = 0$) the number of normal modes is practically reduced to a single one: the simultaneous stretching of all elastic dumbbells within the necklace. This comprises only one eigenvalue, which always results in a value of J_{eR} equal to unity.

A restriction of the number of beads in the RZ-model also decreases the number of normal modes to leave only one normal mode in the case of the single elastic dumbbell: the stretching of the dumbbell. So also in that case only one eigenvalue is involved, which differs in value from the above mentioned one, but that does not influence the value of J_{eR}.

In the foregoing only a small choice is made out of a vast amount of theories, describing the hydrodynamic behaviour of macromolecules in solution. However, it falls far outside the scope of this work to describe all theories. Only one theory still must be mentioned, as this one will be used in a later chapter.

As pointed out in section 3.2, the best description of the dimensions of stiff macromolecules could be given with the aid of the statistics of the "wormlike chain". Eizner and Ptitsyn[55] have treated the intrinsic viscosity of infinitely thin wormlike chains of finite length in terms of the intrinsic viscosity equation of Peterlin[56]. Their relation reads:

$$[\eta]_o = \frac{2^{3/2}(b^3/M_o)\ \Phi_o N\ X(N/\lambda)}{[45(2\pi/3)^{\frac{1}{2}}/32(3-2^{\frac{1}{2}})]\ (b/\lambda r_o) + (1/\lambda^{3/2})\ \varphi(\lambda,N)N^{\frac{1}{2}}} \qquad (3.62)$$

where in the notation of the authors:

Φ_o = the Flory-Fox constant, given in eq. (3.55b),
N = the degree of polymerization,
M_o = the molecular weight of the monomer unit,
b = the length of the monomer unit,
λ = the number of monomers per persistence length a, i.e. $\lambda = \frac{1}{2}s$,
r_o = the hydrodynamic radius of the monomer unit. It should be mentioned that r_o cannot be related to the finite diameter of a short chain; r_o only characterizes a kind of friction factor.

The ratio N/λ equals the parameter $x = L/a$, used in eq. (3.3). The function $X(N/\lambda)$ describes the ratio of the mean square radius of gyration of the wormlike chain to that of an infinitely long Gaussian coil; it has separately been calculated by Eizner and Ptitsyn. The function $\varphi(\lambda,N)$ describes the intramolecular hydrodynamic interaction as a function of λ and N. It was tabulated by Kurath et al.[57].

Actually eq. (3.62) turns out to be a kind of modified Flory-Fox equation (3.55a), in which the non-Gaussian character of the end-to-end distribution of the stiff chain is taken into account. In the form pre-

sented, also this theory is only valid for theta solvents in which the excluded volume vanishes. For a graphic representation of the type of molecular weight dependence of the intrinsic viscosity obtained see the dashed line in Fig. 6.17. Equation (3.55a) would give a straight line in this double logarithmic plot.

Finally, the question remains in how far the above described models reflect the hydrodynamic behaviour of real macromolecules. In fact, it needs no discussion that all these models only very crudely approximate the real structure of a macromolecule. However, the essential idea of model building in rheology is probably not so much a realistic description but the development of equations containing a small number of measurable and readily interpretable constants[51], in order to provide a coupling of the experiments with theoretical quantities. In that case a model theory derives its value from the experiments. Only if a certain model gives a reasonable description of experimental results, it proves its value. Probably one will never succeed in comprising all properties of a real macromolecule in a single model. Therefore an experimentalist will choose the one which furnishes the best agreement with his special measurements. But he should not believe that his model describes all aspects of reality.

3.8 The stress-optical properties of model chains

3.8.1 The stress-optical law

It has been pointed out in section 2.4 that the stress-optical properties of very flexible polymers can be described by a stress-optical law. In this paragraph the theoretical backgrounds of this law will be discussed in further detail.

The stress-optical law for polymer solutions has been first formulated by Lodge[58]. It appears to be generally valid not only for dilute polymer solutions but also for higher concentrated systems up to polymer melts. Actually, the existence of a stress-optical law for permanent polymer networks, i.e. for rubber elastic solids, was already known since long[11].

The theoretical derivation of this stress-optical law starts with the assumption that for very flexible macromolecules of sufficient length the end-to-end distance obeys a Gaussian distribution, as described by the Kuhn-statistics[7]. Hydrodynamically such a molecule is considered as an elastic dumbbell, with a spring force constant determined by the statistical entropy force of a Gaussian coil, eq. (3.46). The contributions of such dumbbells to the stress tensor of a streaming solution are given by the eqs. (3.38 a-d) with N equal to unity and $\langle h_o^2 \rangle$ replacing b_o^2:

$$p_{ij} = -\nu\, kT\, \delta_{ij} + \nu \frac{3kT}{\langle h_o^2 \rangle} \langle r_i r_j \rangle \tag{3.63}$$

where δ_{ij} = the Kronecker delta,
r_i = the projection of the end-to-end vector of the dumbbell on the i-axis.

There exists an analogous expression for the mean polarizability tensor of a solution of Gaussian coils. This expression, derived by Kuhn and Grün[59], reads:

$$\nu\gamma_{ij} = \nu\langle\gamma_\perp\rangle\delta_{ij} + (3/5)[\nu(\alpha_1 - \alpha_2)/\langle h_o^2\rangle]\langle r_i r_j\rangle \tag{3.64}$$

where $\langle\gamma_\perp\rangle$ = a function depending on the mean square end-to-end distance, but not on the orientation of the coils,
$\alpha_1 - \alpha_2$ = the average difference of polarizabilities of the statistical random link with respect to the directions parallel and perpendicular to its extension.

For a solution at rest it is of particular interest that according to eq. (3.64) the mean polarizability difference $\gamma_{/\!/} - \gamma_\perp$ of the whole coil molecule with respect to directions parallel and perpendicular to its end-to-end distance is given by:

$$\gamma_{/\!/} - \gamma_\perp = (3/5)(\alpha_1 - \alpha_2) \tag{3.65}$$

A comparison of eqs. (3.63) and (3.64) shows that the deviatoric components of both tensors are proportional to each other[60]. As a consequence both tensors are coaxial. The proportionality factor reads:

$$(1/5)(\alpha_1 - \alpha_2/kT) \tag{3.66}$$

For a further derivation of the stress-optical coefficient, as given by eq. (2.16), one can proceed along the lines traced out by Kuhn and Grün[59]. The following relation for the stress-optical coefficient is obtained:

$$C = \frac{2\pi}{45} \frac{(n_s^2+2)^2}{n_s} \frac{\alpha_1-\alpha_2}{kT} \tag{3.67}$$

where n_s = the average refractive index of the solution.
For the above given derivation the form birefringence is left out of consideration.

It appears that C mainly depends on two quantities: the temperature and the anisotropy $\alpha_1 - \alpha_2$ of the statistical random link. Molecular weight, concentration and shear rate do not occur in eq. (3.67). As to the temperature dependence of C very little is known. For the very flexible polymers polystyrene and polyethylene, for instance, the temperature dependence of C is very small[31]. On the contrary there exists

a strong temperature dependence for cellulose tricarbanilate in benzophenone[61] and for poly(dimethyl siloxanes) in the melt[62]. The temperature dependence for cellulose tricarbanilate in a series of other solvents will extensively be discussed in a later chapter.

The anisotropy of the statistical random link is extremely sensitive to the length of the random link, the chemical structure of the chain and the degree and kind of solvatation of the chain[63]. A change of one of these quantities will lead to a change of the anisotropy, which can be observed as a change of the stress-optical coefficient. Especially the first two quantities are related to the conformation of the macromolecule. As a consequence it must be expected that very valuable information concerning conformational transitions of polymers can be deduced from the experimental values of the stress-optical coefficient. However, if a change of solvent composition is involved in such a conformational transition, change of solvatation may have a disturbing influence. Investigations done on atactic polystyrene[31] have shown that this influence can amount up to 30% of the value of the stress-optical coefficient of the melt. A correction method or a way to exclude this influence are not known, so that the preferent solvatation will cause an uncertainty in the interpretation of the experimental results.

3.8.2 Short stiff chain molecules

Solutions of relatively stiff or short chain molecules do not obey the stress-optical law. For these cases the value of the above called stress-optical coefficient appears to be dependent on the molecular weight of the polymer: it decreases with decreasing molecular weight. Moreover, a decrease is found for the measured value of the stress-optical coefficient with increasing shear rate. As a consequence, eq. (2.17) remains valid only in the limit of zero shear rate. As one cannot really speak of a stress-optical coefficient in those cases, sometimes another notation is used, derived from dilute solution theories:

$$[n]/[n]_o = \lim_{q \to 0} 2C \tag{3.68a}$$

where [n] = the Maxwell constant, defined by:

$$[n] = \lim_{\substack{q \to 0 \\ c \to 0}} (\Delta n - \Delta n_s)/qc\eta_s \tag{3.68b}$$

The validity of eq. (3.68a) can easily be verified by combining the eqs. (2.11), (2.12 a-b) and (2.17), using the fact that sin 2χ becomes equal to unity in the limit of zero shear rate.

The molecular weight dependence of the ratio of the Maxwell constant and the intrinsic viscosity was calculated first by Tsvetkov[64] for free draining wormlike chains. These calculations were improved by Gotlib and

Svetlov[65]. As the stress-optical coefficient has been shown to be independent of the draining of the Gaussian coil, these authors assumed that the same is also valid for short macromolecules.

For the calculation of the Maxwell constant the assumption is made that an assembly of flexible macromolecules with continuously changing configurations can be replaced at small shear rates by an assembly of molecules with "frozen" configurations, where the distribution over the different configurations is described by a weight function[66]. This was already earlier intuitively assumed by Kuhn et al.[67]. Brownian motion is taken into account only so far as rotary diffusion of the rigid configuration is concerned. In that case only the orientation of the macromolecules in the flow determines the hydrodynamic and optical properties of the solution. The diffusion equation for a rigid macromolecule with an arbitrary configuration is solved, using a first order approximation with respect to the shear rate. The obtained probability density for the orientation of the macromolecule gives the Maxwell constant for this molecule. Finally, the averaging over all possible configurations is carried out with the aid of the weight function. The intrinsic viscosity is calculated in the same way. As for higher shear rates also deformation effects would play a role, which can only be described by a second order approximation of the probability density, this theory is valid only in the limit of zero shear rate. This implies also that no extinction angles other than 45 degrees can be given.

The obtained result reads:

$$\frac{[n]}{[\eta]_o} = \frac{4\pi}{45} \frac{(n_s^2+2)^2}{n_s} \frac{1}{2} \frac{a\Delta\beta}{k\,T} \frac{x\cdot\phi_1(x)}{\phi_2(x)} \qquad (3.69)$$

where $\Delta\beta$ = the anisotropy of the polarizability per unit length of the wormlike chain,

$\frac{x\cdot\phi_1(x)}{\phi_2(x)}$ = a complicated function of $x = L/a$, given by Gotlib and Svetlov[65], which describes the dependence of $[n]/[\eta]_o$ on x.

As a matter of fact, eq. (3.69) gives a very good description of the dependence of $[n]/[\eta]_o$ on molecular weight[61]. Both, a change in stiffness of the macromolecule and a change of the chemical structure cause an alteration of the term $a\Delta\beta\ x\cdot\phi_1(x)/\phi_2(x)$, so that also the ratio $[n]/[\eta]_o$ is extremely sensitive to conformational transitions.

From section 3.2 we know that the results of the persistence-statistics and the Kuhn-statistics are identical in the limit of Gaussian coils. Hence one must expect that eq. (3.69) becomes identical with eq. (3.67) in the limit of very large x. This actually appears to be the case. To show this, one needs two results, viz. the limits of the function of x and of the optical factor. The first one reads:

$$\lim_{x\to\infty} \frac{x\cdot\phi_1(x)}{\phi_2(x)} = \frac{10}{3} \tag{3.70}$$

As to the second one, Gotlib[68] has derived that the average polarizability difference of a persistent chain in the coil limit is given by:

$$\gamma_{/\!/} - \gamma_{\perp} = a\Delta\beta \tag{3.71}$$

which according to eq. (3.65) is equal to $(3/5)(\alpha_1 - \alpha_2)$. Eq. (3.71) gives an important result. It means that the polarizability difference of a statistically coiled chain is equal to the polarizability difference of a rod with a length equal to the persistence length of the macromolecule. When eqs. (3.70) and (3.71) are inserted into eq. (3.69) and combined with eq. (3.68a), one obtains eq. (3.67), which once again demonstrates the equivalence of both statistical theories in the coil limit.

3.9 Some remarks on the coaxiality of the stress tensor and the refractive index ellipsoid

One of the main conditions for the validity of the stress-optical law is the coaxiality of the stress tensor and the refractive index ellipsoid. For a deformed rubber-like solid the coaxiality of both ellipsoids is taken for granted.

For the molecular theories, described in the foregoing, coaxiality is not self-evident any longer. For the elastic dumbbell model, which served as a model for the derivation of the stress-optical coefficient, the coaxiality appears to hold only in so far as the eqs. (3.63) and (3.64) are valid. The validity of these equations, however, is restricted to small disturbances of the equilibrium conditions. As will be seen in a later chapter, for larger deformations higher order terms occur which disturb the proportionality between the statistical restoring force and the optical anisotropy of a coil molecule. On adding the contributions of all oriented elastic dumbbells the coaxiality of both ellipsoids is then lost.

The RZ-model could be considered as an assembly of a great number of elastic dumbbells connected with each other. As a matter of fact, a conclusion about the optical properties of this model can only be made after the introduction of a certain kind of anisotropy in this model. This is usually done by endowing each spring, resp. dumbbell, with a polarizability tensor, equal to the polarizability tensor for a single elastic dumbbell, as given by eq. (3.64)[30]. It only remains to define the vector denoting the end-to-end distance of the single dumbbell ($\underline{r}$ in eq. (3.64)) in the configuration space, in which the lengths of the springs, resp. dumbbells, can be expressed. Also in that case the con-

tributions of the separate dumbbells to the stress tensor and the refractive index ellipsoid simply add up. As they are proportional to each other, the coaxiality of the macroscopic tensors is preserved. Therefore also for the RZ-model both ellipsoids are coaxial, provided that the deformation of the dumbbells is restricted. A decrease of the number N of the springs does not alter this aspect of the model. So also for finite N the extinction angle and the orientation angle of the stress tensor coincide, which clearly benefits to the value of the flow birefringence as a technique for the determination of the state of stress in solutions of flexible macromolecules.

Also for the HH-model one can define a polarizability tensor for the separate dumbbells in the same was as done for the RZ-model[33]. So also in this case the orientation of the refractive index ellipsoid depends on the orientation and deformation of the separate dumbbells. However, besides a contribution due to the orientation and deformation of the dumbbells, the stress tensor now also contains a contribution due to bending forces around the beads. As these forces are not assumed to influence the polarizability of the dumbbells, coaxiality does not exist any longer. The extinction angle and the orientation angle of the stress tensor will no longer coincide. As an illustration of the difference between both angles one can look at the calculations of Noda and Hearst[33]. These authors calculated the extinction angle as a function of β_N for several values of ΛN^2 in the limit of non-draining. In Table 3.1, column 4, the ratio of $[\cot 2\chi/\beta_N]$ is given for several values of ΛN^2. For the RZ-model the ratio of $[\cot 2\chi/\beta_N]$ was equal to the value of the reduced steady state shear compliance J_{eR}. In the HH-case there exists some difference between both quantities. Only for very large, resp. very small, values of ΛN^2 both are equal. Very large ΛN^2 corresponds to the RZ-case, very small ΛN^2 means that all dumbbells of a chain take exactly the same orientation in the flow and, moreover, have the same deformation. This means that the contributions to the stress tensor and the refractive index ellipsoid are only by a certain factor higher than the contributions of a single dumbbell. Also in that case one arrives at coaxiality, at least for low shear rates.

After what has been said in section 3.7 this coaxiality for the straight elastic pearl necklace is obviously the result of an imperfection of this model in describing the behaviour of stiff macromolecules, viz. its axial deformability. For a really rigid dumbbell J_{eR} would be equal to 3/5, while the corresponding optical quantity $[\cot 2\chi/\beta_N]$ equals one[53]. The same consideration applies to a straight rigid pearl necklace, which should be considered as a better approximation of a stiff rodlike macromolecule. Consequently, also for this model no coaxiality exists.

In this paragraph it has been shown that a certain degree of stiffness

in a model causes a disturbance of the coaxiality of the stress tensor and the refractive index ellipsoid. As a consequence, one must be careful in assuming coaxiality for non-coiled stiff macromolecules. As to the experimental part of this work, therefore, the optically measured quantity [cot $2\chi/\beta_N$] can only be identified with the hydrodynamic quantity J_{eR} if the investigated polymer clearly behaves like a Gaussian coil molecule.

3.10 Summary of the most important results

Because of the comprehensiveness of the foregoing it seems useful to summarize at this stage the most important theoretical results.

For solutions of very flexible polymers there exists a stress-optical law, describing the flow birefringence over a great range of concentrations and shear rates. For many polymers the stress-optical coefficient appears to be a constant dependent to some extent on the type of solvent, but independent of shear rate and, at the absence of form birefringence, also independent of molecular weight and concentration. One of the most important conditions for the validity of the stress-optical law is the coaxiality of the stress tensor and the refractive index ellipsoid. For macromolecules, possessing a certain degree of chain stiffness, this is usually not the case. In those cases only theoretical predictions can be made, valid in the limit of zero shear rate, where coaxiality is trivial.

On the basis of a number of model theories the dependence of the orientation angle χ', resp. the extinction angle χ, on shear rate has been studied. For small shear rates a linear relation is predicted between cot $2\chi'$, resp. cot 2χ, and the reduced shear rate β_N. For models whose overall dimensions do not obey Gaussian statistics the value of J_{eR} is increased with respect to its value for Gaussian coils. The same applies to the ratio of $[\cot 2\chi/\beta_N]_{opt}$, the optical equivalent of the hydrodynamic quantity J_{eR}. While for Gaussian coils both quantities can be identified (coaxiality) they show a small difference for models with a certain degree of chain stiffness.

It appears that all values of J_{eR} lie within a small range: 0.2 to 1.0. For the non draining case of the HH-model the value of J_{eR} increases only with a factor of 5, going from a completely flexible coil to a completely straight pearl necklace with only axial deformability. An increase of the draining of that model even reduces the effect. The highest value of $[\cot 2\chi/\beta_N]_{opt}$, reported in literature[69], amounts to 1.25 for a completely rigid prolate ellipsoid of infinite axial ratio. The conclusion can be drawn that the effects of varying chain stiffness will be comparatively small and, as will be seen in the next paragraph, will hardly be discernable due to the great influence of polydispersity.

3.11 Influence of polydispersity

According to assumption (i) in section 3.3 we have discussed only monodisperse systems so far. However, in practice it is very difficult if not impossible to obtain monodisperse polymer samples. As a matter of fact, the polydispersity has a tremendous influence on the extinction angle. In comparison with experiment, eq. (3.43) would predict much too small values of J_{eR}, if polydispersity were disregarded.

The influence of polydispersity was already described by Hermans[41] for the dumbbell model. It can be deduced, that eq. (3.43) reads for a polydisperse system:

$$\cot 2\chi' = J_{eR} \frac{\langle \beta_N^2 \rangle_n}{\langle \beta_N \rangle_n} \tag{3.72a}$$

where $\langle \ \rangle_n$ = the number average.
With the introduction of a polydispersity-factor p, where

$$p = \frac{\langle \beta_N^2 \rangle_n}{\langle \beta_N \rangle_n^2} \tag{3.73}$$

eq. (3.72a) reads:

$$\cot 2\chi' = p \, J_{eR} \langle \beta_N \rangle_n . \tag{3.72b}$$

The quantity $\langle \beta_N \rangle_n$ can directly be obtained from eqs. (3.45), if the number average molecular weight of the polymer is inserted. According to Peterlin[70] and Daum[71] the polydispersity-factor p can be calculated, if the molecular weight distribution and the exponent α in the Mark-Houwink relation are known for the polymer. As is well known, this relation reads $[\eta]_o = K M^{\alpha}$, where $0.5 \leqslant \alpha \leqslant 1.0$*. Using the latter relation one obtains:

$$p = \frac{\langle M^{2\alpha+2} \rangle_n}{\langle M^{\alpha+1} \rangle_n^2} \tag{3.74}$$

These complicated molecular weight averages can be calculated with the aid of an assumed molecular weight distribution. For example, Daum[71]

* In a consequent treatment only $\alpha = 0.5$ should be used, since this value holds for Gaussian statistics (in θ-solvents). However, as has been pointed out in literature[31], for a sharp fraction in a good solvent J_{eR} is scarcely greater than in a θ-solvent. It appears that the influence of the polydispersity depends on the quality of the solvent, just by virtue of exponent α, which is greater than 0.5 in a good solvent. The physical reason for this surprising result is that the averaging actually is carried out over the β_N-values, i.e. over the $[\eta]_o$'s of the molecular weight fractions. Only the ratio $(p_{11}-p_{22})/2p_{21}$ is unsensitive to α (see eq. (3.43)).

gave a relation for p, if the molecular weight distribution is of the Schultz-Zimm type. For this type of distributions one obtains:

$$\frac{\langle M\rangle_w}{\langle M\rangle_n} = \frac{z+2}{z+1} \tag{3.75}$$

where $\langle M\rangle_n$ and $\langle M\rangle_w$ are the number- and weight-average molecular weights, respectively, and z is an adjustable parameter. The corresponding relation for p reads:

$$p = \frac{z!\ (z+2+2\alpha)!}{(z+1+\alpha)!^2} \tag{3.76}$$

Peterlin and Munk[72] gave p-values for a series of chosen values of $\langle M\rangle_w/\langle M\rangle_n$ and α.

Literature

1. M.V. Volkenstein, Configurational Statistics of Polymeric Chains (High Polymers Vol. XVII) Interscience, New York (1963).
2. T.M. Birshtein, O.B. Ptitsyn, Conformations of Macromolecules (High Polymers Vol. XXII) Interscience, New York (1966).
3. P.J. Flory, Statistical Mechanics of Chain Molecules, Interscience, New York (1969).
4. W. Kuhn, H. Kuhn, Helv. Chim. Acta *28*, 1533 (1945); *29*, 71, 609, 830 (1946).
5. R. Cerf, J. Polymer Sci. *23*, 125 (1957); Adv. Polymer Sci. *1*, 382 (1959).
6. P.J. Flory, Principles of Polymer Chemistry, Cornell Univ. Press, Ithaca, New York (1953) p. 523.
7. W. Kuhn, Kolloid-Z. *68*, 2 (1934); *76*, 258 (1936).
8. E. Guth, H. Mark, Monatsh. Chem. *65*, 93 (1934).
9. B. Zimm, J. Polymer Sci. *16*, 245 (1955).
10. K. Nagai, J. Chem. Phys. *38*, 924 (1963).
11. L.R.G. Treloar, The Physics of Rubber Elasticity, 2nd ed., Clarendon Press, Oxford (1958).
12. O. Kratky, G. Porod, Rec. Trav. Chim. *68*, 1106 (1949).
13. M.C. Wang, G.E. Uhlenbeck, Revs. Modern Phys. *17*, 323 (1945).

14. S. Chandrasekhar, Revs. Modern Phys. *15*, 1 (1943).
15. Ref. (2), preface.
16. H.A. Kramers, J. Chem. Phys. *14*, 415 (1946); *16*, 565 (1948).
17. J.G. Kirkwood, R.M. Fuoss, J. Chem. Phys. *9*, 328 (1941).
18. J.G. Kirkwood, Rec. Trav. Chim. *68*, 649 (1949); J. Polymer Sci. *12*, 1 (1954).
19. J.G. Kirkwood, Macromolecules, Ed. P.L. Auer, Gordon and Breach, New York (1967).
20. H.J. Merk, Stochastische problemen in de lineaire constitutie theorie, Delft (1971).
21. H.J. Merk, On the derivation of the Fokker-Planck and Smoluchowski equations for deformable particles suspended in Newtonian fluids, Delft (1973).
22. N. Saito, I. Prigogine, discussion remarks to be found in Ref. 19, p. 31.
23. J.M. Burgers, Second Report on Viscosity and Plasticity of the Amsterdam Academy of Sciences, N.V. Noord-Hollandsche Uitgeversmij., Amsterdam (1938).
24. J.G. Kirkwood, J. Riseman, J. Chem. Phys. *16*, 565 (1948).
25. C.W. Oseen, Hydrodynamik Vol. I, Akademische Verlagsgesellschaft, Leipzig (1927).
26. R.A. Harris, J.E. Hearst, J. Chem. Phys. *44*, 2595 (1966).
27. J.G. Kirkwood, P.L. Auer, J. Chem. Phys. *19*, 281 (1951).
28. P.E. Rouse, J. Chem. Phys. *21*, 1272 (1953).
29. F. Bueche, J. Chem. Phys. *22*, 603 (1954).
30. B.H. Zimm, J. Chem. Phys. *24*, 269 (1956).
31. H. Janeschitz-Kriegl, Adv. Polymer Sci. *6*, 170 (1969).
32. J.E. Hearst, E. Beals, R.A. Harris, J. Chem. Phys. *48*, 5371 (1968).
33. I. Noda, J.E. Hearst, J. Chem. Phys. *54*, 2342 (1971).
34. A.S. Lodge, Yeen-jing Wu, Rheol. Acta *10*, 539 (1971).
35. N.W. Tschoegl, J. Chem. Phys. *44*, 4615 (1966).
36. A. Peterlin, J. Chem. Phys. *39*, 224 (1963).
37. W. Kuhn, H. Kuhn, Helv. Chim. Acta *26*, 1394 (1943).
38. C.W. Pyun, M. Fixman, J. Chem. Phys. *42*, 3838 (1965).
39. R. Ullman, J. Chem. Phys. *76*, 1755 (1972).
40. Yu.E. Svetlov, Vysokomolekul. Soedin. *13*, 521 (1971).
41. J.J. Hermans, Physica *10*, 777 (1943).
42. K. Osaki, Macromolecules *5*, 141 (1972).
43. G.B. Thurston, J.D. Morrison, Polymer *10*, 421 (1969).
44. A.S. Lodge, Yeen-jing Wu, Paper presented at the Society of Rheology's Winter Meeting, Salt Lake City, February (1971).
45. B.H. Zimm, G.M. Roe, L.F.J. Epstein, J. Chem. Phys. *24*, 279 (1956).
46. Ref. (6), p. 611.
47. N.W. Tschoegl, J. Chem. Phys. *39*, 149 (1963).
48. J.E. Hearst, J. Chem. Phys. *37*, 2547 (1962).
49. M. Fixman, J. Kovac, J. Chem. Phys. *58*, 1564 (1973).
50. R. Simha, J. Chem. Phys. *44*, 25 (1940).
51. R.B. Bird, H.R. Warner, D.C. Evans, Adv. Polymer Sci. *8*, 1 (1971).
52. H. Janeschitz-Kriegl, Rheol. Acta *5*, 78 (1966).
53. W. Kuhn, H. Kuhn, Helv. Chim. Acta *28*, 97 (1945).
54. T. Kotaka, J. Chem. Phys. *30*, 1566 (1959).
55. Yu.E. Eizner, O.B. Ptitsyn, Vysokomolekul. Soedin. *4*, 1725 (1962).
56. A. Peterlin, J. Polymer Sci. *5*, 470 (1950); J. Chem. Phys. *33*, 1799 (1960).
57. S.F. Kurath, Ch.A. Schmitt, J.J. Bachhuber, J. Polymer Sci. A *3*, 1825 (1965).
58. A.S. Lodge, Nature *176*, 838 (1955); Trans. Faraday Soc. *52*, 127 (1956).
59. W. Kuhn, F. Grün, Kolloid-Z. *101*, 248 (1942).
60. H. Janeschitz-Kriegl, Makromol. Chem. *40*, 140 (1960).
61. H. Janeschitz-Kriegl, W. Burchard, J. Polymer Sci. A2, *6*, 1953 (1968).
62. J.L.S. Wales, private communication.
63. E.V. Frisman, A.K. Dadivanyan, G.A. Dyuzhev, Dokl. Akad. Nauk SSSR *153*, 1062 (1963).
64. V.N. Tsvetkov, Vysokomolekul. Soedin. *4*, 894 (1962).
65. Yu.Ya. Gotlib, Yu.E. Svetlov, Dokl. Akad. Nauk SSSR *168*, 621 (1966); Ukr. Fiz. Zh. *12*, 331 (1967).
66. Yu.Ya. Gotlib, Yu.E. Svetlov, Vysokomolekul. Soedin. *8*, 1517 (1966).
67. W. Kuhn, H. Kuhn, P. Buchner, Ergeb. Exakt. Naturw. *25*, 1 (1951).
68. Yu.Ya. Gotlib, Vysokomolekul. Soedin. *6*, 389 (1964).
69. H.A. Scheraga, J.T. Edsall, J.O. Gadd, J. Chem. Phys. *19*, 1101 (1951).
70. A. Peterlin, J. Chem. Phys. *39*, 224 (1963).
71. U. Daum, J. Polymer Sci. A2, *6*, 141 (1968).
72. A. Peterlin, P. Munk, Physical Methods of Chemistry, Vol. I, part 3c, A. Weissberger and B. Rossiter Eds., Wiley, New York (1972) p. 271.

CHAPTER 4

EXPERIMENTAL ARRANGEMENTS

4.1 Materials

4.1.1 Poly(amide carboxylic acid)

For the investigations on the poly(amide carboxylic acid) (PACA) from pyromellitic anhydride and benzidine a sample was supplied by Dr. A. Horvath (Karlsruhe). Its weight average molecular weight $\langle M \rangle_w$ was 125,000, and its polydispersity index $\langle M \rangle_w / \langle M \rangle_n$ was 2.4.

The solvent N,N-dimethyl acetamide (DMA) (Fluka A.G.) was dried over KOH and P_2O_5, resp., and distilled in vacuo. The viscosity of the DMA was 0.8711×10^{-2} poise, its density 0.9317 g/cm^3, both at 30°C. Triethyl amine (TEA) (Fluka A.G.) was distilled from KOH in a nitrogen atmosphere.

The solutions were prepared by adding about half the required amount of DMA to a weighed portion of a 5%-solution of PACA in DMA. To this solution an amount of a solution of TEA in DMA was added. This amount depended on the required number of gramequivalents. Finally, DMA was suppleted until the right dilution was attained. At high concentrations of PACA (2×10^{-3} g/ml) and great amounts of TEA (5 g-equiv. and more) a precipitation occurred.

The refractive index increment of the PACA in DMA is 0.375 cm^3/g [1]. Normally such a high value results in a rather large form birefringence. This effect can be calculated as a contribution C_f to the stress-optical coefficient C [Eq.(5.3) of Janeschitz-Kriegl[2]]. Even for the unionized PACA, however, one obtains the rather small relative contribution:

$$C_f/C = 1.67 \times 10^{-2} \qquad (4.1)$$

when the value of C is taken from the measurements to be described. Due to the extraordinary large value of the anisotropy of the PACA-chain, this contribution is small enough to lie completely within the limits of accuracy of the flow birefringence measurements. Therefore it can be disregarded throughout the investigations.

The pure DMA does not show any measurable flow birefringence. This means that all formulas can be used without a correction for the solvent contribution to the flow birefringence.

4.1.2 Cellulose tricarbanilate

The investigations on cellulose tricarbanilate (CC) were done on a number of samples supplied by Prof. W. Burchard (Freiburg i. Br.). Only CC(Lonza) has been prepared in this laboratory from cellulose-2½-acetate

(Lonza), also supplied by Burchard.

The low molecular weight samples CC I and CC II were prepared by partial precipitation from acetone solutions with the aid of water. The CC(L 610) sample was directly prepared from bleached Linters cotton. The way in which CC III was prepared, is unknown.

Data on these samples are gathered in Table 4.1. The weight average molecular weights $\langle M \rangle_w$ were determined by light scattering from dioxane

Table 4.1

Data of the Cellulose tricarbanilate samples

Sample	$\langle M \rangle_w \times 10^{-3}$	$[\eta]_o$ (cm^3/g) 20°C Dioxane	$\langle M \rangle_w / \langle M \rangle_n$
CC I_3	14.1	13.7	-
CC I_4	14.0	13.4	-
CC I_5	15.1	13.0	-
CC I_7	15.1	11.3	-
CC I_9	12.8	10.8	-
CC I_{12}	8.2	9.1	-
CC II_2	3.1	5.35	-
CC (Lonza)	185	168	1.59
CC (L 610)	620	555	∿1.5
CC III	2180	-	<1.2

solutions. About the heterogeneity of the low molecular weight fractions no details are known. However, for such small degrees of polymerization (6 - 30) one cannot expect that a partial precipitation gives a narrow distribution. So the polydispersity indices may be rather high ($\geqslant 2$).

The solvents were prepared in the following ways. 1,4-Dioxane (UCB) was dried over $MgSO_4$ and distilled subsequently. Phenyl benzoate (Fluka A.G.) was recristallized from ethanol and thoroughly dried. Tri-o-cresyl phosphate (K&K Laboratories) was dried over $MgSO_4$ and distilled in high vacuo. A colourless product was obtained. Diphenylether (Fluka A.G.) was dried over $MgSO_4$ and distilled in vacuo. Also a colourless product was obtained.

All solvents, except dioxane, can be considered to be matching solvents, which means that the refractive index increment of CC in these solvents is nearly zero. In dioxane the refractive index increment of CC amounts to 0.156 cm^3/g at 20°C [3]. In the same was as done for PACA, the contribution of the form birefringence to the stress-optical coefficient can be calculated. One obtains for the sample CC(L 610) at 25°C:

$$C_f/C = 2.3 \times 10^{-2} \qquad (4.2)$$

when the value of C is taken from the measurements to be described. As a consequence, this contribution lies within the limits of accuracy again.

All solvents, except dioxane, show a measurable flow birefringence. This means that all measurements, done in those solvents, have to be corrected for the solvent contributions. As with all low molecular weight fluids, the birefringences increase exactly linearly with the shear rate. For the pure unmixed solvents the slopes of these lines are given in Table 4.2, column 5, for the temperatures at which measurements were carried out. In addition, in this table also the densities and the viscosities of the pure solvents are given.

Table 4.2

Data of the pure solvents for Cellulose tricarbanilate

Solvent	Temp. (°C)	Density (g/cm^3)	Viscosity x 10^2 (poise)	$\Delta n_s/q$ x 10^{11} (s)
Dioxane	25	1.0283	1.193	-
	35	1.0171	1.017	-
	50	0.9998	0.816	-
	60	0.9893	0.718	-
	75	0.9735	0.611	-
	90	0.9543	0.514	-
Phenylbenzoate	75	1.0893	2.699	1.137
	90	1.0766	1.982	0.843
	100	1.0682	1.693	0.733
Tri-o-cresyl phosphate	30	1.1523	60.208	10.1
	60	1.1284	14.019	3.67
	90	1.1051	5.839	1.31
Diphenylether	30	1.0666	3.219	0.633
	60	1.0411	1.764	0.322
	90	1.0152	1.124	0.211

4.2 Apparatus

4.2.1 The coaxial cylinder apparatus for the measurement of flow birefringence

The apparatus for the measurement of flow birefringence was designed by Janeschitz-Kriegl and Nauta at the Central Laboratory TNO, Delft. As it has been described extensively in literature[2,4], only a short description will be given in the present report.

Figure 4.1 gives a survey of the rotor unit. Pot and cover together form a container enclosing the essential parts of the unit. The whole

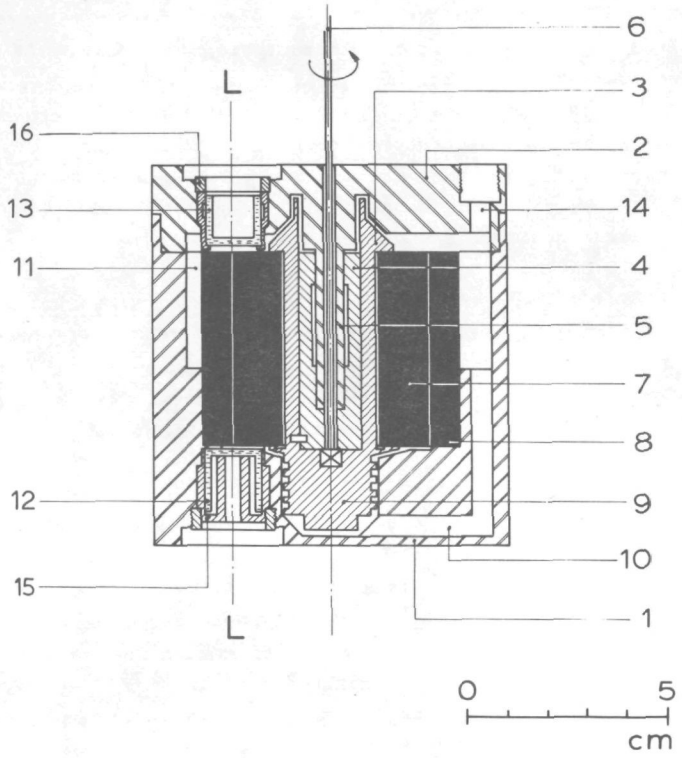

Fig. 4.1. Cross-section of the rotor unit. (1) pot, (2) cover, (3) rotor, (4) bronze bush, (5) axle, (6) driving shaft, (7) internal cylinder of black glass, (8) external (stationary) cylinder of black glass, (9) screw pump, (10) bore for fluid circulation, (11) chamber, (12) lower window, (13) upper window, (14) filling hole, (15) fitting lower window, (16) fitting upper window. LL, direction of the light-beam.

fits in a thermostat, which is not shown. All parts of the unit are made of stainless steel, except those for which the material is explicitely mentioned. The measuring cell consists of two concentric glass cylinders, of which the inner one (rotor) is driven (Couette flow). The width of the annular gap between the cylinders amounts to 0.25 mm, the height of the gap is 5 cm. For the chosen diameter of the rotor (5 cm) the ideal case of two infinite parallel plates, moving with regard to each other at constant speed, is quite well approximated. The curvature of the flow field can be neglected for the calculation of the shear rate. The speed of rotation of the driving unit can be continuously varied over a range of

3 decades. For the described apparatus this corresponds to shear rates between 10 and 10^4 (s^{-1}).

The light beam passes through the solution in a direction parallel to the cylinder axes. The maximum shear rate at which measurements are still possible is determined by the frictional heat produced in the fluid under shear. A radial temperature gradient in the gap of only a few tenths of a degree centigrade per millimeter will prevent the light-beam from passing directly through the fluid. The light-beam will be bent towards the region of lower temperature and reflected from the corresponding cylinder wall. As the reflection of a polarized light-beam from a metal wall causes a considerable phase difference, systematic errors would be introduced into the measurements. To suppress these effects the cylinders are made of black glass with a refractive index of 1.53. As a second useful property, glass has a low heat-conductivity. This enables us to prevent the formation of radial temperature gradients in the gap, as nearly no heat can flow to the wall. A slow convection stream is applied in axial direction with the aid of a screw pump, mounted at the lower side of the rotor. The maximum velocity gradient of the axial velocity profile amounts to one tenth of the velocity gradient of the main flow. The fluid describes a kind of helical flow-pattern. Due to this construction the fluid temperature will increase linearly from entrance to exit. However, this increase of temperature of at most a few degrees will hardly influence the measurements in most practical cases.

A very important feature is the construction of the windows. Both windows are cylindrical cuvettes made of one piece of glass, with a flat bottom which is polished on both sides. These windows have only a very small constant birefringence, caused by residual strains in the glass.

The lower window fits (with the bottom on the upper side) slidingly in a fitting. It rests with the inner side of its bottom on a rim mounted in the interior of the fitting (Fig. 4.1, position 15, inner cylinder). The sealing of the window is achieved by spreading a thin layer of highly viscous silicone oil on the internal rim. When the rotor unit is filled with fluid, this fluid penetrates between the fitting and the outer cylindrical surface of the window but encloses an air cushion, which prevents the fluid from reaching the mentioned silicone layer.

For the upper window the sealing is less critical. The cuvette fits, with the bottom downwards, slidingly in a fitting and rests on three small ledges. A thin oil layer on the upper side of the cuvette also prevents the window from leaking by enclosing an air cushion in a small chamber, cut in the wall of the fitting.

The above described construction of the windows enables us to carry out measurements at temperatures between 0°C and 160°C, without disturbances by leakage or parasitic birefringences in the windows due to changing internal stresses.

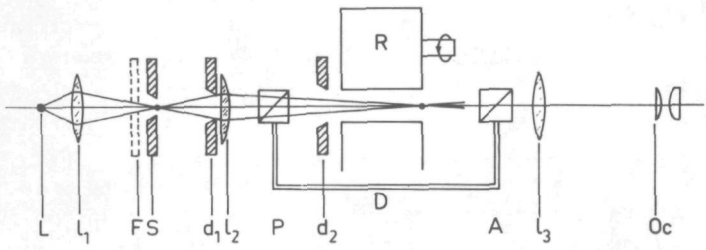

Fig. 4.2. Optical alignment of the apparatus.

Figure 4.2 gives a survey of the optical alignment of the apparatus. As a light source a high-pressure mercury arc is used. The spherical lens l_1 forms an image of the lamp L on a slit diaphragm S. The astigmatic lens l_2 forms an image of the slit at the place where the light-beam leaves the gap of the rotor unit R. The breadth of this image must be somewhat smaller than the gap width so that, from a point of view of classical optics, all light passes through the rotor unit without being reflected from the cylinder walls. In reality diffraction occurs between the cylinder walls of the rotor unit. With the aid of the spherical lens l_3 an image of the diffraction pattern is formed in a Ramsden ocular Oc. This diffraction pattern is confined in radial direction by the edges of the cylinders and in tangential direction by a diaphragm d_2 ($\emptyset$ = 2 mms). Besides a zero order maximum, due to the light passing through the rotor unit without reflection, also a number of higher order maxima can be observed, parallel to the zero order maximum. As only the zero order maximum can be extinguished between crossed nicols, this maximum is used for the measurements. If cylinders of black glass are used, the higher order maxima do not disturb the measurements because of their weak intensity. As polarizer and analyser Thompson-Glan prisms are used. If in the centre of the observed image the main directions of the crossed polarizer P and analyser A coincide with the main axes of the birefringent medium, a dark area should be observed, corresponding to one of the four arms of the "cross of isoclines". A distance of 2 millimeters (the diameter of d_2) along the circumference of the rotor corresponds to an angle of 5 degrees. Owing to the finite curvature of the cylinders the dark zone should therefore be much narrower than the mentioned 2 millimeters. In other words, the isocline should be embraced on both sides by bright areas.

By means of the use of the astigmatic lens l_2 a sharpening of the isocline is achieved; this lens produces a second image of slit S in the tangential plane. This image is far behind the exit from the gap. A simul-

taneous shift in the radial plane by simply using a weaker spherical lens on the place of l_2 would result in an unnecessary reduction of the light-flux. In this way the position of the isocline can be determined, down to a birefringence of 0.5×10^{-7}, with an accuracy of 0.1 degree by simultaneous rotation of the crossed polarizer and analyser, coupled by a rigid arm D.

The apparent parasitic birefringence in the windows and the polarizing prisms can be compensated with the aid of a weakly birefringent glass plate, mounted revolvably on the housing of the polarizer. This compensation method is extensively described by Janeschitz-Kriegl[6]. However, it must be said that the windows and polarizing prisms were of an extremely good quality, almost free of residual birefringences.

The apparatus is calibrated with dioctyl-phtalate, a low molecular weight fluid, which gives an extinction angle of 45 degrees at all shear rates.

The birefringence is measured by means of a compensation method. For the measurement of very small phase differences, up to $0.06 \times 2\pi$ radians, the method of de Sénarmont has been used, for greater phase differences the compensator of Ehringhaus (Fa. Zeiss) has been applied. The de Sénarmont compensation method requires green light, achieved by a green filter F, the Ehringhaus compensator can be used in white light.

4.2.2 Viscosity measurements

Viscosity measurements were carried out with ordinary Ubbelohde viscometers, while densities were determined with the aid of pycnometers. The temperatures of the thermostats in which the measurements were done, were constant within 0.05°C. It has been assumed that, for the low polymer concentrations used in this work, the influence of concentration on the density of the solvent could be neglected.

For several solutions the dependence of the viscosity on shear rate had to be measured. These measurements were done on an apparatus at the Central Laboratory TNO, Delft, described by Daum and Janeschitz-Kriegl[7] The principle of this apparatus which avoids drainage of fluid along any vessel wall, is based on a cylindrical chamber, in which a piston can be moved up and down with known speeds. In the piston a cylindrical capillary is mounted with known length and diameter. When the piston is moved, a certain amount of fluid passes through the capillary. With the aid of a sensitive detection method the pressure on the fluid can be measured. From the calibration constants the shear stress at the wall of the capillary is obtained as a function of the apparent shear rate. To obtain the true shear rate at the wall the well-known Rabinowitsch[8] correction has to be applied to these measurements. This correction reads:

$$q_w = D_s[(3/4) + (1/4)\ d \ln D_s/d \ln \tau_w] \qquad (4.3)$$

where q_w = the true shear rate at the wall of the capillary,
$D_s = 4Q/\pi R^3$ = the apparent shear rate,
$\tau_w = PR/2L$ = the shear stress at the wall of the capillary,
Q = the volumetric output rate,
R = the radius of the cross-section of the capillary,
L = the length of the capillary,
P = the pressure drop over the capillary.

In this way the viscosity as a function of the true shear rate is obtained as the ratio of τ_w and q_w.

Literature

1. A. Horvath, Thesis Karlsruhe (1970).
2. H. Janeschitz-Kriegl, Adv. Polymer Sci. *6*, 170 (1969).
3. W. Burchard, Makromol. Chem. *88*, 11 (1965).
4. H. Janeschitz-Kriegl, R. Nauta, J. Sci. Instr. *42*, 880 (1965).
5. E. van Kuik-van Meerten, H. Janeschitz-Kriegl, J. Sci. Instr. *39*, 301 (1962).
6. H. Janeschitz-Kriegl, Lab. Pract. *10*, 802 (1961).
7. U. Daum, H. Janeschitz-Kriegl, Rheol. Acta *7*, 349 (1968).
8. B. Rabinowitsch, Z. Phys. Chem. A *145*, 1 (1929).

CHAPTER 5

A COIL EXPANSION OF POLY(AMIDE CARBOXYLIC ACID) CAUSED BY IONIZATION

5.1 Results of flow birefringence measurements

The flow birefringence of a great number of solutions with various concentrations of poly(amide carboxylic acid) (PACA) in N,N-dimethyl acetamide (DMA) and with several amounts of triethyl amine (TEA) added was measured. All measurements were carried out at 30°C.

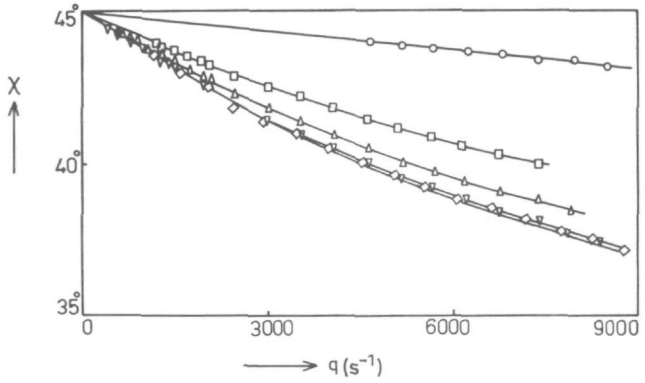

Fig. 5.1. Extinction angle against shear rate of a series of solutions of PACA in DMA with varying amounts of TEA added. Concentration of PACA: 0.3 x 10^{-3} g/ml. Amounts of TEA added, expressed in g-equiv. per COOH-group: (o) 0; (□) 1; (Δ) 2; (▽) 5; (◇) 15. Temperature of measurements: 30°C.

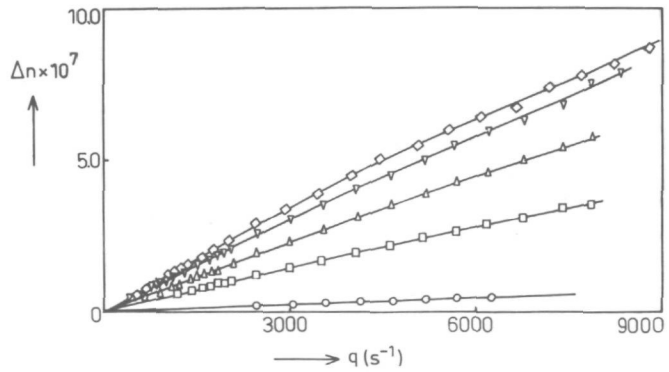

Fig. 5.2. Flow birefringence against shear rate for the solutions specified in the caption to Fig. 5.1.

Figure 5.1 gives an example for the type of extinction angle curves found. In this figure the number of g-equiv. TEA per carboxylgroup serves as a parameter. The concentration of the chosen solution is 0.3×10^{-3} g PACA per ml. The corresponding measurements of the birefringence Δn are given in Fig. 5.2.

It is observed that, with increasing amounts of TEA, the deviation of the extinction angle from 45° rapidly increases, while also the birefringence appreciably increases. For the unionized PACA (0 g-equiv. of TEA), however, the deviation of the extinction angle from 45° and the birefringence at low shear rates are so small, that reliable measurements are possible only at rather high shear rates.

In both figures a tendency to saturation can be observed with regard to the influence of large quantities of TEA. If only a small quantity of TEA is added, the relation between the measured birefringence and the shear rate is linear. If larger quantities of TEA are added, a downward curvature is noticed at high shear rates. This points to a deviation from the stress-optical law (eq. (2.17)).

As was pointed out in section 4.1.1, at high concentrations of PACA and great amounts of TEA a precipitation occurred. This can be observed on an anomalous extinction angle curve. Figure 5.3 gives the extinction angle curve for the solution with a PACA-concentration of 2×10^{-3} g/ml and 5 g-equiv. TEA added. A rapid decrease of the extinction angle is observed at small shear rates. As has been pointed out by v.d. Put et al.[1], this indicates that a rather small number of large particles or aggregates is formed in the solution. On the birefringence curve, Fig. 5.4, nothing particular can be observed. This is, as well, in accordance with the findings in ref. 1.

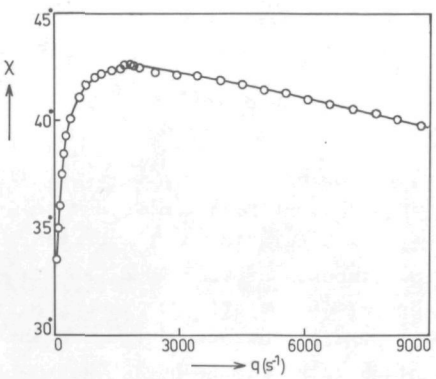

Fig. 5.3. Extinction angle against shear rate for a solution of PACA in DMA; concentration of PACA: 2.0×10^{-3} g/ml; 5 g-equiv. of TEA added.

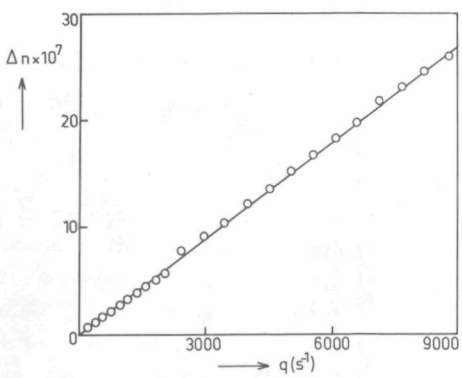

Fig. 5.4. Flow birefringence against shear rate for the same solution as in Fig. 5.3.

With the aid of eq. (2.17) stress-optical coefficients can be calculated from the measurements. The obtained values are given in Fig. 5.5 as functions of the number of g-equiv. TEA per COOH-group and with the concentrations of PACA as parameters. Since several solutions show deviations from the proportionality between birefringence and shear rate, all values are taken after extrapolation to zero shear rate.

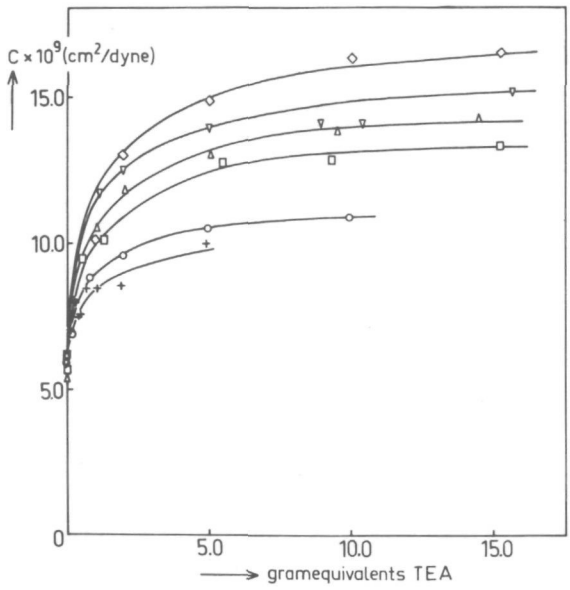

Fig. 5.5. Stress-optical coefficient C, calculated for all solutions, against number of g-equiv. TEA per COOH-group added. Concentrations in g PACA per ml are: (◇) 0.1 x 10^{-3}; (▽) 0.2 x 10^{-3}; (△) 0.3 x 10^{-3}; (□) 0.5 x 10^{-3}; (o) 1.0 x 10^{-3}; (+) 2.0 x 10^{-3}.

From an inspection of Fig. 5.5 the following facts can be deduced: On addition of TEA the stress-optical coefficient first shows a considerable increase. On the other hand, a clear saturation of the stress-optical coefficient is noticed at larger amounts of TEA added. An increase of the concentration of PACA suppresses the effect.

Figure 5.6 gives the same results, now as functions of the concentration of PACA and with the numbers of g-equiv. of TEA per COOH-group as parameters. One clearly observes that a decrease of the concentration of PACA results in an increase of the stress-optical coefficient.

The curves in Figs. 5.5 and 5.6 show a striking resemblance to the η_{sp}/c-curves of this PACA, as given in Figs. 5.7 and 5.8. These figures

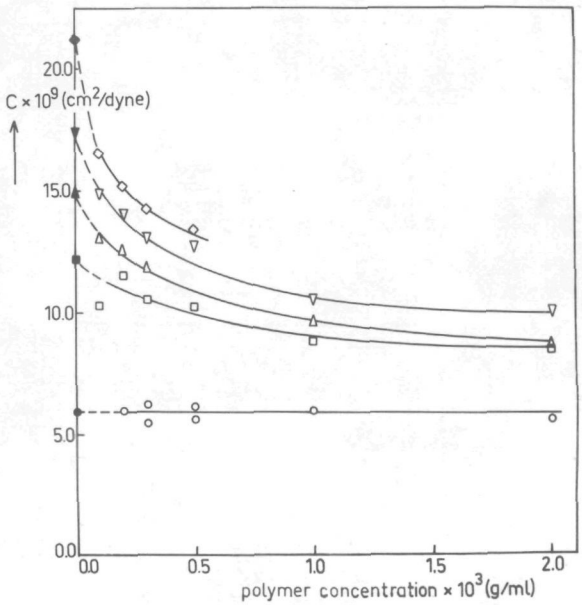

Fig. 5.6. Stress-optical coefficient C against concentration of PACA. Number of g-equiv. TEA per COOH-group added: symbols as in Fig. 5.1. Closed points: values of C extrapolated to zero concentration, according to eq. (5.2).

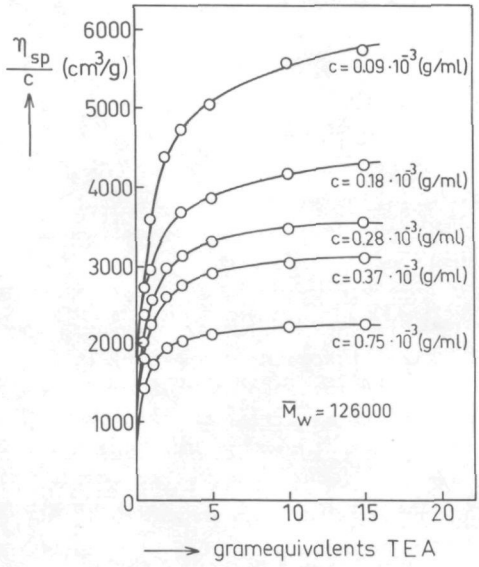

Fig. 5.7. η_{sp}/c against number of g-equiv. TEA per COOH-group added. Figure taken from the work of Horvath[2].

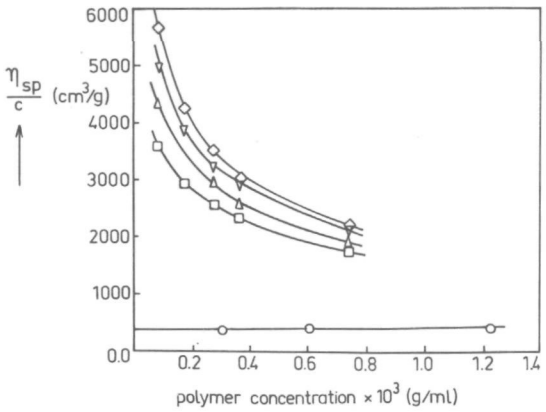

Fig. 5.8. η_{sp}/c against concentration of PACA, obtained from data in Fig. 5.7. Symbols as in Fig. 5.1.

are taken from Horvath and Vollmert[2,3]. A detailed discussion of this fact will be given in the next paragraph.

It should be noticed that the stress-optical coefficient of the unionized PACA (0 g-equiv. TEA) is independent of concentration. This is normally found for uncharged polymers of molecular weights high enough for the formation of Gaussian coils.

In Fig. 5.9 an example is given of the usefulness of the reduced shear rate $\langle\beta_N\rangle_n$. The points correspond to measurements at a variety of concentrations of PACA. About 5 g-equiv. of TEA per COOH-group are added to each solution. All points fall on the same line within the accuracy of these measurements: for the rather low concentrations of PACA, used in this investigation, the reduction with respect to these concentrations, according to eq. (3.45a), seems successful.

At the highest $\langle\beta_N\rangle_n$-values a slight deviation can be observed from the proportionality between cot 2χ and $\langle\beta_N\rangle_n$. This points, like the deviation from linearity in Fig. 5.2, to a deviation from the Gaussian behaviour of the chains. At lower $\langle\beta_N\rangle_n$-values, where the relation between cot 2χ and $\langle\beta_N\rangle_n$ is still linear, we can assume that the stress tensor and the refractive index ellipsoid of the solution are sufficiently coaxial that pJ_{eR} can be determined directly from these optical measurements as the ratio $[\cot 2\chi/\langle\beta_N\rangle_n]_{opt}$. The obtained values of pJ_{eR} are given in Fig. 5.10. This figure surveys the results of the entire investigation, as far as the extinction angle is concerned. Both, the concentration and the added amount of TEA, seem to have no significant influence on pJ_{eR}. The averaged value of pJ_{eR} amounts to 1.60.

The larger scatter, which is obtained when less TEA is added, is

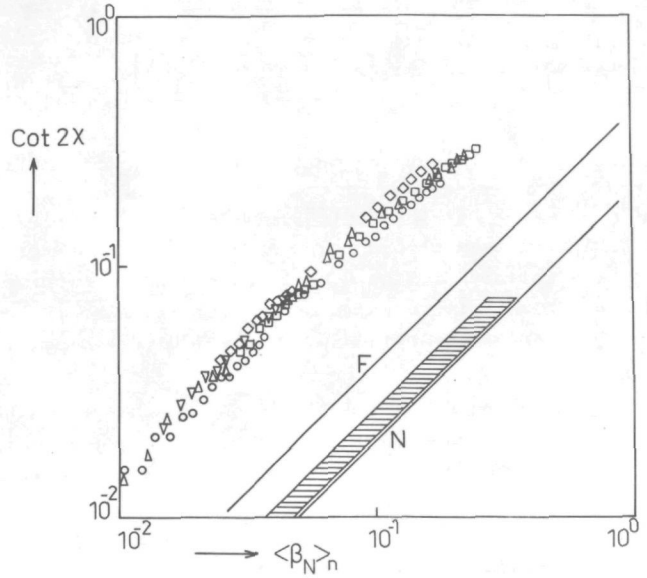

Fig. 5.9. Example of a reduction of the extinction angle χ with respect to concentration. Concentrations in g PACA per ml solution are: (◇) 0.1×10^{-3}; (▽) 0.2×10^{-3}; (△) 0.3×10^{-3}; (□) 0.5×10^{-3}; (o) 1.0×10^{-3}. To all solutions 5 g-equiv. of TEA per COOH-group are added. F = free-draining approximation; N = non-draining approximation. Shaded area: location of the measured points after a correction for polydispersity.

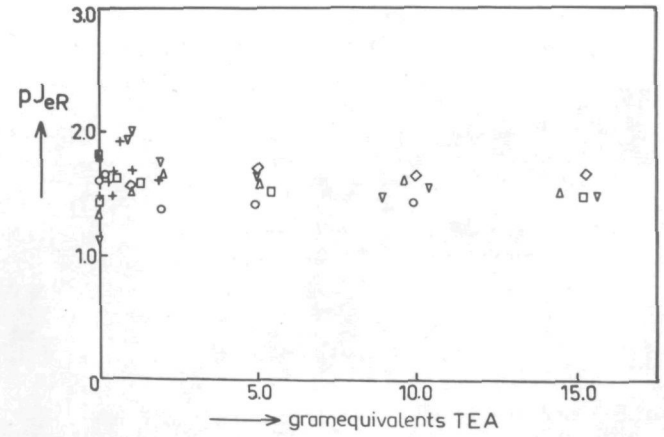

Fig. 5.10. Values of pJ_{eR} for all investigated solutions, as calculated from their extinction angle curves. The values are plotted against the number of g-equiv. TEA per COOH-group added. Symbols as in Fig. 5.5.

caused by the inaccuracy in measuring small deviations of the extinction angle from 45° (compare Fig. 5.1). Moreover, with these measurements also the birefringence is very small, making an accurate determination still more difficult.

5.2 The influence of coil expansion on the stress-optical coefficient

It is quite obvious that the increase of the stress-optical coefficient of the PACA must be ascribed to an expansion of the macromolecules. Especially the resemblance of Fig. 5.6 to the η_{sp}/c vs. c-curves characteristic for polyelectrolytes seems to prove this. Also the equilibrium character of the acid-base reaction is clearly manifested by the saturation effect in Fig. 5.5.

On the other hand, the unionized PACA shows no changes in the stress-optical coefficient, when the concentration of PACA is changed. From this fact the conclusion may be drawn that PACA in DMA is incapable of a spontaneous ionization. Admittedly, such an ionization will be detectable only at low concentrations. The question remains, whether at these concentrations changes in the stress-optical coefficient can be observed with a sufficient accuracy.

As is well known, quantitative conclusions about the coil expansion of polyelectrolytes cannot be drawn from viscosity measurements, as the results of these measurements cannot safely be extrapolated to zero concentration. As a matter of fact, the same is true for the stress-optical coefficient. Only when isoionic dilution, according to Pals and Hermans[4] is applied to viscosity measurements on polyelectrolytes, normal results are obtained, which can be extrapolated to zero concentration.

However, Fuoss and Strauss[5] found an empirical relation which seems to describe the dependence of η_{sp}/c on c at low polyelectrolyte concentrations with a reasonable accuracy. This Fuoss-Strauss relation reads:

$$(\eta_{sp}/c) = \frac{A}{1 + B \times (c)^{\frac{1}{2}}} \qquad (5.1)$$

where A and B are adjustable parameters. This equation has been extremely useful for many polyelectrolytes. In fact, Horvath and Vollmert[2,3] have shown that it can also be applied to the changes of the viscosity of the PACA-solutions.

Because of the resemblance of the curves in Fig. 5.6 to the η_{sp}/c vs. c-curves of this PACA (Fig. 5.8) a similar relation was tried for the dependence of the stress-optical coefficient on the concentration of the PACA[6]:

$$C = \frac{A'}{1 + B' \times (c)^{\frac{1}{2}}} \qquad (5.2)$$

When 1/C is plotted as a function of the square root of PACA concentration, a straight line should be obtained. This is demonstrated in Fig. 5.11 for several quantities of TEA added. Within the limits of accuracy a reasonable extrapolation to zero concentration can be carried out with the aid of eq. (5.2). The values of the stress-optical coefficient, extrapolated in this way, are given in Table 5.1, column 2. They are also shown in Fig. 5.6 as closed points at the ordinate axis.

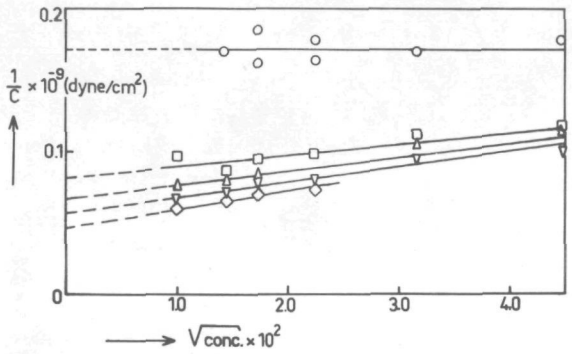

Fig. 5.11. Extrapolation of the stress-optical coefficient to zero concentration, according to eq. (5.2). Number of g-equiv. TEA per COOH-group added: symbols as in Fig. 5.1.

Table 5.1

Stress-optical coefficient and coil-expansion for several amounts of TEA added

TEA (g-equiv.)	$\lim_{\substack{q\to 0 \\ c\to 0}} C \times 10^9$ (cm^2/dyne)	$\frac{\langle h^2 \rangle}{\langle h_o^2 \rangle}$
0	5.9	1
1	12.2	2.1
2	14.9	2.5
5	17.4	2.9
10	19.6	3.3
15	21.2	3.6

At infinite dilution no mutual shielding of charges on separate macromolecules takes place. The coil expansion is then determined only by the charges on the same molecular chain.

The expansion of the molecular coil can be described by an increase of the mean square end-to-end distance of the coil with regard to the

unionized state[7,8]. For the expanded state Gaussian statistics may still be applied, if the expansion is not too large.

The charges on the molecular chain lead to a "long-range" repulsion, as well as to a "short-range" repulsion, which particularly influences the local chain-stiffness. Both effects together lead to an increase of the coil-dimensions. For a moderate expansion, we may apply a relation, which may be obtained from eqs. (3.64) and (3.65):

$$\gamma_{/\!/} - \gamma_{\perp} \sim \frac{\langle h^2 \rangle}{\langle h_o^2 \rangle} \tag{5.3}$$

where $\langle h_o^2 \rangle$ in this case means the mean square end-to-end distance in the undisturbed, i.e. uncharged, state and h is an arbitrarily chosen end-to-end distance. If an external couple of forces is applied to the end-points, an averaging over the square of this end-to-end distance seems reasonable. In this way the action of the electrostatic repulsion forces is rudely taken into account. Admittedly, this procedure is equivalent to the introduction of an effective statistical random link which increases in length with the degree of ionization.

From eqs. (5.3), (3.65) and (3.67) it can be concluded that an expansion of the coil must result in an increase of the stress-optical coefficient C. The more the coil expands, the more C increases.

On the other hand, the anisotropy $\gamma_{/\!/} - \gamma_{\perp}$ of the macromolecule will also be influenced by a change of the chemical structure of the macromolecule, as caused by the ionization of the chain. This means that, in principle, the changes in the stress-optical coefficient must be ascribed to several effects.

However, the COOH-groups on our PACA-molecule are located opposite to each other on the aromatic rings in the chain. The charges, introduced by ionization, are uniformly distributed along the molecular chain. Therefore it seems probable that the anisotropy per unit length of the PACA-chain will hardly be changed by the ionization. This makes the assumption plausible that the increase of the stress-optical coefficient is mainly caused by the expansion of the macromolecular coil.

In that case the degree of expansion, expressed as an increase of the mean square end-to-end distance, can be calculated with the aid of eqs. (3.67) and (5.3). The results of this calculation are given in Table 5.1, column 3.

Another way of interpretation is found by a look on Fig. 5.12. In this figure the stress-optical coefficient, as extrapolated to zero concentration, is plotted on a double logarithmic scale versus the intrinsic viscosity, measured at corresponding degrees of ionization[2,3]. If the above made assumption with respect to the usefulness of the stress-optical coefficient as a measure of coil expansion is correct, one should

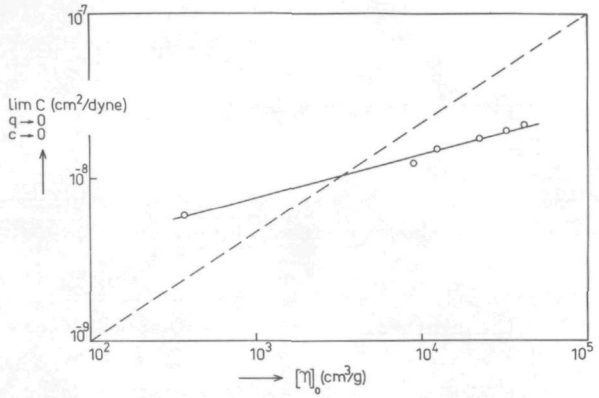

Fig. 5.12. Stress-optical coefficient C, extrapolated to zero concentration, against intrinsic viscosity $[\eta]_o$, at various degrees of ionization. Dashed line: slope 2/3.

obtain a curve of slope 2/3, since the intrinsic viscosity should be proportional to the 3/2th power of the mean square end-to-end distance of the coiled molecule, eq. (3.55a).

In Fig. 5.12 a dashed line of slope 2/3 is drawn for comparison. From this figure it becomes clear, however, that the growth of the stress-optical coefficient with increasing degree of ionization is considerably slower than would be expected from the corresponding growth of the intrinsic viscosity. More detail should probably not be deduced from this figure because of the limited reliability of the extrapolation methods. The interpretation of the just mentioned fact may probably be that the difference of main polarizabilities $\gamma_{/\!/} - \gamma_{\perp}$ of the chain is more sensitive to the local stiffening of the chain than to the expansion by long range interaction forces, whereas the intrinsic viscosity is influenced by both effects more equally. This interpretation should, nevertheless, be considered with some extra reserve as we do not know the influence of the growing number of charges on the polarizabilities.

5.3 Hydrodynamic properties of the PACA-molecules

For a discussion of the hydrodynamic properties of the PACA-molecules Fig. 5.9 is considered. Except for the highest $\langle\beta_N\rangle_n$-values, where a slight downward tendency can be observed, the linear relation between cot 2χ and $\langle\beta_N\rangle_n$, as postulated by eq. (3.43), is obeyed by this polymer. This means that the macromolecules behave hydrodynamically as flexible coils.

For a comparison of these measurements with the results of the Rouse-Zimm treatment of the "bead-spring" model, as given in Chapt. 3, two

theoretical lines are also given in Fig. 5.9. The upper line, denoted by F, stands for the free-draining approximation, the lower one, designated by N, for the non-draining case.

However, all experimental points lie far outside the theoretical expected area between the F- and N-line. From the experience with other polymers one may expect that this deviation is mainly caused by the polydispersity of the polymer sample. In order to confirm this assumption, Peterlin's method, which was explained in section 3.11, is applied to the experimental results.

As is well-known, a polycondensation reaction, like the one which takes place during the synthesis of this PACA, actually gives rise to a molecular weight distribution of the Schultz-Zimm type. A polydispersity index of 2.4 as found for this PACA corresponds to a value of -0.286 for the adjustable parameter z in eq. (3.75).

Unfortunately, Horvath and Vollmert[2,3] only give the Mark-Houwink equation at 25°C for the unionized PACA in DMA containing LiBr:

$$[\eta]_o = 3.40 \cdot 10^{-2} \times \langle M \rangle_w^{0.78} \tag{5.4}$$

A few measurements in pure DMA give higher values for the intrinsic viscosity of the PACA as a function of $\langle M \rangle_w$. The exponent in the Mark-Houwink equation, however, does not seem to be changed. The difference of 5°C between the temperatures at which the measurements of Horvath and Vollmert and the present measurements were carried out, seems of minor importance. Thus, a value of 0.78 is used for the constant α which occurs in eq. (3.76). In this way one obtains for the polydispersity factor p a value:

$$p = 6.25 \tag{5.5}$$

Using the average value for $pJ_{eR} = 1.60$, as derived from Fig. 5.10, one finally obtains for J_{eR} the value:

$$J_{eR} = 0.25 \tag{5.6}$$

This value actually lies between the free-draining and the non-draining limits of Rouse and Zimm, as was found earlier for many uncharged molecules. In Fig. 5.9 the location of the measurements, corrected for polydispersity, is indicated by a shaded area.

5.4 Conclusions

From the foregoing the following conclusions can be drawn. The value of the stress-optical coefficient appears to be very much influenced by an ionization of the molecule. Due to the high anisotropy of this PACA, even semi-quantitative conclusions can be drawn with respect to the de-

gree of expansion. This will be impossible, however, for most of the more conventional polyelectrolytes in aqueous solution, because of the rather low optical anisotropy of these polymers.

The hydrodynamic behaviour of the expanded chain does not deviate from that of an uncharged polymer (Fig. 5.10). No influence of the ionization on J_{eR} can be observed. According to the linear theory, described in chapter 3, this should mean, that both the charged and uncharged PACA-molecules are flexible enough to form Gaussian coils. In that case low values of J_{eR} are expected, according to the Rouse-Zimm theory. These low values of J_{eR} are indeed obtained. This gives also a justification of the use of eq. (5.3) for the calculation of the coil expansion.

From the exact value of J_{eR} obtained, one can conclude that both the charged and the uncharged chains behave like molecular coils, in which the solvent is non-draining. This conclusion agrees pretty well with the opinion expressed by Vollmert and Horvath[9] that the PACA-molecules must be highly solvated in DMA.

Literature

1. A.G. v.d. Put, A. Ghijsels, H. Janeschitz-Kriegl, Monatsh. f. Chemie *103*, 1138 (1972).
2. A. Horvath, Thesis Karlsruhe (1970).
3. A. Horvath, B. Vollmert, Angew. Makromol. Chem. *23*, 141 (1972).
4. D.T.F. Pals, J.J. Hermans, J. Polymer Sci. *5*, 733 (1950).
5. R.M. Fuoss, U.P. Strauss, J. Polymer Sci. *3*, 602 (1948).
6. J.W.M. Noordermeer, H. Janeschitz-Kriegl, A. Horvath, Polymer *14*, 178 (1973).
7. W. Kuhn, O. Künzle, A. Katchalski, Helv. Chim. Acta *31*, 1994 (1948).
8. H. Morawetz, Macromolecules in Solution (High Polymers Vol. XXI) Interscience, New York (1965), Chapter VII.
9. B. Vollmert, A. Horvath, Angew. Makromol. Chem. *23*, 117 (1972).

CHAPTER 6

THE INFLUENCE OF HYDROGEN BONDS ON THE CHAIN STIFFNESS OF CELLULOSE TRICARBANILATE

6.1 Results of flow birefringence and viscosity measurements

On starting this part of the investigation, the flow birefringence of a great number of solutions of the sample CC(L 610) was measured. Mixtures of esters and ethers were used as solvents, their compositions varying from pure ester to pure ether. The compositions of the solvents will be expressed in weight percentages. The following two combinations of solvents will be discussed:

a) Phenyl ester of Benzoic Acid (PhB) - Dioxane,

b) Tri-o-cresyl Phosphate (TOCPh) - Diphenyl Ether (DPhE).

The measurements were carried out at several temperatures.

Figure 6.1 gives the extinction angle curves for solutions of CC(L 610) in dioxane, with concentrations varying from 0.2×10^{-2} to 0.8×10^{-2} g/ml. These measurements were carried out at a temperature of 25°C. The corresponding measurements of the birefringence are given in Fig. 6.2. It is observed that the relation between the measured birefringence and the shear rate is linear only for the lowest concentration (0.2×10^{-2} g/ml). At higher concentrations the birefringence increases less than linearly with the shear rate.

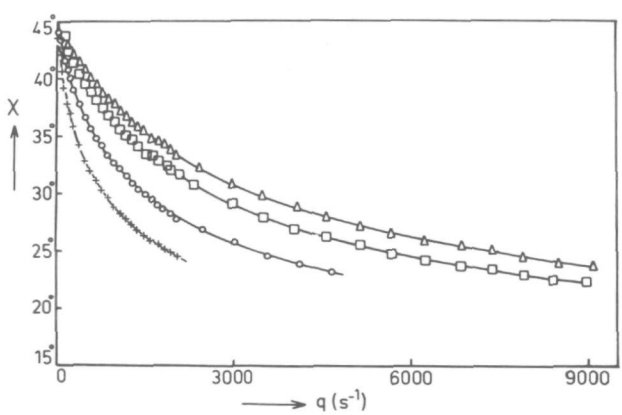

Fig. 6.1. Extinction angle against shear rate for a series of solutions of CC(L 610) in dioxane at 25°C. Concentrations of CC(L 610) expressed in g/ml: (Δ) 0.2×10^{-2}; (□) 0.3×10^{-2}; (o) 0.5×10^{-2}; (+) 0.8×10^{-2}.

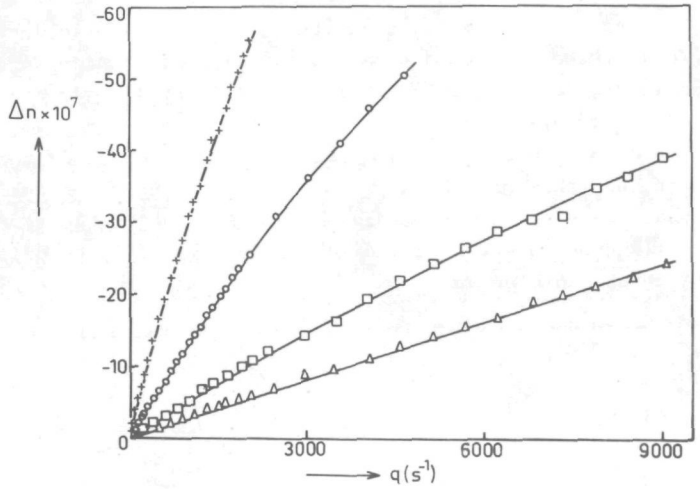

Fig. 6.2. Flow birefringence against shear rate for the solutions specified in the caption to Fig. 6.1.

An example for the influence of temperature on the extinction angle curves is given in Fig. 6.3. The results given in this figure were obtained from measurements on a 0.564% (w/v)-solution of CC(L 610) in TOCPh at the indicated temperatures. A comparison of Figs. 6.1 and 6.3 shows that the temperature has a much greater influence on the extinction angle curves than the concentration of the solutions.

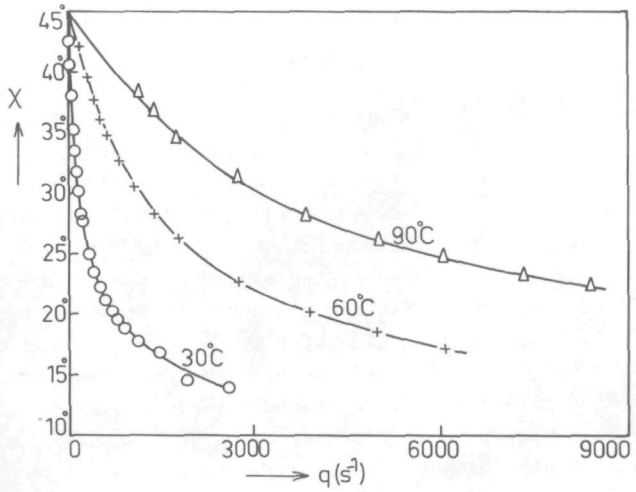

Fig. 6.3. Extinction angle curves for a solution of CC(L 610) in TOCPh at different temperatures. Concentration: 0.564 x 10^{-2} g/ml.

Due to the high molecular weight of the sample CC(L 610) the extinction angle curves deviate considerably from 45 degrees. With decreasing molecular weight, the deviation from the 45° angle decreases rapidly, as can be seen in Fig. 6.4. In this figure the extinction angle curves are given for a 1.3% (w/v)-solution of the sample CC(Lonza) in pure PhB at 75° and 90°C. As quoted in Table 4.1, the molecular weight of this sample is much lower than that of the sample CC(L 610). In this connection it is important that the viscosities of dioxane and PhB are of the same order of magnitude (see Table 4.2). So they cannot account for the difference in the extinction angle curves.

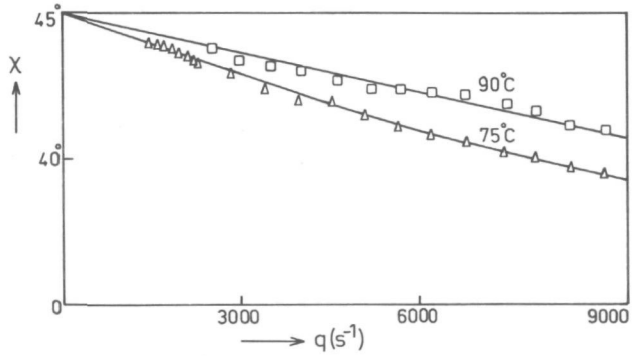

Fig. 6.4. Extinction angle curves for a solution of CC(Lonza) in PhB at different temperatures. Concentration: 1.32 x 10^{-2} g/ml.

With the aid of eq. (2.17) the values of the stress-optical coefficient can be calculated from these measurements. As was pointed out in section 4.1.2, all measurements, except those made in pure dioxane, had to be corrected for the solvent contribution to the flow birefringence. Furthermore, only the Newtonian viscosities of the solutions, as measured with the aid of Ubbelohde viscometers, were used for these calculations. As will be shown in chapter 8, Ubbelohde measurements are nearly always in fair agreement with the Newtonian viscosities at low shear rates for the sample CC(L 610). For the moment, we are only interested in the linear behaviour of this polymer: the values of the apparent stress-optical coefficients, as calculated with the aid of these Newtonian viscosities, yield the correct value of C by an extrapolation to zero shear rate. In Fig. 6.5 a few examples are given of the obtained results. In this figure the values are given of the stress-optical coefficients for the sample CC(L 610) in pure dioxane, resp. pure PhB, as functions of polymer concentration and with the temperature as a parameter. In both solvents no significant influence of concentration on the results is observed. A relative scatter of about 10% is quite normal for this sort of

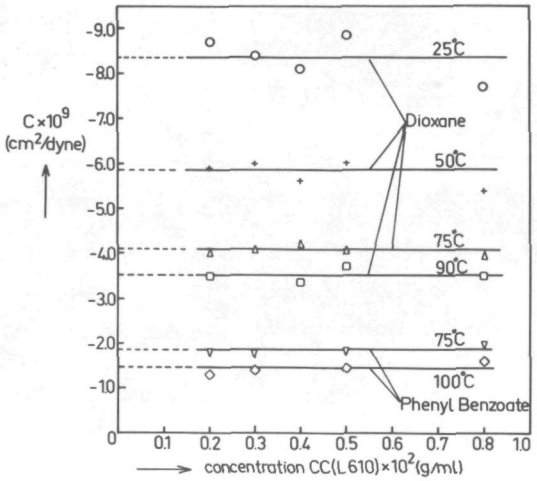

Fig. 6.5. Stress-optical coefficient C, extrapolated to zero shear rate, against concentration for solutions of CC(L 610) in dioxane and PhB. Temperatures are given in the figure.

measurements. This concentration-independence was found for all the measurements with all different CC-samples in all kinds of solvents. The significance of this fact for the interpretation will be discussed in the next paragraph. In this respect the behaviour of CC does not differ from that of other polymers.

On the other hand, the stress-optical coefficient of CC(L 610) strongly depends on temperature in both solvents. It decreases strongly with an increase of temperature. This is quite a striking result, because up till now no other polymer is known to have a stress-optical coefficient, which is so strongly temperature dependent. The largest changes of the stress-optical coefficient of CC(L 610) were found in a mixture of TOCPh - DPhE 25/75. The stress-optical coefficient of CC(L 610) decreases in the mentioned solvent mixture from a value of -33×10^{-9} cm²/dyne at 30°C to -13.3×10^{-9} cm²/dyne at 120°C.

The stress-optical coefficient of CC(L 610) in dioxane appears to be considerably larger than in PhB at corresponding temperatures. To investigate this difference in more detail, the values of the stress-optical coefficient have been determined for CC(L 610) in a series of mixtures of both solvents. The results, given in Fig. 6.6, are averages of the values obtained on at least two concentrations. No systematic concentration dependence was found in any case. PhB melts at about 70°C. As a consequence, on the ester side no measurements could be carried out at low temperatures. In Fig. 6.6 a clear transition can be observed, which

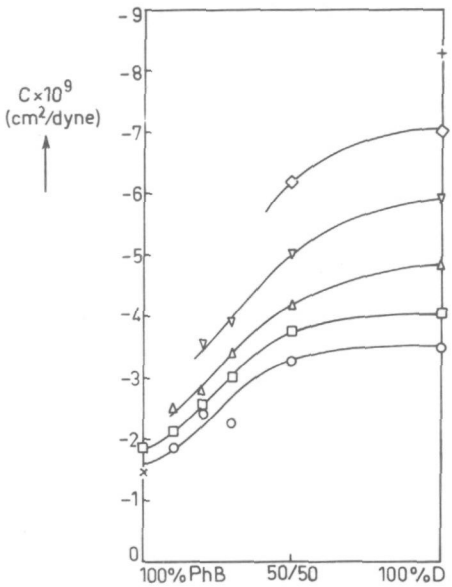

Fig. 6.6. Stress-optical coefficient C, extrapolated to zero shear rate, for CC(L 610) in solvent mixtures PhB - dioxane. Temperatures: (+) 25°C; (◇) 35°C; (▽) 50°C; (△) 60°C; (□) 75°C; (o) 90°C; (x) 100°C.

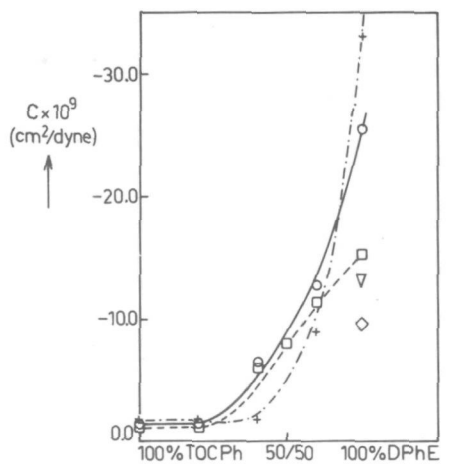

Fig. 6.7. Stress-optical coefficient C, extrapolated to zero shear rate, for CC(L 610) in solvent mixtures TOCPh - DPhE. Concentrations: 0.5 x 10^{-2} g/ml. Temperatures: (+) 30°C; (o) 60°C; (□) 90°C; (▽) 120°C; (◇) 135°C.

almost entirely takes place in the range of high PhB-contents of the solvent.

A similar transition of the stress-optical coefficient was found for CC(L 610) in mixtures of TOCPh and DPhE, which is shown in Fig. 6.7. However, CC dissolves in DPhE only at high temperatures, so that the flow birefringence in pure DPhE could not be measured at the given temperatures. The measurements, reproduced in Fig. 6.7, were made only on solutions with a concentration of 0.5×10^{-2} g/ml. Measurements at other concentrations were not carried out in these solvent mixtures, in view of the high price of the TOCPh and practical difficulties in preparing good solutions. As a matter of fact, the measurements in the solvent mixture PhB - dioxane are much more accurate. Nevertheless, an increase of the stress-optical coefficient is observed as well on changing from ester to ether. The effect is even considerably greater in mixtures of TOCPh and DPhE. Another striking feature is that, at 30°C, the transition occurs at a higher content of DPhE than with the other temperatures, whereas in the solvent mixture PhB - dioxane no influence of temperature on the transition region could be observed.

A further confirmation of the presence of a transition is obtained from the change of the intrinsic viscosity of CC(L 610) with composition of the solvent mixture PhB - dioxane. The values of the intrinsic viscosity, as measured at the same temperatures at which also flow birefringence measurements were carried out, are given in Fig. 6.8. A comparison with Fig. 6.6 shows that both transitions occur at about the same solvent composition. However, the total effect, as observed on the

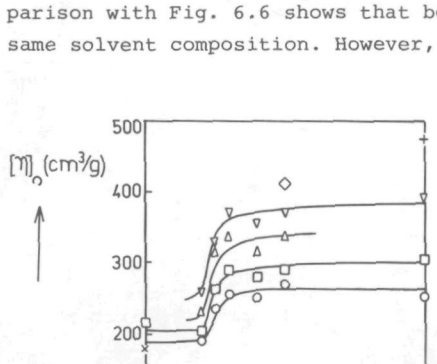

Fig. 6.8. Intrinsic viscosity of CC(L 610) in solvent mixtures PhB - dioxane. Symbols as in Fig. 6.6.

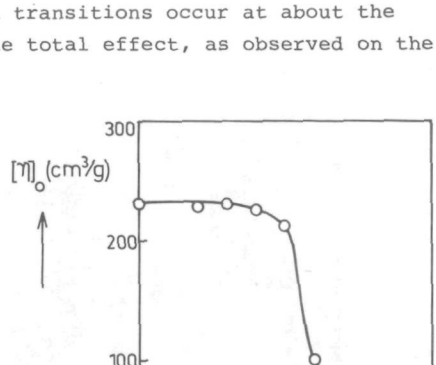

Fig. 6.9. Intrinsic viscosity of CC(L 610) in solvent mixtures TOCPh - DPhE. Temperature 30°C.

intrinsic viscosity, appears to be much smaller than on the stress-optical coefficient, although the transition in the intrinsic viscosity is much sharper.

In Fig. 6.9 the intrinsic viscosity of CC(L 610) is shown as a function of solvent composition for mixtures of TOCPh - DPhE at 30°C. This figure shows a remarkable result, as the change of the intrinsic viscosity is just opposite to that of the stress-optical coefficient. One may incline to interpret this in terms of the formation of aggregates or a precipitation of the polymer. However, this should have influenced the extinction angle curve (compare Fig. 5.3). In contrast to this figure, no abnormalities are shown by the extinction angle curves of a solution, containing 0.5 x 10^{-2} g/ml of CC(L 610) in a mixture of TOCPh - DPhE 25/75. This seems to indicate that the CC(L 610) is still completely dissolved. Yet, these results on the TOCPh - DPhE mixtures should be considered with some reserve.

The above mentioned results seem to confirm Burchard's supposition[1], viz. that a stiffening of CC occurs on changing the solvent composition from pure ester to pure ether. To study this stiffening somewhat more quantitatively, the dependence of the stress-optical coefficient of CC on molecular weight has been determined. For these measurements also the other CC-samples, mentioned in Table 4.1, were used. In Fig. 6.10 stress-optical coefficients, as obtained in pure PhB and pure dioxane,

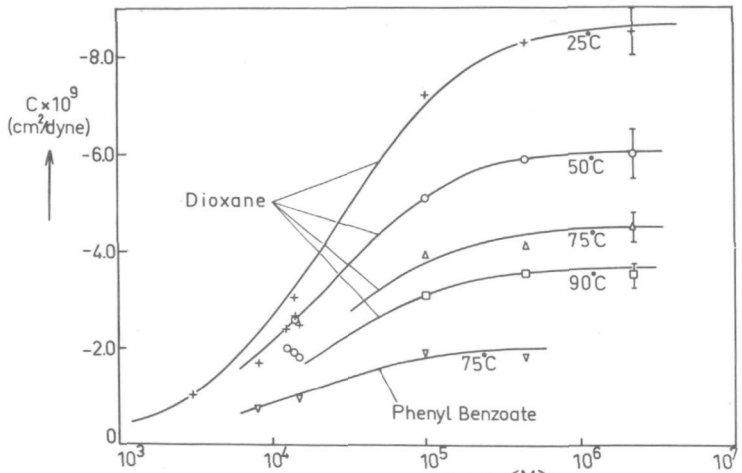

Fig. 6.10. Plot of the values of the stress-optical coefficient C against molecular weight for a series of samples of CC in dioxane and PhB, at different temperatures. The full lines are theoretical curves according to the theory of Gotlib and Svetlov.

are given as functions of the estimated number average molecular weights of the samples. For the samples with weight average molecular weights between 3000 and 15000 only these molecular weight averages were known. As a consequence, for these samples results are plotted against the weight average molecular weights. Most C-values are averages of measurements on at least two concentrations. Of the high molecular weight sample CC III unfortunately only a small quantity was available, so that measurements could be carried out at only one concentration. The non-Newtonian behaviour of the viscosity of the solution, which is expected to be pronounced for this sample, could not be measured either. As even Ubbelohde measurements are expected to lie in the non-Newtonian region of shear rates, no exact values of the stress-optical coefficient could be determined. Shear rates in the Ubbelohde viscometers have been estimated for this solution on the only approximately valid assumption of a parabolic flow profile. The stress-optical coefficients, however, as calculated from the flow birefringence measurements at those shear rates, can at the expected imperfect flexibility of the chain only be lower than the true stress-optical coefficients, as defined for zero shear rate. On the other hand, an extrapolation of the flow birefringence measurements to zero shear rate with the aid of the mentioned non-New-

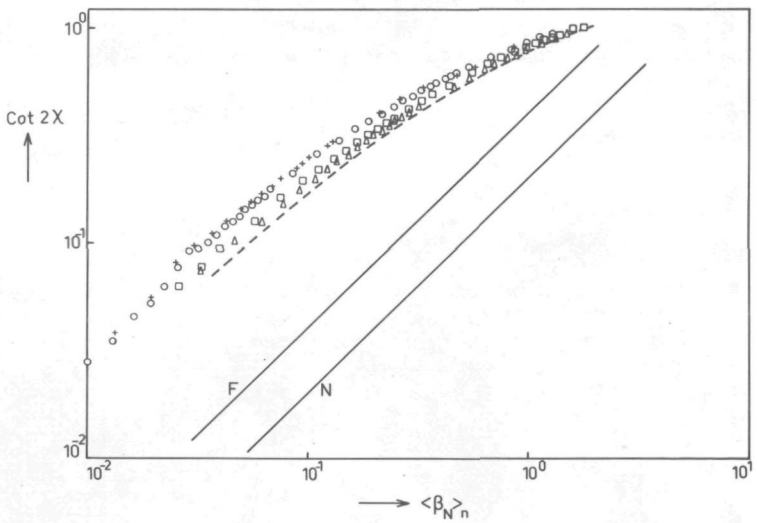

Fig. 6.11. Example of the poor reduction of the extinction angle curves with respect to concentration for CC(L 610) in dioxane at 25°C. Concentrations: symbols as in Fig. 6.1.(-----): curve extrapolated to zero concentration. F = free-draining approximation for Gaussian coils; N = non-draining approximation.

tonian viscosities must give too high values of the stress-optical coefficient. Both limits are given in Fig. 6.10 by the end-points of the vertical lines. As the best approximations for the true zero shear values of the stress-optical coefficient the averages of both limits have been taken, given by the places of the symbols.

In Fig. 6.11 an example is given for the reduction of the extinction angle curves with respect to concentration with the aid of the reduced shear rate $\langle\beta_N\rangle_n$. The points correspond to the measurements reproduced in Fig. 6.1. It is clearly observed that the curves show an upwards shift with increasing concentration. The reduction of the measured extinction angle curves with respect to concentration is not successful. This was found earlier for anionic polystyrenes by Daum[2] and Janeschitz-Kriegl[3]. Furthermore, a clear curvature can be observed for all concentrations at high $\langle\beta_N\rangle_n$-values. Only for the lowest $\langle\beta_N\rangle_n$-values a linear relationship between cot 2χ and β_N, as predicted by theory, seems to hold. This means that CC(L 610) shows a linear behaviour only at the lowest $\langle\beta_N\rangle_n$-values, which could be reached. As for the moment we are interested only in that linear behaviour, the zero shear rate values of $[\cot 2\chi/\langle\beta_N\rangle_n]$ have to be determined at the lowest possible values of $\langle\beta_N\rangle_n$. The best way of doing this is to plot the calculated values of $[\cot 2\chi/\langle\beta_N\rangle_n]$ against $\langle\beta_N\rangle_n$. In Figs. 6.12 and 6.13 a few examples are given of this procedure. Fig. 6.12 corresponds to the measurements given in Figs. 6.1 and 6.11. The larger scatter, which is obtained at the lowest $\langle\beta_N\rangle_n$-values, is caused by the inaccuracy in measuring extinction

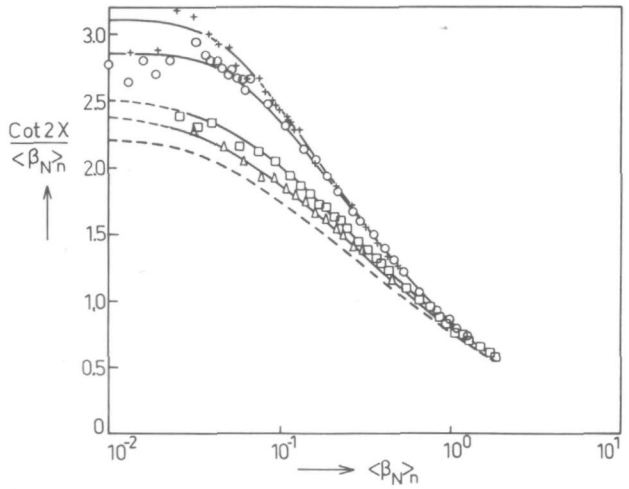

Fig. 6.12. Values of $[\cot 2\chi/\langle\beta_N\rangle_n]$ against $\langle\beta_N\rangle_n$ for CC(L 610) in dioxane at 25°C. Extrapolation to zero shear rate ($\langle\beta_N\rangle_n = 0$). Concentrations: symbols as in Fig. 6.1. (-----): curve extrapolated to zero concentration.

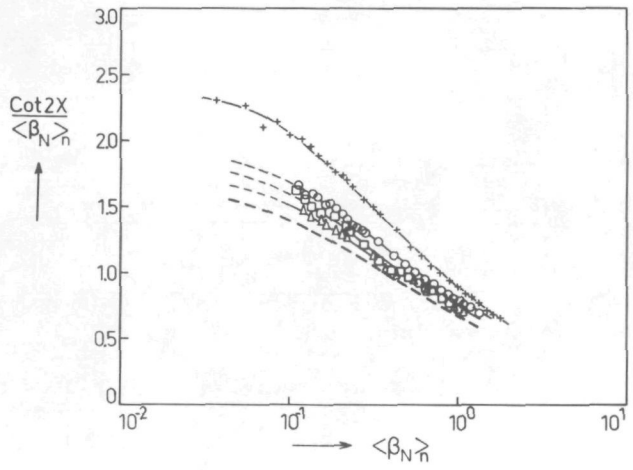

Fig. 6.13. Values of [cot $2\chi/\langle\beta_N\rangle_n$] against $\langle\beta_N\rangle_n$ for CC(L 610) in PhB at 75°C. Concentrations: symbols as in Fig. 6.1. (-----): curve extrapolated to zero concentration.

angles close to the 45° angle. One observes that a linear region is hardly found. However, at $\langle\beta_N\rangle_n \sim 10^{-2}$ the value of [cot $2\chi/\langle\beta_N\rangle_n$] seems to become independent of $\langle\beta_N\rangle_n$, so that an extrapolation to that $\langle\beta_N\rangle_n$-value seems justified. Fig. 6.13 gives the results for CC(L 610) in PhB at 75°C. For these measurements, unfortunately, no extrapolation can be tried. However, a comparison with Fig. 6.12 shows that these curves, on the whole, are situated lower than the curves in Fig. 6.12 at corresponding concentrations.

In Fig. 6.14 the values of Ω * for CC(L 610) in pure dioxane, as extrapolated to zero shear rate according to the above description, are plotted against concentration, with temperatures as parameters. From this figure it may be concluded that Ω not only depends on concentration but also on temperature. However, the temperature influence seems to diminish when the concentration is lowered. In other words, for finite concentrations also the temperature reduction with the aid of β_N does not hold for CC(L 610) in dioxane. An extrapolation to zero concentration can be made with reasonable accuracy. At infinite dilution the temperature dependence of Ω practically disappears within the accuracy limits of the extrapolation procedures.

In fact, the determination of the zero shear rate value of Ω is equivalent with the direct determination of the initial slope of the extinction angle/curve. The accuracy of this determination depends on

* In the text Ω is used for typographic reasons instead of $[\cot 2\chi/\langle\beta_N\rangle_n]_{q=0}$.

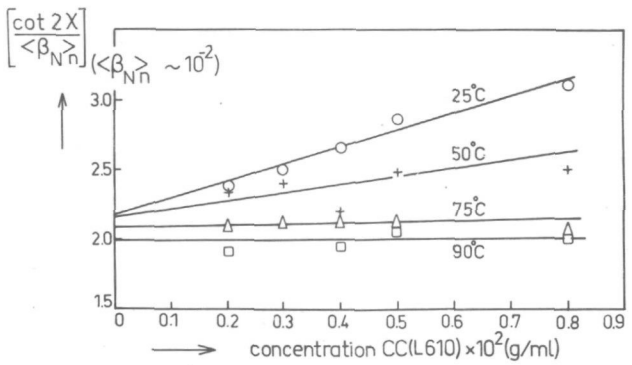

Fig. 6.14. Values of $[\cot 2\chi/\langle\beta_N\rangle_n]$, extrapolated to $\langle\beta_N\rangle_n \sim 10^{-2}$, against concentration for CC(L 610) in dioxane at different temperatures.

the number of reliable extinction angle measurements carried out in the vicinity of 45°. However, as can be seen in Figs. 6.1 and 6.3, for CC(L 610) only a few experimental points could be obtained between say 40° and 45°. Because of the high molecular weight of the sample CC(L 610) the extinction angle rapidly deviates from 45° at small shear rates, while the created birefringence is still feeble*. This causes the difficulties in extrapolating $[\cot 2\chi/\langle\beta_N\rangle_n]$ to zero shear rate.

In this respect, measurements on the lower molecular weight sample CC(Lonza) look more promising. For this purpose a number of extinction angle curves were measured for this sample in pure PhB, resp. pure dioxane. An example for the extinction angle curves has already been given in Fig. 6.4. As theoretically predicted, the extinction angle decreases linearly with increasing shear rate, as long as the measured values lie above 40°. The initial slope of the curves can now be determined directly and with great accuracy. For solutions in dioxane, however, reliable results can only be obtained at low temperatures. At 90°C extinction angles deviate so little from 45° that a reasonable estimation of Ω becomes impossible.

The values of Ω as obtained for CC(Lonza) according to this more direct method, are given in Fig. 6.15: in the upper part for dioxane, in the lower part for PhB, for the indicated temperatures. As to the dioxane part of this figure, the same trends are observed as in Fig. 6.14. In the PhB-part the temperature difference between both series of measurements is too small to show up in the results. A comparison of the results in

* Roughly speaking, the initial slope of the extinction angle curve increases with the square of molecular weight, whereas the slope of the birefringence curve only increases linearly with molecular weight[3].

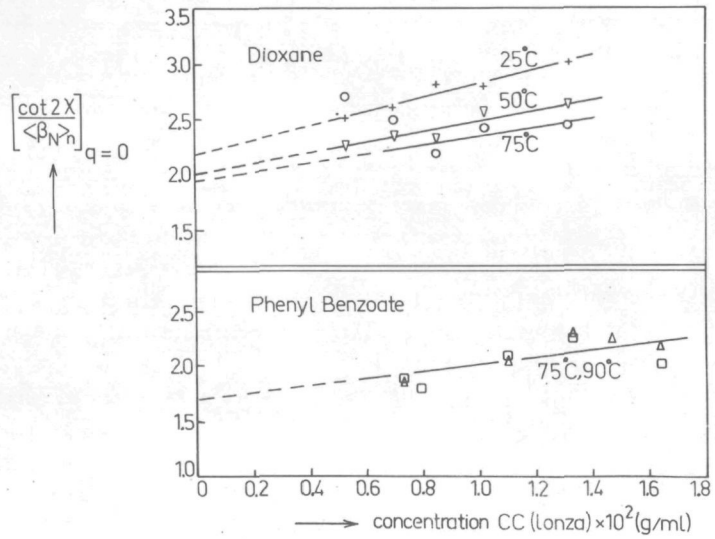

Fig. 6.15. Values of $[\cot 2\chi/\langle\beta_N\rangle_n]$, extrapolated to zero shear rate, against concentration for CC(Lonza) in dioxane, resp. PhB, at different temperatures.

both solvents shows again that the values of Ω for the solutions in PhB are generally lower than those for the dioxane solutions, also when the difference in temperature is taken into account. The same trend was already observed on the solutions of CC(L 610), although for this polymer no zero shear rate values could be obtained in PhB-solutions. As is seen from Fig. 6.15, the extrapolation to zero concentration can easily be carried out. The resulting values are given in Table 6.1. Strictly speaking, the differences between these values are so small that they nearly lie within the accuracy limits of the extrapolation method. So it must

Table 6.1

Values of $[\cot 2\chi/\langle\beta_N\rangle_n]_{q=0}$, as obtained for CC(Lonza), after extrapolation to zero concentration. Approximate values of J_{eR}, as obtained after correction for polydispersity, are given between brackets

Solvent	$[\cot 2\chi/\langle\beta_N\rangle_n]_{q=0}$			
	25°C	50°C	75°C	90°C
Dioxane	2.17 (0.571)	2.00 (0.526)	1.90 (0.500)	-
Phenyl ester of Benzoic Acid	-	-	1.70	1.70

be concluded that, if the transition in the stress-optical coefficient is accompanied by a change of the value of Ω (extrapolated first to zero shear rate and then to infinite dilution), this change must certainly be a very small one.

6.2 Influence of solvent and temperature on the chain stiffness

The experimental results clearly demonstrate that CC undergoes a kind of conformational transition when the solvent composition is changed from ester to ether. The simultaneous growths of the stress-optical coefficient and the intrinsic viscosity, as observed in the mixtures of PhB and dioxane, probably point to a stiffening of the chain. However, a direct semi-quantitative interpretation of the increase of the stress-optical coefficient in terms of coil expansion, as it seemed permissible for poly(amide carboxylic acid), is certainly not possible in this case. Primarily, the cellulose derivatives are so stiff that at the used molecular weights, no Gaussian coils are formed. As a consequence, eq. (5.3) cannot be applied to this system. Secondly, the molecular structure of CC is so complicated that one should not expect that the anisotropy per unit length of the CC-chain remains unchanged at a conformational transition of the molecule.

The most direct proof for the character of the transition can be derived from Fig. 6.10. The measurements represented in this figure can be interpreted straightforwardly by the theory of Gotlib and Svetlov, dealt with in section 3.8.2. In fact, the full lines connecting these points are theoretical curves with the following parameters:

Dioxane:	25°C	$C_\infty = -8.76 \times 10^{-9}$ cm^2/dyne,	$s = 50.0$
	50°C	$C_\infty = -6.17 \times 10^{-9}$ cm^2/dyne,	$s = 42.5$
	75°C	$C_\infty = -4.55 \times 10^{-9}$ cm^2/dyne,	$s = 42.5$
	90°C	$C_\infty = -3.70 \times 10^{-9}$ cm^2/dyne,	$s = 38.6$
PhB	: 75°C	$C_\infty = -2.06 \times 10^{-9}$ cm^2/dyne,	$s = 30.0$

where $C_\infty = \frac{1}{2}([\eta]/[\eta]_o)_\infty$ = the value of the stress-optical coefficient for an infinitely long Gaussian macromolecule,

s = the number of monomer units per statistical random link, which is twice the number of monomers per persistence length.

The lowest molecular weight samples usually give too low values of the stress-optical coefficient, compared with theory. In the first place, this is caused by the use of the weight average molecular weights of these samples. As is well known, these averages are always higher than the number averages, which means that the measured points are apparently shifted to higher molecular weights. In the second place, this can be caused by the fact that, for these low molecular weights, the assumption

of the infinitely thin persistent thread does not hold. At these low degrees of polymerization the diameter of the chain is of the same order of magnitude as its length. Sample CC II_2 even corresponds to a total length of only six monomer units. For those cases Tsvetkov[4] has shown that the anisotropy of the side-groups takes over the function of the anisotropy of the main chain, which for CC must result in a decrease of the absolute value of the stress-optical coefficient and, in the worst case, even in a change of sign of the birefringence. It should also be noted that a logarithmic molecular weight scale is used in Fig. 6.10. This overemphasizes the importance of the experimental points at low molecular weights.

Special attention should be paid to the number s of monomer units per random link for CC in dioxane at 25°C. From light-scattering measurements on CC in a θ-mixture dioxane-methanol 56.5/43.5 (vol.%) at 20°C Burchard[5,6] has calculated a persistence length a = 141 Å, on assuming a symmetric rotational potential around β-glycosidic bonds with respect to the straight zig-zag conformation of the chain. This corresponds to a length of the statistical random link A = 2a = 282 Å. The best fit of experimental results was obtained when an average monomer length of 5.50 Å was assumed. Using these values one obtains s = 51.3, which is rather close to the value given above for the dioxane solutions at 25°C. The difference of 5°C between the temperatures at which both kinds of measurements were carried out, seems of minor importance. In fact, the monomer length of cellulose is well-known from x-ray diffraction to be 5.15 Å. With this value even larger values of s would have been found, although this monomer length would not fit in the calculations of Burchard[6]. The fact that the value of s in the θ-mixture is a little higher than the above quoted value in pure dioxane is in accordance with the poorer solvent nature of a θ-mixture.

From Fig. 6.10 it can be concluded that the stiffness of the CC-chain increases with a decrease of temperature: the number of monomers per random link grows with this decrease. The same naturally holds for the length of this link. On the other hand, it seems reasonable that also the transition of the stress-optical coefficient, as observed with a change of the solvent composition (see Fig. 6.6), must be ascribed to a changing stiffness of the chain. In the ester PhB the CC-chain is less stiff than in the ether dioxane. An interpretation of growing stiffness in terms of the formation of intramolecular hydrogen bonds is quite obvious.

However, the stiffness of CC, as expressed in terms of the number of monomer units per random link, changes less than one would expect from the large changes of the stress-optical coefficient. Apparently, the stress-optical coefficient does not simply depend on the length of

Table 6.2

Properties of two samples of CC in a series of solvents

Code	Mol.wt. $x10^{-5}$	Solvent	Temp. (°C)	$[\eta]_o$ (cm^3/g)	$Cx10^9$ (cm^2/dyne)	$(\alpha_1-\alpha_2)x10^{25}$ (cm^3)	s
CC(L 610)	4.4	Dioxane	25	472	- 8.30	-2270	50.0
			50	390	- 5.90	-1730	42.5
			75	305	- 4.05	-1370	42.5
			90	255	- 3.50	-1167	38.6
		Phenyl Benzoate	75	215	- 1.86	- 510	30.0
			100	180	- 1.45	- 426	
		Tri-o-cresyl	30	230	- 1.40	- 334	
		Phosphate	60	185	- 1.25	- 328	
			90	155	- 1.15	- 329	
		TOCPh-Diphenyl	30	65	-33.0	-7773	
		ether (25/75)	60		-25.5	-6601	
			90		-15.2	-4289	
			120		-13.3	-4063	
		Dibutyl ketone	15		- 3.10	- 776	
			25		- 2.10	- 544	
			35		- 1.50	- 402	
			40		- 1.20	- 327	
CC IX_4	5.0	Benzophenone	55	206	- 1.98	- 519	36.6
			80	174	- 1.54	- 430	34.7

the random link. In Table 6.2 a survey is given of the results obtained on CC(L 610) in the different solvents. In this table also results are mentioned, which were obtained on CC(L 610) in dibutylketone[7] and on a sharp fraction CC IX_4 of comparable molecular weight in benzophenone by Janeschitz-Kriegl and Burchard[8]. Before drawing conclusions from the values of the stress-optical coefficient about the chain-stiffness of CC, one should realize that the stress-optical coefficient C_∞ is, according to eq. (3.67), explicitely influenced by the refractive index of the solution and by the temperature. This means that the values of the anisotropy $\alpha_1 - \alpha_2$ of the random link should be used, which can be calculated from the stress-optical coefficients with the aid of eq. (3.67). As far as possible, these calculations were carried out with the aid of the values of C_∞, as obtained from the method of Gotlib and Svetlov. If these values were not known, the experimental values for CC(L 610) were used. From Fig. 6.10 it can be deduced that the errors made by this procedure are comparatively small. The calculated values of $\alpha_1 - \alpha_2$ are given in Table 6.2, column 7. Two groups of solvents can clearly be dis-

cerned: on the one hand the ethers, in which CC possesses a relatively high anisotropy, on the other hand the esters and ketones, in which CC possesses a lower anisotropy. Apparently, the stiffness of CC is of the same order of magnitude in esters and ketones, but differs from that in ethers.

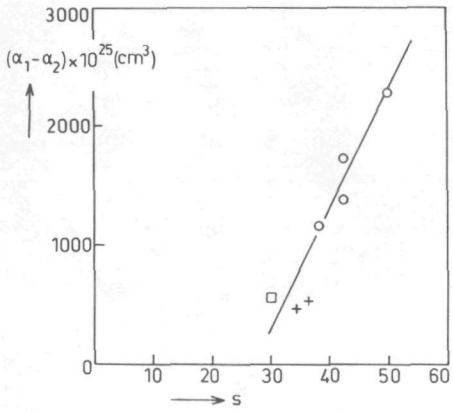

Fig. 6.16. Anisotropy of the statistical random link $(\alpha_1-\alpha_2)$ against the number of monomer units per random link s, for CC in different solvents and at different temperatures. Solvents: (o) dioxane; (+) benzophenone; (□) phenyl benzoate.

In Fig. 6.16 the results shown in the last two columns of Table 6.2 are plotted graphically to illustrate the tremendous influence of s on the anisotropy of the random link. From eqs. (3.65) and (3.71) it can be deduced that the anisotropy of the statistical random link should be proportional to the length of that link, provided that the anisotropy per unit length of the chain $\Delta\beta$ remains the same. For CC this is certainly not the case, as can be seen in Fig. 6.16. The non-linear relation must therefore be due to other influences.

Besides a stiffening of the chain also other reasons can be responsible for a change of the anisotropy of the statistical random link:

a) A changing form-birefringence,
b) A changing polymer-solvent interaction resulting in changes with regard to solvatation as well as excluded volume,
c) A change of the chemical structure of the molecular chain.

This classification is certainly quite arbitrary, as the different effects are usually interrelated. Therefore it will, in the general case, be impossible to determine the influences of all these effects separately from only a restricted number of measurements. There are reasons, however, to expect a simpler situation with CC.

As to the first effects, it can be said that these will become apparent when the solvent is changed. In this context one should remind that

dioxane and also dibutylketone are no "matching solvents". Therefore the anisotropies of the CC-molecules in these solvents must contain a certain positive contribution of the form-birefringence. However, in section 4.1.2 it was already demonstrated that the latter effect lies within the measuring accuracy. Moreover, if form-birefringence occurs, the stress-optical coefficient shows a systematic concentration dependence[9], viz. a decrease with increasing concentration, when the total birefringence effect is positive, or an increase in absolute value, if the total effect is negative. This was never observed, which again confirms that this effect may be neglected.

Solvatation influences will probably play a role. From Fig. 1.2 it can easily be seen that CC has a kind of tape structure which contains the cellulose backbone in the centre. This backbone is surrounded on both sides by rather closely packed phenyl-groups. Both regions are easily accessible to solvent molecules and will probably show their own solvatation behaviour. Indeed, the peculiar behaviour of CC in mixtures of ketones and water, resp. methanol, as observed by Burchard[10], may be due to this fact. Therefore it cannot be excluded that the transition of the anisotropy, as observed with a change of the solvent composition, is at least partly caused by a change of the solvatation of the molecular chain.

For CC(L 610) in dioxane at 25°C a number of 50 monomer units was found per random link. This means that the total length of the molecule comprises only 17 random links. With such a small number of random links the molecule can scarcely form a Gaussian coil. In such a case, the excluded volume cannot play a role of importance.

Undoubtedly, however, the strong change of the anisotropy of the random link with temperature and also with solvent-composition, is mainly due to an alteration of the chemical structure of the chain. As a matter of fact, the negative anisotropy of CC is caused by the presence of the strongly anisotropic phenyl-rings in the side-groups. Since the polarizability of a phenyl-group is much greater in the plane of the ring than in a direction perpendicular to that plane, the contributions of these groups to the anisotropy of the chain can be expected to depend to a great extent on the average orientation of the rings with regard to the longitudinal direction of the chain. A similar hypothesis has been put forward and checked some time ago for polystyrene[11]. From Fig. 1.2 it can be seen that, when the indicated hydrogen bonds are formed, the phenyl groups are closely packed. A rotation of the phenyl groups is nearly completely blocked. Any breakage of hydrogen bonds results in a greater flexibility of the chain and, simultaneously, in a greater freedom for rotation of the phenyl-rings. This certainly causes the observed decrease of the anisotropy of the chain.

Table 6.3

Temperature coefficients of intrinsic viscosity and anisotropy and the conformational energy differences of two samples of CC in a series of solvents

Code	Solvent	$d(\ln[\eta]_o)/dT$ ($°C^{-1}$)	$d(\ln\lvert\alpha_1-\alpha_2\rvert)/dT$ ($°C^{-1}$)	ΔE (kcal/mol)
CC(L 610)	Dioxane	-0.98×10^{-2}	-1.02×10^{-2}	2.20
	Phenyl Benzoate	-0.71×10^{-2}	-0.72×10^{-2}	1.85
	Tri-o-cresyl Phosphate	-0.66×10^{-2}	0.0	0.0
	TOCPh-Diphenyl ether (25/75)		-0.90×10^{-2}	2.09
	Dibutyl ketone		-3.53×10^{-2}	6.15
CC IX_4	Benzophenone	-0.68×10^{-2}	-0.74×10^{-2}	1.75

The transition of CC(L 610) in mixtures of TOCPh - DPhE must obviously be interpreted in the same way. In TOCPh - DPhE 25/75 the anisotropy is even higher than in dioxane, which probably indicates a still greater stiffness related to a different polymer-solvent interaction. In this respect one should be reminded that CC cannot be dissolved in pure DPhE at the temperatures used. This probably means that the mixture TOCPh - DPhE 25/75, especially at the lower temperatures, is nearly a θ-solvent. In such a case the thermodynamic polymer-solvent interaction is minimal, which certainly promotes the formation of intramolecular hydrogen bonds.

The effects of temperature on the anisotropy $\alpha_1 - \alpha_2$ of the chain of CC(L 610) in the different solvents can be compared by calculating the temperature coefficients of this anisotropy from the data in Table 6.2, column 7. The results are given in Table 6.3, column 4. It appears that TOCPh and dibutylketone differ clearly in their behaviour. Further both ethers dioxane and DPhE give a somewhat higher value than PhB and benzophenone. The latter solvents give nearly equal values. This again demonstrates the extraordinary position of the ethers as solvents, promoting the formation of intramolecular hydrogen bonds within CC. With the aid of light scattering Öhman and Shanbhag[12] have found that CC behaves quite peculiarly in dibutylketone. This appears to be accompanied, according to the present results, by a marked temperature coefficient of the anisotropy. As the temperature coefficient for CC in TOCPh is extraordinary as well, it is probable that CC will behave quite exceptionally also in this solvent. This may have something to do with

the temperature influence on the transition region for CC(L 610) in TOCPh - DPhE, which was reported above (see Fig. 6.7).

As a final point of discussion it must be mentioned that, on the basis of birefringence measurements on stretched poly(dimethyl siloxane) elastomers, Mills and Saunders[13] have proposed a relation, which describes the temperature dependence of the anisotropy of the random links over a limited temperature range. This relation reads:

$$\alpha_1 - \alpha_2 = (\alpha_1 - \alpha_2)_{T=\infty} \times \exp(\Delta E/RT) \qquad (6.1)$$

where $(\alpha_1 - \alpha_2)_{T=\infty}$ = an adjustable constant,

ΔE = a kind of conformational energy difference.

As a matter of fact, also the results given in Table 6.2, column 7, can be described quite well by this relation. In this way the conformational energy difference of CC in all mentioned solvents can be calculated. The results are given in Table 6.3, column 5. However, the question remains in how far ΔE has any real significance.

6.3 The hydrodynamic aspects of the conformational transition

In this paragraph only the linear effects, accompanying the conformational changes of CC, will be discussed. An evaluation of the non-linear behaviour of CC is postponed to a later chapter.

6.3.1 The intrinsic viscosity

Unfortunately, a quantitative interpretation of the observed transitions in the intrinsic viscosity cannot be given in terms of the chain stiffness. As a matter of fact, all known theories on the intrinsic viscosity of polymer solutions are derived for monodisperse samples. The polydispersity, however, has a great influence which varies with the degree of stiffness of the polymer. As the polydispersity of all samples used in this investigation is quite appreciable, only some qualitative conclusions can be obtained.

Equations (3.55 a-b) describe the dependence of the intrinsic viscosity on the molecular dimensions of a coil molecule. For the derivation of these equations the following assumptions were made:

a) Excluded volume effects are negligible (θ-conditions),
b) The macromolecules are sufficiently long to behave as Gaussian coils,
c) The macromolecules are non-draining.

As to the first assumption, it has already been mentioned in section 6.2 that the influence of excluded volume may in fact be negligible for cellulose derivatives. However, both other assumptions are certainly not satisfied. Cellulose derivatives are in general too stiff to behave like Gaussian coils. This also implies that these coils are far from non-

draining. Consequently, the Flory-Fox parameter Φ_o is not a universal constant: it has not yet reached its asymptotic value for very high molecular weights. In this connection the reader is reminded that Φ_o is explicitely influenced by the draining parameter h*. It decreases with decreasing h* (< 0.25). However, in spite of these restrictions Flory et al.[14] believe that the influence of temperature on the intrinsic viscosity of cellulose derivatives must mainly be due to changes of the mean square end-to-end distance $\langle h_o^2 \rangle$ of the chains. These changes are caused by alterations of the stiffness of the cellulose chain, due to restrictions of the free rotation around the β-glycosidic bonds. Also the height of the jump in the intrinsic viscosity in mixtures of PhB - dioxane, as shown in Fig. 6.8, must then be ascribed to this stiffening effect. Qualitatively the values of the intrinsic viscosity of CC(L 610), as given in Table 6.2, column 5, are in accordance with the observed changes of the stiffness of CC.

The temperature coefficients of the intrinsic viscosity of CC(L 610) in the different solvents are given in Table 6.3, column 3. Except for dioxane, values are obtained which are of the same order of magnitude as those found for other cellulose derivatives[14]. The value found in dioxane is somewhat higher than normal, which again should be due to the extra stiffening of CC in this solvent by the formation of intramolecular hydrogen bonds. As a matter of fact, in ethers also a higher temperature coefficient of the optical anisotropy was found than in most other solvents.

As a next point of discussion it must be mentioned that Burchard et al.[15] have measured the molecular weight dependence of the intrinsic viscosity of CC in dioxane at 20°C. For these measurements a great number of samples with narrow molecular weight distributions ($\langle M \rangle_w / \langle M \rangle_n$ < 1.1) was used. These results are given in Fig. 6.17. In this figure also a number of measurements of Janeschitz-Kriegl and Burchard[8] on sharp fractions of CC in benzophenone at 55°C is reproduced as well as the intrinsic viscosities of the samples CC I_5, CC I_{12}, CC(Lonza) and CC(L 610) in PhB at 75°C.

With the aid of the theory of Eizner and Ptitsyn, as dealt with in section 3.7, the molecular weight dependence of the intrinsic viscosity was calculated for CC in dioxane at 20°C by the present author. For the molecular weight of the monomer unit M_o of CC one obtains a value of 519. For b, the length of the monomer unit, a value of 5.15 Å was taken, equal to the value obtained from x-ray diffraction data. For the number of monomer units per random link s = 2λ the value of 50 was used, the value found above for CC in dioxane at 25°C. The difference of 5°C between both kinds of measurements will be of minor importance. For r_o a value of 9.2 Å was chosen, in correspondence with the mean radius of the cross

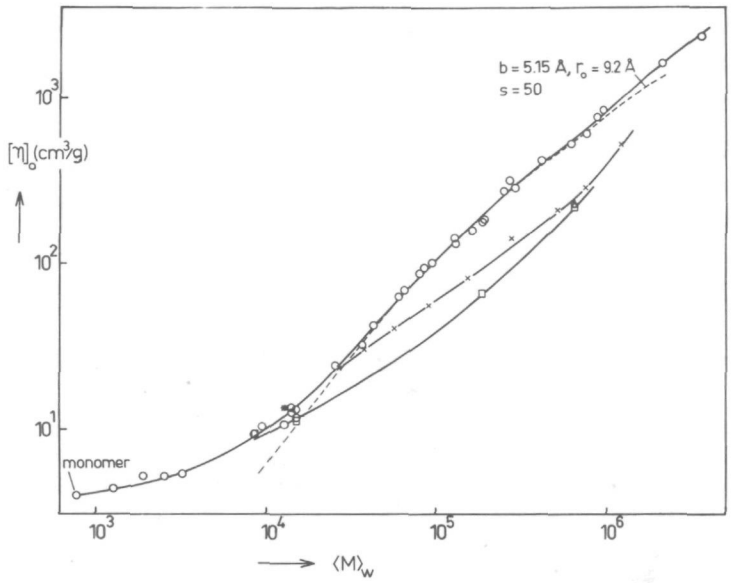

Fig. 6.17. Intrinsic viscosity of cellulose tricarbanilate fractions against molecular weight in various solvents: (o) dioxane 20°C; (x) benzophenone 55°C; (□) phenyl benzoate 75°C. (-----) curve according to the theory of Eizner and Ptitsyn for the parameters indicated; (*) theoretical point for a prolate ellipsoid of one persistence length.

section of the chain, as obtained from x-ray small-angle measurements on acetone solutions[16]. It must be said that the influence of r_o is not very pronounced; even a value of $r_o = \infty$ does not give much difference. The result of these calculations is given by the dashed line in Fig. 6.17. Except for the lowest molecular weight samples the experimental and theoretical lines almost completely coincide, which means that the flow birefringence and viscosity measurements on CC in dioxane are in excellent agreement. For the low molecular weight samples the model of the infinitely thin wormlike chain is not quite realistic. In fact, the finite thickness of the chain will have a pronounced influence on the intrinsic viscosity. This is the reason why, at low molecular weights, the character of the theoretical curve is quite different from the one drawn through the experimental points.

As has been pointed out by Janeschitz-Kriegl and Burchard[8], short wormlike chains of finite thickness can better be approximated by prolate ellipsoids. In the same way as done by these authors the intrinsic viscosity of a particle, possessing just the persistence length, can be calculated. In fact a mistake was made by these authors in their calculation

of the volume of the equivalent ellipsoid. As this particle should contain 25 monomer units, its molecular weight would be 13 x 10^3. The value of the intrinsic viscosity can be obtained from the works of Simha[17] and Scheraga[18]. The value as obtained by the present author on assuming a value of 5.15 Å for the monomer length and a value of 9.2 Å for the mean radius of the cross section of the chain, is indicated in Fig. 6.17 by an asterix. This value again agrees quite well with the experimental results.

The character of the curve drawn through the experimental results for CC in benzophenone and PhB, however, is quite different from the theoretically predicted curve in the whole range of molecular weights. The difference between the experimental curves in benzophenone and PhB is probably due to the fact that the samples measured in the latter solvent had a comparatively great polydispersity. In fact the curves obtained for benzophenone and for PhB are below the one obtained for dioxane. According to the Eizner-Ptitsyn theory this fact would correspond to lower values of λ, in accordance with flow birefringence data. However, the curvatures of these experimental lines are just opposite to that of the theoretical line. As assumed already by Janeschitz-Kriegl and Burchard[8], the reason for this fact must be sought in the excluded volume. In the solvents benzophenone and PhB, in which CC is much more flexible than in dioxane, the CC-chain will start to show a Gaussian behaviour in a lower molecular weight range than in dioxane. In that range also the influence of the excluded volume will become perceptible. As a matter of fact, even in dioxane the highest molecular weight samples can be seen to deviate slightly from the theoretical line, due to excluded volume effects. This causes the upward curvature of the experimental curves. Finally it can be observed in Fig. 6.17 that all experimental curves seem to converge to the same values at small molecular weights, where the influences of both chain stiffness and excluded volume on the intrinsic viscosity vanish.

6.3.2 The behaviour of the extinction angle

It should be reminded that for the rather stiff CC-samples the optically measured quantity $[\cot 2\chi/\langle\beta_N\rangle_n]$ cannot be identified, after extrapolation to zero shear rate, with the hydrodynamic quantity pJ_{eR}, as defined by eq. (3.72b). This procedure is strictly correct only in the case of Gaussian coil molecules. For the respective argumentation see section 3.9. For the following, however, we must suppose for simplicity that all investigated samples are sufficiently coiled to justify the assumption that the values of Ω (see footnote on page 87) and pJ_{eR} do not differ to a great extent. This means that we shall assume to be allowed to use the hydrodynamic theories, described in chapter 3, for an interpretation of the optically measured quantities, without introducing great errors.

It is a rather difficult task to draw conclusions from the observed changes of Ω. However, a general trend can be deduced from the values of this quantity for CC(Lonza), as quoted in Table 6.1, and also from Figs. 6.12 and 6.13: the value of Ω shows a tendency to grow with increasing stiffness of the chain. Both the temperature- and the solvent-influence on the chain stiffness can be recognized in a change of the value of Ω. As far as the behaviour of Ω reflects that of the quantity pJ_{eR} for these samples, it can be stated that the prediction put forward in chapter 3, viz. that J_{eR} should increase with a growing stiffness of a macromolecule, seems to be confirmed by these experiments. However, in view of the limited accuracy of the extrapolation procedures the question remains in how far the observed changes can be considered as significant.

As to the found influence of temperature on Ω it must be mentioned that the reduction of the extinction angle curves of other polymers with the aid of the reduced shear rate β_N was always found to give temperature independent values of $[\cot 2\chi/\beta_N]$[3]. Obviously, the changes of stiffness with temperature were so small for those other polymers that the temperature reduction was not disturbed.

Just as for poly(amide carboxylic acid) also in the case of CC the polydispersity of the samples has a tremendous influence on the experimental results. For a comparison of these results with theory again a correction for polydispersity must be made. If we assume that the molecular weight distribution of the sample CC(Lonza) is also of the Schultz-Zimm type, the correction method of Peterlin can again be used in the form given in section 3.11. For this purpose one needs the polydispersity-index of this sample, as given in Table 4.1, column 4, and the exponent α in the Mark-Houwink equation. However, the value of α is not a constant for CC in all solvents and at all temperatures used (see the curved lines in the double logarithmic plot of Fig. 6.17). As a consequence, an exact correction for polydispersity cannot be made.

To get an idea yet of the values of J_{eR} certain additional approximations can be made. From Fig. 6.17 it can be deduced that a smoothed exponent α for CC(Lonza) in dioxane at 20°C amounts to about 1.0. On using this value one obtains a polydispersity-factor $p = 3.80$. If one further assumes that this value will approximately hold in dioxane at all temperatures applied, it can be used for a correction of the experimental values of Ω for the sample CC(Lonza), as quoted in Table 6.1. The results are given in Table 6.1, between brackets, behind the measuring results from which they were derived. These values will probably be rather good approximations of the values of the hydrodynamic quantity J_{eR} for this sample.

As a matter of fact, the obtained values are above the range quoted for Gaussian coils, i.e. $0.2 \leqslant J_{eR} \leqslant 0.4$. But even this sample CC(Lonza)

which comprises only about 4 random links in dioxane at 25°C, does still give values which deviate only slightly from those expected for Gaussian coils.

The most promising way to find significant influences of chain stiffness on J_{eR} is to measure the flow birefringence of a great number of samples over a wide range of molecular weights. This was done by Janeschitz-Kriegl and Burchard[8] for sharp fractions of CC in benzophenone. They found a clear increase of the values of $[\cot 2\chi/\beta_N]$ with decreasing molecular weight which, according to section 3.2, also corresponds to an increasing chain stiffness. However, due to a lack of material their number of measurements was insufficient for an extrapolation to zero concentration. As a consequence, also in their case a certain degree of uncertainty is retained with regard to the interpretation of the obtained results.

From the foregoing the conclusion may be drawn that both flow birefringence investigations have given some evidence of the theoretically predicted influence of chain stiffness on the reduced steady state shear compliance J_{eR}. However, it is also clear that the extinction angle can never be a sensitive quantity from which information concerning the conformation or stiffness of macromolecules can be derived. Moreover, the influence of polydispersity nearly masks all other influences on the behaviour of the extinction angle. Consequently, the behaviour of the extinction angle can better be used as a measure for polydispersity itself. This aspect of flow birefringence should certainly be explored more extensively.

6.4 Conclusions

As previously found for a variety of polymers, the theory of Gotlib and Svetlov gives a very good description of the molecular weight dependence of the stress-optical coefficient also for CC. The great usefulness of this theory may be demonstrated by the fact that the stiffness of CC, as expressed by the number of monomer units per statistical random link, can be found in a straightforward manner. Furthermore, the obtained experimental results reveal a transition of the stiffness of CC, when the solvent composition is varied from pure ester to pure ether. In the ether dioxane CC has a stiffer structure than in the ester PhB, at comparable temperatures. Further, the stiffness of CC increases appreciably with decreasing temperature. An increase of its stiffness causes a tremendous growth of the stress-optical coefficient, appreciably greater than the corresponding growth of the intrinsic viscosity. This demonstrates the great advantage of measuring the stress-optical coefficient on studying conformational transitions of polymers.

The high optical anisotropy, the high temperature coefficients of this quantity and of the intrinsic viscosity of CC in pure dioxane show that the behaviour of CC in this solvent clearly deviates from that in non-ether solvents. An explanation of this difference in terms of the formation of hydrogen bonds between neighbouring monomers was quite obvious. The great changes in the stress-optical coefficient are probably due to sterical hindrance of the free rotation of the anisotropic phenyl-rings in the side groups of the chain.

The value of 50 monomers per statistical random link, as found for CC in dioxane at 25°C, agrees quite well with the results obtained from light scattering measurements in the same solvent at 20°C. This value was introduced into the equation of Eizner and Ptitsyn for the calculation of the intrinsic viscosity of CC as a function of molecular weight. The theoretical curve excellently coincides with the experimental one, except for the lowest molecular weights, where the model of the worm-like chain is not realistic, and for the highest molecular weights, where the excluded volume plays a role. This coincidence proves that the value s = 50 is a very realistic one.

The influence of chain stiffness on the behaviour of the extinction angle appears to be very small; it nearly lies within the limits of experimental error. Moreover, the influence of polydispersity masks the effect to a great extent. Nevertheless, with some reserve it may be concluded that the theoretically predicted increase of J_{eR} and, consequently, of the optical quantity $[\cot 2\chi/\langle\beta_N\rangle_n]_{q=0}$ with growing stiffness of a macromolecule is found in practice. However, it also appears that $[\cot 2\chi/\langle\beta_N\rangle_n]_{q=0}$ hardly gives any valuable information concerning the observed stiffening of the CC-chain.

Literature

1. W. Burchard, private communication.
2. U. Daum, unpublished results.
3. H. Janeschitz-Kriegl, Adv. Polymer Sci. *6*, 170 (1969).
4. V.N. Tsvetkov, Dokl. Akad. Nauk SSSR *192*, 380 (1970).
5. W. Burchard, Makromol. Chem. *88*, 11 (1965).
6. W. Burchard, Brit. Polymer J. *3*, 214 (1971).
7. Unpublished results.
8. H. Janeschitz-Kriegl, W. Burchard, J. Polymer Sci. A2, *6*, 1953 (1968).
9. H. Janeschitz-Kriegl, Makromol. Chem. *33*, 55 (1959); *40*, 140 (1960).
10. W. Burchard, Z. Physik. Chem. *42*, 293 (1964).
11. V.N. Tsvetkov, S.Ya. Magarik, Dokl. Akad. Nauk SSSR, *127*, 840 (1959).
12. J. Öhman, V.P. Shanbhag, Arkiv. f. Kemi *31*, 137 (1969).
13. N.J. Mills, D.W. Saunders, J. Macromol. Sci. B, *2*, 369 (1968).
14. P. Flory, O.K. Spurr, D.K. Carpenter, J. Polymer Sci. *27*, 231 (1958).
15. W. Burchard, W. Sutter, B. Pfannemüller, unpublished results.
16. O. Kratky, I. Pilz, W. Burchard, unpublished results.
17. R. Simha, J. Phys. Chem. *44*, 25 (1940).
18. H.A. Scheraga, J. Chem. Phys. *23*, 1526 (1955).

CHAPTER 7

THEORETICAL DESCRIPTION OF NON-LINEAR BEHAVIOUR OF MODEL CHAINS

7.1 Introduction

In chapter 3 the hydrodynamic behaviour of a macromolecule was described with the aid of an idealized model. This theory was based on a generalized diffusion equation, which only holds for "systems slightly departing from equilibrium". This linear theory resulted in the eqs. (3.42) and (3.44) for the intrinsic viscosity and the reduced steady state shear compliance, which showed no dependence on shear rate. Hence, an interpretation of experimental results could only be carried out with the aid of this theory, as far as no dependence on shear rate was observed. As a consequence, the experimental results usually had to be extrapolated to zero shear rate in the foregoing chapters. Only at the lowest shear rates the supposed linearity was found (see e.g. Fig. 6.12). For values of $\langle \beta_N \rangle_n$ higher than 10^{-1} non-linearity became already quite well perceptible.

For high shear rates the deviations from the supposed equilibrium conditions will probably become so large that the required linearizations in the momentum space, as mentioned in section 3.3, will no longer be permissible. In such a case higher order moments will become involved, which disturb the Markoffian character of the usual diffusion processes[1]. As a matter of fact, this Markoffian character was an essential condition for the derivation of the conventional diffusion equation (3.8). A foundation of non-linear behaviour asks for an extension of the kinetic theory to stochastic processes of non-Markoffian character. However, these new approaches are still nearly unexplored up till now.

From the foregoing it becomes clear that a correct theoretical description of non-linear behaviour is an intractable task so far. However, in the past several attempts were made to derive constitutive equations, which are non-linear in terms of shear rate. For this purpose, in some way non-linearity is introduced into the theory. According to a well-known procedure[2,3] the supposed linear relation between the deformations of the particles and the resulting elastic forces, as given for example by eqs. (3.18a) and (3.19a), is rejected. In fact, for real macromolecules such a linear relation will only hold at very small deformations. At larger deformations the elastic restoring forces will increase more than linearly with deformation until they become nominally infinite, when the macromolecule is fully extended and a further deformation results in chain rupture.

When the diffusion equation is modified in this way, it will yield non-linear effects, although it does not comprise all possible reasons for non-linearity. Particularly diffusion is still described by the unmodified diffusion terms of eq. (3.8). Hence, from a diffusion equation modified in this way, a theory is derived which can better be called a "quasi-linear theory".

It has also been shown that other effects, such as the excluded volume in good solvents[4], an anisotropy of the hydrodynamic interaction[4,5] or the kinetic stiffness of the polymer chain[6-8] can cause non-linear behaviour. So the question will remain, which one of the above called parameters must be considered to be the main reason for non-linear effects.

7.2 Introduction of the inverse Langevin function into the Rouse-model

A first attempt to make allowance for the restricted deformability of a macromolecule was made by Peterlin[2] for the elastic dumbbell model. Later on this idea was also applied to the more general Rouse-model by Reinhold and Peterlin[3]. Their method will be described here.

We can define a kind of contour length for the RZ-model, as:

$$L = N\, b \tag{7.1}$$

where b^2 = the average of the mean square end-to-end distances of the Gaussian subchains (springs), which are supposed to build up the molecule:

$$b^2 = N^{-1} \sum_{n=1}^{N} b_n^2 = N^{-1} \sum_{n=1}^{N} \langle (\underline{r}_n - \underline{r}_{n-1})^2 \rangle \tag{7.2}$$

In the absence of external forces b^2 becomes equal to b_o^2, defined previously in eq. (3.46). For the RZ-model quantity b^2 can easily be calculated. With the aid of the normal coordinate transformation, as given by the eqs. (3.27 a-b), it can easily be derived that the relation between the mean square length of the n^{th} spring and the normal coordinates is given by:

$$b_n^2 = \sum_{m=1}^{N} \{\langle \zeta_m^2 \rangle + \langle \eta_m^2 \rangle + \langle \vartheta_m^2 \rangle\} \{Q_{nm} - Q_{n-1,m}\}^2 \tag{7.3}$$

where Q_{nm} = the elements of the transformation matrix $\bar{\bar{Q}}$.
For sufficiently large N eq. (7.3) can be approximated by:

$$b_n^2 = \sum_{m=1}^{N} \{\langle \zeta_m^2 \rangle + \langle \eta_m^2 \rangle + \langle \vartheta_m^2 \rangle\} \{\partial Q_{nm}/\partial n\}^2 \tag{7.4}$$

After inserting the eqs. (3.39 a-c) and combining the result with eq. (7.2) one obtains the following relation:

$$b^2 = \frac{3kT}{\sigma} N^{-1} \sum_{m=1}^{N} (\mu_m)^{-1}[1 + \frac{2}{3}(\gamma_m^2)^{-1}(\frac{q\rho}{2\sigma})^2] \times \sum_{n=1}^{N} [\partial Q_{nm}/\partial n]^2 \qquad (7.5)$$

For the Rouse case, i.e. in the absence of hydrodynamic interaction, μ_m and γ_m are equal (see eq. (3.30)). After inserting the values of μ_m and Q_{nm}, as given by eqs. (3.48b) and (3.49 a-c), one obtains the following relation:

$$b^2 = \frac{3kT}{\sigma} [1 + \frac{N^3}{135} \frac{q^2\rho^2}{4\sigma^2}] = \frac{3kT}{\sigma} [1 + \frac{4}{15N} \beta_N^2] \qquad (7.6)$$

since:

$$\beta_N = \frac{M[\eta]_o \eta_s q}{R T} = \sum_{n=1}^{N} (\gamma_n^{-1}) \frac{q\rho}{2\sigma} \qquad (7.7)$$

From this result the conclusion may be drawn that the mean square length of the springs depends on the reduced shear rate β_N. For a fluid at rest, i.e. $\beta_N = 0$, eq. (3.46) is regained.

The obtained result implies that the contour length of the model chain increases with growing shear rate. This would clearly be a very non-physical property of the model, because the contour length of a real macromolecule is completely determined by chemical bonds, which cannot be extended.

To correct for this effect, Reinhold and Peterlin[3] have introduced a restricted extensibility of the subchains into the Rouse model. According to a method of Kuhn and Grün[9] the inverse Langevin function is introduced into the formula for the longitudinal elastic force in the subchain. This means that the elastic force becomes infinite at a certain maximum length b_∞ of the subchain. In this way eq. (3.18a) becomes:

$$\underline{f}^e_{n,L} = \sigma E_n \underline{b}_n$$

with

$$E_n = \mathcal{L}^{-1}(t_n)/3t_n \quad \text{and} \quad t_n = b_n/b_\infty \qquad (7.8)$$

where $\mathcal{L}^{-1}$ = the inverse Langevin function.
The function $E_n(t_n)$ can be approximated by:

$$E = 1 + \frac{3t^2}{5} + \frac{99\ t^4}{175} + \ldots , \quad \text{for } t \to 0$$

$$= 1/(3t - 3t^2), \quad \text{for } t \to 1 \qquad (7.9)$$

Because of the relationship $b_n = |\underline{r}_n - \underline{r}_{n-1}|$ the value of E_n depends in a non-linear manner on the coordinates $\underline{r}_n$ and $\underline{r}_{n-1}$. For simplicity, however, in E_n some preaveraging is carried out over the root mean square length of the link b_n. In this way a set of modified eigenvalues is obtained. These eigenvalues are functions of β_N and, as a consequence of this dependency, also functions of the shear rate. The intrinsic viscosi-

ty, eq. (3.42), and the reduced steady state shear compliance, eq. (3.44), show a decrease at increasing β_N. The magnitude of these effects can be varied by adjusting the value of b_∞/b_o, which is the ratio of the maximum length of the subchain to its length in the fluid at rest. The smaller b_∞/b_o is chosen, the stronger the non-linear effects.

At the values chosen for b_∞/b_o by Reinhold and Peterlin, namely 2 and 5, the deviations from linear behaviour become perceptible at β_N-values higher than 1. However, experimentally such deviations are already observed at β_N-values of the order of 10^{-1} and even at smaller values. Consequently, the conclusion may be drawn that the Reinhold-Peterlin method underestimates the non-linear effects.

7.3 Condition of constant contour length

In the Reinhold-Peterlin theory a simultaneous extension of all subchains is allowed. This means that the contour length of their model still increases with growing shear rate. Therefore Noda and Hearst[10] have introduced a more stringent condition into the RZ-model and HH-model, requiring the total contour length, as defined by eq. (7.1), to remain constant for all shear rates.

7.3.1 The Rouse-Zimm model

For the RZ-model the condition requiring the total contour length to remain constant is accomplished by adjusting the spring force constant σ. It is used as a kind of Lagrange multiplier which forces the condition upon the model. If, in this way σ is permitted to grow with increasing rate of shear, one obtains the paradoxical effect that somewhere along the chain subchains have to contract in order to enable other subchains to extend. These two effects have to balance each other to keep the total contour length, as defined by eq. (7.2), constant. Thus, this theory is different from that of Reinhold and Peterlin.

For the Rouse-model the average of the mean square length of the springs was already given in eq. (7.6). Now the spring force constant is adjusted to the shear rate q, in such a way that b^2 remains constant. Unlike the Reinhold-Peterlin method the eigenvalues remain unchanged. If we put the spring force constant in the resting fluid (q = 0) equal to σ_o, the relation between the spring force constant σ and the shear rate can be calculated from eq. (7.6):

$$b^2 = \frac{3kT}{\sigma_o} = \frac{3kT}{\sigma}\left[1 + \frac{N^3}{540}\frac{q^2\rho^2}{\sigma^2}\right] \tag{7.10}$$

which after some rearrangements results in:

$$X^3 - X^2 = \frac{N^3}{540}\frac{q^2\rho^2}{\sigma_o^2} \tag{7.11}$$

where $X = \sigma/\sigma_o$.

Equation (7.11) predicts that σ is a unique function of q. A similar relation can be derived for the Zimm-case, which describes the non-draining coil.

It can now easily be shown how large the influence of eq. (7.11) is on the intrinsic viscosity and the reduced steady state shear compliance. Defining a relative intrinsic viscosity $[\eta]_{rel}$ as the ratio of the intrinsic viscosity at finite shear rate q to that at zero shear rate, we have the following relation from eq. (3.42):

$$[\eta]_{rel} = [\eta]/[\eta]_o = (\sigma/\sigma_o)^{-1} = 1/X \qquad (7.12)$$

which, together with eq. (7.11), determines the dependence of the intrinsic viscosity on the shear rate completely.

Due to the fact that the set of eigenvalues remains unchanged, the value of J_{eR} will remain unchanged as well, according to eq. (3.44). However, in eq. (3.43) J_{eR} has been defined as the ratio of cot $2\chi'$ and the reduced shear rate β_N. Actually, eq. (3.43) should be interpreted as a linear relation between cot $2\chi'$ and the shear stress p_{21}. As long as only linear effects are concerned, the shear stress p_{21} is directly proportional to the shear rate q (see eq. (2.11)), which allows the above given definition of J_{eR}. On the other hand, for the occurrence of non-Newtonian solution viscosities the definition of J_{eR} should be revised. In that case for p_{21}, occurring in eq. (3.43), eq. (2.11) must be used with the non-Newtonian solution viscosities inserted. Therefore, the last term of eq. (3.43) should read:

$$\cot 2\chi' = J_{eR}\beta \qquad (7.13)$$

where β = the reduced shear *stress*, defined in the same way as the reduced shear *rate* β_N (eq. (3.45 a-b)), but now with the non-Newtonian solution viscosities inserted, corresponding to the chosen values of q. Only for very small shear rates the difference between β_N and β vanishes.

In the above given definition the ratio of β/β_N is identical with $[\eta]_{rel}$. Consequently, as the value of J_{eR} remains unchanged, eq. (7.13) predicts that [cot $2\chi'/\beta_N$] must show the same dependence on shear rate as $[\eta]_{rel}$.

7.3.2 The Harris-Hearst model

If the condition of a constant contour length is introduced into the RZ-model, the set of eigenvalues remains unchanged. This is obviously not the case for the HH-model. A look on the eqs. (3.58) and (3.59) shows that for the HH-model the value of the spring force constant σ enters the eigenvalues in the form of Λ. The latter takes the function of the La-

grange multiplier in the HH-model. Adjusting the bending force constant α makes no sense of course, as its magnitude does not influence the mean lengths of the springs.

For the HH-model the same definition of the contour length, eq. (7.1), can be used. Noda and Hearst, however, give another definition, which in some cases leads to other results. As mentioned in section 3.6.2, there should exist a correlation between the HH-model and the statistical model of the wormlike chain. For the latter model the idea of a finite number of separate beads must be abandoned and replaced by a continuous model, for which the position of each point on the contour of the chain may be given by a continuous parameter. This requires a rewriting of all equations in terms of this continuous parameter. As this subject, however, falls outside the scope of this work, the discrete bead method will be followed.

For the HH-model the average of the mean square end-to-end distances of the subchains can be deduced in a simple way from the equation for the RZ-model by the substitutions given in section 3.4 and used repeatedly in chapter 3. With these substitutions eq. (7.5) becomes:

$$b^2 = \frac{3kT}{\alpha} N^{-1} \sum_{m=1}^{N} (\mu_{m,HH})^{-1}[1 + \frac{2}{3} (\gamma^2_{m,HH})^{-1} (\frac{q\rho}{2\alpha})^2] \times \sum_{n=1}^{N} [\partial Q_{nm,HH}/\partial n]^2 \qquad (7.14)$$

Again, the simplest treatment corresponds to the absence of hydrodynamic interaction, i.e. the free-draining situation, for which $\gamma_{m,HH} = \mu_{m,HH}$. Let us consider the two limiting cases of the HH-model, as they were discussed in section 3.6.2: the coil limit and the limit of the straight elastic pearl necklace.

The coil limit appears to be the simplest case. Inserting the eqs. (3.49) and (3.58) into eq. (7.14) and rearranging the obtained results one obtains an equation identical with eq. (7.10) which is quite obvious. The dependence of Λ on shear rate is expressed by:

$$X = \Lambda/\Lambda_o = \sigma/\sigma_o \qquad (7.15)$$

where Λ_o is Λ at zero shear rate. As a matter of fact, Noda and Hearst obtain another result for the coil limit due to their different definition of the contour length.

Introduction of the constant contour length into the straight elastic pearl necklace gives a completely different result. As mentioned already in section 3.6.2, only the first eigenvalue plays a role of importance. For the free-draining case this eigenvalue is given by eq. (3.59a). The eigenvalue at zero shear rate is then obtained by replacing Λ by Λ_o. Pursuing this concept Noda and Hearst assumed that, to a first approximation, $\nu_{1,n}$ may be kept constant in the first eq. (3.57a), whereas only

the Λ occurring explicitely in this equation is varied. In this way they obtain:

$$\mu_{1,HH} = \gamma_{1,HH} = 12\ \Lambda_o/N^2 + \Lambda(12\ \Lambda_o/N^2)^{\frac{1}{2}} \tag{7.16}$$

After inserting this equation into eq. (7.14) one obtains:

$$Z^3 - Z^2 = q^2\ \rho^2\ N^8/6\ \alpha^2(12\ \Lambda_o N)^2 \tag{7.17}$$

where

$$Z = \mu_{1,HH}N^2/12\Lambda_o = 1 + [(12\ \Lambda_o N^2)^{\frac{1}{2}}/12]\ X \tag{7.18}$$

These relations also give Λ as a unique function of shear rate. This result is, in spite of the different definition of the contour length, identical to that of Noda and Hearst.

The influence of the constraint of constant contour length on the intrinsic viscosity is obtained from eq. (3.42):

$$[\eta]_{rel} = [\eta]/[\eta]_o = \sum_{n=1}^{N} (\mu_{n,HH})^{-1} / \sum_{n=1}^{N} (\mu_{n,HH})_o^{-1} =$$

$$= \frac{\sum_{n=1}^{N} [\nu_{1,n}^4 + \Lambda\nu_{1,n}^2]^{-1}}{\sum_{n=1}^{N} [(\nu_{1,n})_o^4 + \Lambda_o(\nu_{1,n})_o^2]^{-1}} \tag{7.19}$$

The right hand side of eq. (7.19) is equal to 1/X in the coil limit and equal to 1/Z in the limit of the straight elastic necklace. Hence the dependence of $[\eta]_{rel}$ on q is completely determined by eq. (7.19).

The value of the reduced steady state shear compliance, as defined by eq. (3.44), now depends on shear rate, as the value of Λ occurs in the eigenvalues:

$$J_{eR} = \frac{\sum_{n=1}^{N} [\nu_{1,n}^4 + \Lambda\nu_{1,n}^2]^{-2}}{\{\sum_{n=1}^{N} [\nu_{1,n}^4 + \Lambda\nu_{1,n}^2]^{-1}\}^2} \tag{7.20}$$

However, for very large ΛN^2, i.e. for the coil limit, again a value of J_{eR} is found which does not depend on shear rate, as was also the case for the RZ-model. Surprisingly, also the straight necklace limit gives a J_{eR} independent of shear rate, as for that case only the first term of the sums is of importance. For intermediate values of ΛN^2 a slight decrease of J_{eR} is obtained with increasing shear rate. As before, the calculated values of J_{eR} should be correlated with the orientation angle χ' of the stress tensor in the way given by eq. (7.13), in which the reduced shear stress β refers to the shear rate dependent non-Newtonian viscosity.

Noda and Hearst have calculated these effects for several values of ΛN^2, and not only for the free-draining, but also for the non-draining case. Besides $[\eta]_{rel}$ and J_{eR} also the dependence of the extinction angle χ on β_N was calculated. Their most important result probably is the fact that the non-linear effects depend on the value of ΛN^2. For the limit of the straight elastic necklace of constant contour length the first non-linear effects in $[\eta]$ and cot $2\chi'$ can be observed at β_N-values of about 10^{-1}. For very flexible chains, $\Lambda N^2 \sim 10^8$, the beginning of non-linearity becomes observable only at β_N-values of about 10^1. This region between 10^{-1} - 10^1 actually is the region, in which non-linearity appears for nearly all kinds of polymers. The conclusion may be drawn that, in contrary to the Reinhold-Peterlin method, the constraint of constant contour length seems to give results, which are more in agreement with experiments.

Noda and Hearst gave a great number of examples of the results of their calculations. A few will be given in the next chapter.

Literature

1. H.J. Merk, On the derivation of the Fokker-Planck and Smoluchowski equations for deformable particles suspended in Newtonian fluids, Delft (1973).
2. A. Peterlin, Makromol. Chem. *44-46*, 338 (1961); Polymer *2*, 257 (1961).
3. C. Reinhold, A. Peterlin, J. Chem. Phys. *44*, 4333 (1966).
4. M. Fixman, J. Chem. Phys. *45*, 793 (1966).
5. M. Čopič, J. Chim. Phys. *53*, 440 (1956).
6. W. Kuhn, H. Kuhn, Helv. Chim. Acta *28*, 1533 (1945); *29*, 71 (1946).
7. R. Cerf, Adv. Polymer Sci. *1*, 382 (1959).
8. Yu.Ya. Gotlib, V.P. Budtov, Vestn. Leningr. Univ. *16*, 88 (1964).
9. W. Kuhn, F. Grün, Kolloid-Z. *101*, 248 (1942).
10. I. Noda, J.E. Hearst, J. Chem. Phys. *54*, 2342 (1971).

CHAPTER 8

SHEAR RATE DEPENDENCE OF THE VISCOSITY AND FLOW BIREFRINGENCE OF CELLULOSE TRICARBANILATE

8.1 Experimental

8.1.1 Non-Newtonian viscosity

With the aid of the special TNO-apparatus the shear rate dependence of the viscosity of a number of solutions of CC(L 610) was measured in several solvents. In Figs. 8.1 and 8.2 a few examples of the obtained results are given. In Fig. 8.1 the results are represented for solutions of CC(L 610) in PhB at 75°C. Fig. 8.2 deals with measurements done on solutions in dioxane at 25°C. The concentrations of the solutions are expressed in (w/v)-percentages. In both figures appreciable non-Newtonian effects can be observed. In these figures also a number of measurements is given, carried out with Ubbelohde viscometers (crosses in centers of circles). The shear rates in the Ubbelohde viscometers were estimated from the dimensions of the apparatus. The conclusion can be drawn that all viscosities, measured with these Ubbelohde viscometers, are in fair agreement with the Newtonian viscosities at low shear rates. The viscosity of TOCPh is so high that Ubbelohde measurements for solutions in that solvent agree with the Newtonian viscosities only at low concentrations ($< 0.5 \times 10^{-2}$ g/ml).

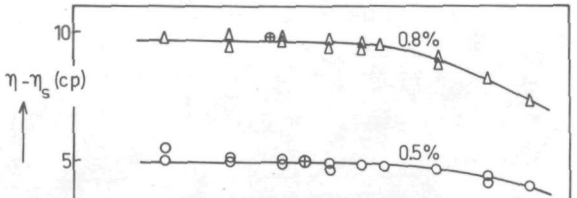

Fig. 8.1. Shear rate dependence of $\eta-\eta_s$, i.e. contribution of solute to viscosity for solutions of CC(L 610) in Phenyl Benzoate at 75°C. Concentrations are expressed in (w/v)-percentages. ⊕: Experimental points obtained with Ubbelohde viscometers.

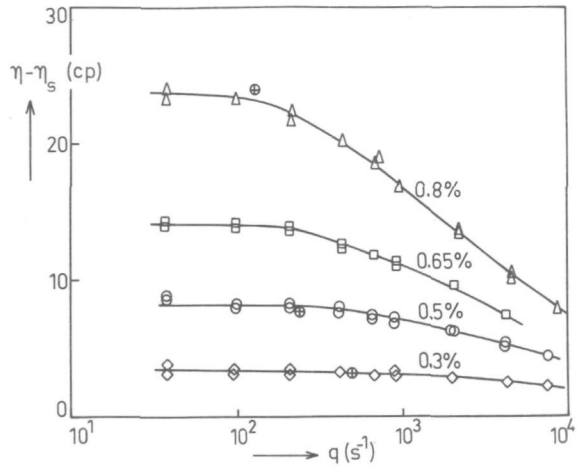

Fig. 8.2. Shear rate dependence of $\eta-\eta_s$ for solutions of CC(L 610) in Dioxane at 25°C. ⊕: Ubbelohde measurements.

Using these results the shear rate dependence of the intrinsic viscosity in the different solvents can be estimated. Figs. 8.3 - 8.5 give the reduced viscosities of CC(L 610) as functions of the reduced shear rate $\langle\beta_N\rangle_n$, where in the latter quantity the Newtonian solution viscosity is inserted. Fig. 8.3, resp. 8.4, correspond to the measurements given in Fig. 8.1, resp. 8.2. Fig. 8.5 gives the results for solutions of CC(L 610) in TOCPh at 30°C. From all figures it becomes evident that the decrease of the reduced viscosity with increasing $\langle\beta_N\rangle_n$ is more pronounced at higher concentrations. An extrapolation to zero concentration can be made

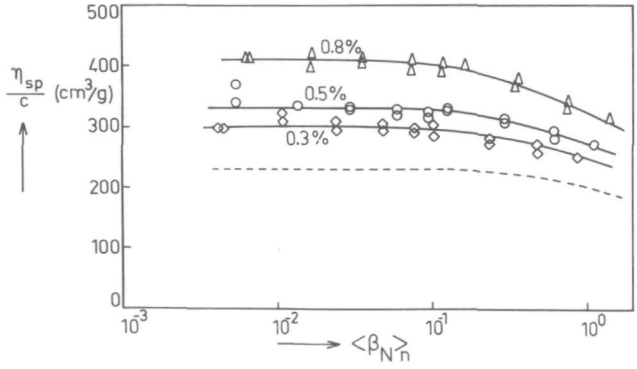

Fig. 8.3. Measurements of Fig. 8.1, replotted as η_{sp}/c against reduced shear rate $\langle\beta_N\rangle_n$. (-----): curve extrapolated to zero concentration.

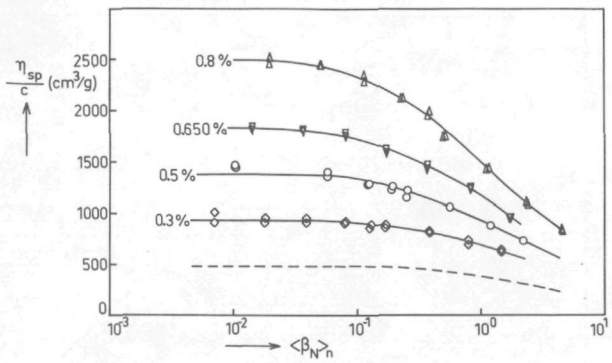

Fig. 8.4. Measurements of Fig. 8.2, replotted as η_{sp}/c against $\langle\beta_N\rangle_n$. (-----): curve extrapolated to zero concentration.

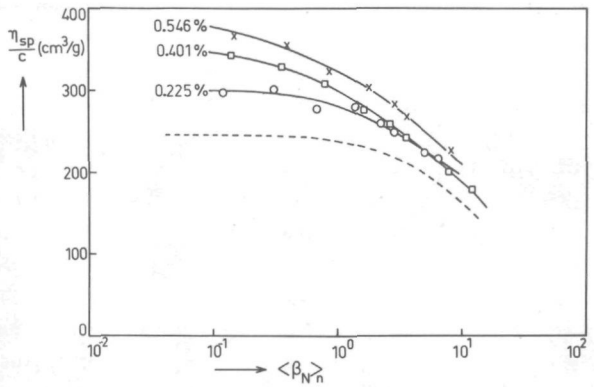

Fig. 8.5. η_{sp}/c against $\langle\beta_N\rangle_n$ for solutions of CC(L 610) in Tri-o-cresyl Phosphate at 30°C. Concentrations are expressed in (w/v)-percentages. (-----): curve extrapolated to zero concentration.

with a reasonable accuracy. The results of this operation, viz. the intrinsic viscosities as functions of $\langle\beta_N\rangle_n$, are given by dashed lines.

The resulting curves, obtained for CC(L 610) in the three different solvents, are plotted together in Fig. 8.6 in terms of the dependence of the relative intrinsic viscosity $[\eta]_{rel}$ on the reduced shear rate $\langle\beta_N\rangle_n$.

The non-Newtonian effects become perceptible in all three solvents at $\langle\beta_N\rangle_n$-values of about 10^{-1}, although there appears to be a slight influence of the solvent on the exact position of the curves. In none of the solvents sufficiently large values of $\langle\beta_N\rangle_n$ can be attained to obtain a new constant value of the intrinsic viscosity ("second Newtonian region").

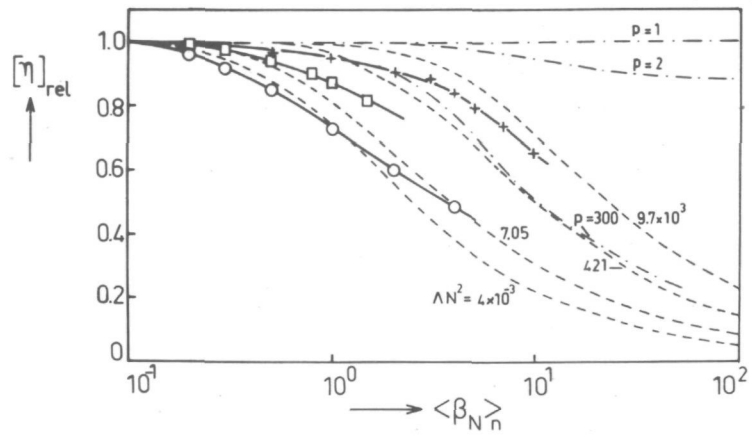

Fig. 8.6. Plot of the relative intrinsic viscosity $[\eta]_{rel}$ of CC(L 610) against $\langle\beta_N\rangle_n$ for a series of solvents: (o) Dioxane, 25°C; (□) Phenyl Benzoate, 75°C; (+) Tri-o-cresyl Phosphate, 30°C. (-----): theoretical lines according to Noda and Hearst; (-·-·-): theoretical lines for prolate ellipsoids with the indicated axial ratios P.

Plotting the reduced viscosity as a function of the reduced shear stress $\langle\beta\rangle_n$, as was done by Munk and Peterlin[1] for solutions of polystyrene in Aroclor 1248, does not make much difference. It only seems to make the non-Newtonian effects still more pronounced. For the results in Fig. 8.4, for instance, this would mean that all curves would converge in a stronger way. The Huggins constant approaches zero with increasing $\langle\beta\rangle_n$, so that the reduced viscosity seems to become more and more independent of concentration. This agrees quite well with the observations of Munk and Peterlin.

8.1.2 Non-linear behaviour of the extinction angle curves

In Fig. 6.11 already an example was given of the shear rate dependence of the extinction angle curves for CC(L 610). The non-linear effects exhibit themselves in a strong downward deviation of the double logarithmic cot 2χ versus $\langle\beta_N\rangle_n$-curves from a straight line of unity slope. In Figs. 6.12 and 6.13 it also was shown that a linear relation between cot 2χ and $\langle\beta_N\rangle_n$ may hold only at low values of $\langle\beta_N\rangle_n$.

We try to use the behaviour of the optically measured extinction angle to obtain some information concerning the behaviour of the hydrodynamic quantity J_{eR}. Therefore, the measuring results depicted in Figs. 6.12 and 6.13 must be used for a calculation of the values of the quantity $[\cot 2\chi/\langle\beta\rangle_n]$, analogous to its hydrodynamic equivalent, defined in eq. (7.13). The shear rate dependent solution viscosities, corresponding to

those results, are known from the preceding paragraph. The results of the calculations are plotted against the reduced shear rate $\langle\beta_N\rangle_n$ in Figs. 8.7 and 8.8. A comparison of these figures with the original Figs. 6.12 and 6.13 reveals that the curves obtained descend less steeply at large values of $\langle\beta_N\rangle_n$.

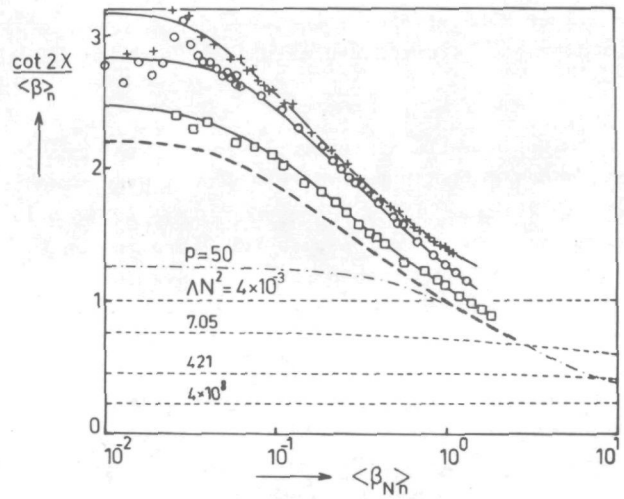

Fig. 8.7. Measurements of Fig. 6.12, replotted as [cot $2\chi/\langle\beta\rangle_n$] against $\langle\beta_N\rangle_n$. Concentrations expressed in g/ml: (□) 0.3×10^{-2}; (o) 0.5×10^{-2}; (+) 0.8×10^{-2}. (----): curve extrapolated to zero concentration. (----): theoretical lines of J_{eR} against β_N according to Noda and Hearst; (-·-·-): theoretical line for prolate ellipsoids with the indicated axial ratio P.

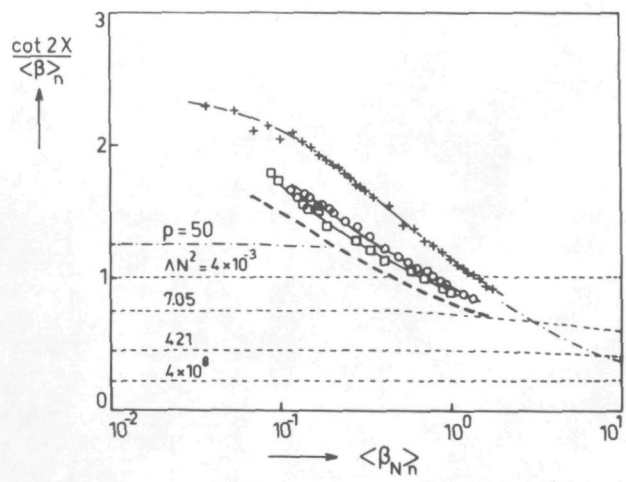

Fig. 8.8. Measurements of Fig. 6.13, replotted as [cot $2\chi/\langle\beta\rangle_n$] against $\langle\beta_N\rangle_n$. Symbols as specified in the caption to Fig. 8.7.

As all theoretical predictions are valid only for infinite dilution, the obtained results must be extrapolated to zero concentration. The resulting curves are given by dashed lines. Probably these lines will give reasonable indications for the dependence of the quantity $pJ_{eR} = [\cot 2\chi'/\langle\beta\rangle_n]$ on the reduced shear rate $\langle\beta_N\rangle_n$. As to the kind of solvent no influence on the general shape of the curves can be observed, although also here the effect remains that the curves for CC(L 610) in PhB are below those in dioxane, as discussed already in section 6.3.2.

8.1.3 Shear rate dependence of the stress-optical coefficient

As a last kind of non-linear behaviour deviations from the stress-optical law can be considered. In Fig. 8.9 a choice is made out of the vast number of experimental data, gathered on this subject in the course of the investigations. The given results were obtained on solutions of CC(L 610) in dioxane at 25°C (concentration: 0.8 x 10^{-2} g/ml), in PhB at 75°C (0.8 x 10^{-2} g/ml) and in TOCPh at 30°C (0.564 x 10^{-2} g/ml). All values were calculated according to eq. (2.17) using the non-Newtonian viscosities of the solutions. In all three solvents the stress-optical coefficients appear to be nearly constant up to a $\langle\beta_N\rangle_n$-value of about 1.0. Thereafter a strong decrease is found. However, in dioxane hardly $\langle\beta_N\rangle_n$- values are obtained, which are sufficiently high to give a significant decrease of the stress-optical coefficient. In TOCPh the deviations are the most pronounced, as the high viscosity of this solvent leads to the highest shear stresses, which could be obtained throughout

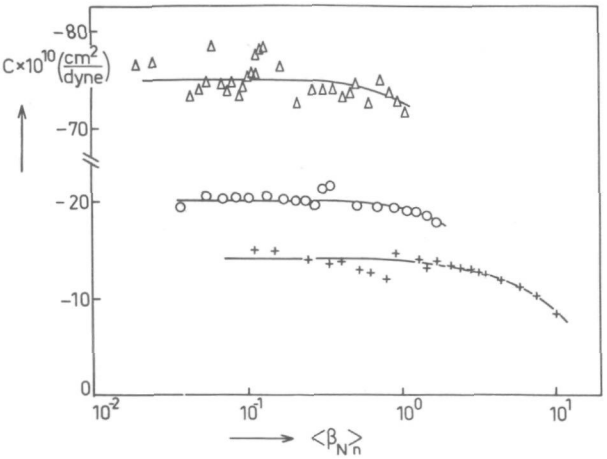

Fig. 8.9. Stress-optical coefficient C against $\langle\beta_N\rangle_n$ for a series of solutions of CC(L 610) in different solvents. (Δ) 0.8 x 10^{-2} g/ml in Dioxane at 25°C; (o) 0.8 x 10^{-2} g/ml in Phenyl Benzoate at 75°C; (+) 0.564 x 10^{-2} g/ml in Tri-o-cresyl Phosphate at 30°C.

this investigation in the various solvents used.

One can clearly observe that the first deviations from the stress-optical law occur at a $<\beta_N>_n$-value, which is more than a decade higher than that, at which the first non-linearities in the viscosity and the values of $[\cot 2\chi/<\beta_N>_n]$ become apparent.

8.2 Discussion

The foregoing results have shown the occurrence of strong non-linear effects for CC(L 610). On the viscosity the first deviations from linear behaviour could already be observed at $<\beta_N>_n$-values of about 10^{-1} and on the ratio of cot 2χ to $<\beta>_n$ even at lower values of $<\beta_N>_n$.

A number of sharp samples of anionic polystyrene in monobromobenzene, investigated by Janeschitz-Kriegl[2], give linear relationships between cot 2χ and β_N up to β_N-values of about 0.5. Also Munk and Peterlin[1,3] found similar results for anionic polystyrene in Aroclor 1248, both on the intrinsic viscosity and on the relation between cot 2χ and β_N. One can conclude that for CC(L 610) an appreciable shift is obtained to lower values of β_N.

This shift can be due to several reasons. First, like all cellulose-derivatives, CC(L 610) is considerably stiffer than most synthetic polymers, such as polystyrene, polyethylene etc. The theory of Noda and Hearst[4], as dealt with in section 7.3.2, predicts a shift of the non-linear effects to lower values of β_N for stiffer molecules. For a comparison of the experimental results with their theory a number of theoretical curves are drawn in Fig. 8.6. The dashed lines are curves according to Noda and Hearst, for several values of ΛN^2 (given at the curves), for the non-draining case. Besides, in Fig. 8.6 also several theoretical curves are drawn for rigid rotational ellipsoids with various axial ratios P (points and dashes), taken from the work of Scheraga[5]. The latter author uses a kind of dimensionless shear rate which, however, can be transformed into the reduced shear rate β_N in a way, given by Kuhn et al.[6] and Tsvetkov[7]. A comparison of both model theories shows that, for rigid rotational ellipsoids, the shape of the curves depends on the axial ratio, while the HH-model according to Noda and Hearst always gives curves of identical shape. However, with increasing chain stiffness (smaller ΛN^2) a shift occurs along the logarithmic β_N-scale to lower values of β_N. The curve for P = 300 has a shape which is nearly identical with the shape characteristic for the curves of Noda and Hearst. The much greater chain stiffness of CC(L 610) compared to that of polystyrene can explain the shift of the non-Newtonian effects to lower values of β_N. In this regard it is quite remarkable that, as far as the value of the anisotropy $\alpha_1-\alpha_2$ can be considered as representative for the chain stiffness (see

Fig. 6.16 and Table 6.2) the relative positions of the curves in different solvents seem to agree with the respective values of $\alpha_1-\alpha_2$. However, this conclusion must be considered with some reserve, because of the errors made at the determination of the intrinsic viscosity as a function of $<\beta_N>_n$.

A second reason for a shift can be sought in the polydispersity of the CC-sample. All theoretical curves for monodisperse systems predict that the total effect of non-Newtonian behaviour of a polymer solution, i.e. the change from constant $[\eta]_o$ to constant $[\eta]_\infty$, should occur within 2 to 3 decades of the shear stress. Indeed, this is found experimentally for monodisperse polymer samples[8,9]. The results in Fig. 8.6 are plotted against the reduced shear rate instead of the reduced shear stress. Still one can see that the non-Newtonian viscosity range for CC(L 610) seems to cover a broader region of shear rates than theoretically predicted for monodisperse samples.The whole transition seems to comprise at least 4 decades in $<\beta_N>_n$. As long as we have no personal experience with the behaviour of monodisperse samples we cannot assess the influence of polydispersity. The deviation from Newtonian behaviour at β_N-values, which are relatively small compared with those predicted by theory, can therefore largely be due to the polydispersity of CC(L 610).

An even greater influence of polydispersity on the measurements can be found in Figs. 8.7 and 8.8. For a comparison with theory in these figures some theoretical curves of J_{eR} vs. β_N are drawn. The dotted lines are theoretical lines according to Noda and Hearst for different values of ΛN^2 for the non-draining case. Again it is clearly observed that a non-linearity in the $[\cot 2\chi/<\beta>_n]$-curves already becomes observable at much lower values of β_N than theoretically predicted for J_{eR}. Moreover, in both figures a much greater decrease of $[\cot 2\chi/<\beta>_n]$ is actually observed, than the theory of Noda and Hearst predicts for J_{eR} in the most pronounced case of $\Lambda N^2 = 7.05$. First, however, it must be stated that the values of J_{eR}, as calculated by Noda and Hearst, are purely hydrodynamic quantities, while the reported measurements, on the other hand, are optical ones giving $[\cot 2\chi/<\beta>_n]$. Only if coaxiality exists between the stress tensor and the refractive index ellipsoid the quantity $[\cot 2\chi/<\beta>_n]$ can be put equal to pJ_{eR}. As long as we do not know the influence of non-linearity on the coaxiality a comparison of these experiments with hydrodynamic theory remains risky. Further, quite certainly the correction for polydispersity, as mentioned in section 3.11, cannot be made in the non-linear region. Hence, it becomes practically impossible to draw conclusions with respect to the validity of the theory from these results: on the one hand, the polydispersity seems to spread the whole effect over a broad region of β_N-values, on the other hand the polydispersity factor p can show appreciable changes with increasing β_N-values.

It must be mentioned that also the HH-model should not be considered as the most ideal model of a stiff macromolecule. The theoretical curve describing J_{eR} as a function of β_N for the most stiff form ($\Lambda N^2 = 4 \times 10^{-3}$), does not show any downward bent at increasing β_N. The limiting case of the straight elastic pearl necklace of the HH-model cannot be considered as an equivalent of a truly rigid rod. The dumbbells, from which the HH-model is built up, always retain their axial extensibility. Even the constraint of constant contour length does not mean that the elastic dumbbells are transformed in rigid dumbbells. A rigid rodlike chain can probably much better be approximated by a rigid rotational ellipsoid. Therefore, in Figs. 8.7 and 8.8 also a theoretical curve of $[\cot 2\chi/\beta_N]$ vs. β_N is drawn for a rodlike rotational ellipsoid with an axial ratio P = 50, derived from the work of Scheraga et al.[10]. As a matter of fact, this model shows a much more pronounced non-linear behaviour, although it must be reminded that the experimental points in these figures correspond to values of $[\cot 2\chi/\beta]$ instead of $[\cot 2\chi/\beta_N]$, as derived from this theory.

Referring to the theoretical work of Fixman[11], Munk and Peterlin[3] ascribe the dependence of $[\cot 2\chi/\beta]$ on β to a changing hydrodynamic interaction within the coil at a deformation of the chain. As a matter of fact, a strongly deformed coil will be better drained than an undeformed one. The theories, discussed in the foregoing, neglect this influence of draining on the value of J_{eR}. However, although the influence of draining on the experimental observations will probably be quite small, it cannot be neglected completely. On the other hand, it does not seem correct to ascribe the whole change of $[\cot 2\chi/\beta]$ to this effect.

Especially with samples of sufficiently large molecular weights the influences of molecular weight and polydispersity on the value of the stress-optical coefficient are quite small. Hence, Fig. 8.9 gives a picture, in which the absolute values at least will not be influenced by polydispersity. On the other side, also in this case it must be taken into account that the polydispersity may have shifted the beginning of the deviations from the stress-optical law to lower values of $\langle\beta_N\rangle_n$. Nevertheless, it can be observed quite clearly that the stress-optical law remains valid for CC(L 610) until far in the non-linear region for the viscosity and the ratio of $[\cot 2\chi/\langle\beta\rangle_n]$. In this respect CC does not deviate from the general behaviour of many other polymers. However, at $\langle\beta_N\rangle_n$-values above 1.0 yet appreciable deviations from the stress-optical law are observed. For very flexible polymers in literature[3,12,13] already many examples are known for a validity up to much higher values of β_N. Therefore the above mentioned results clearly demonstrate that the stress-optical law, as proposed for very flexible Gaussian macro-

molecules, looses much of its general validity in the case of stiff polymers.

8.3 Conclusions

Drawing final conclusions from this sort of measurements is as yet a precarious thing to be done. Primarily, a really good theory is still lacking. Secondly, the measured effects are nearly completely masked by a tremendous influence of polydispersity. Even at the narrowest molecular weight distributions obtainable (e.g. $\langle M \rangle_w / \langle M \rangle_n < 1.05$) a sample still comprises a rather broad region of molecular weights, which influences the extinction angle to a considerable extent. Only the shear rate dependence of viscosity and flow birefringence of a completely monodisperse sample can be used for a critical check of theory.

Still it can be said that the theory of Noda and Hearst[4] and that of the rigid rotational ellipsoids[5,10] give at least a reasonable description of what is found in practice. Primarily, they predict non-linear behaviour at the right β_N-values. Secondly, the predicted general form of the results corresponds to the experiments. One may conclude that the constant contour length of the chain probably is one of the main reasons for non-linear behaviour. However, the non-linearity is also determined by a great number of other influences, which are not worked out in these theories. In so far one cannot expect the experimental results to be completely explained by these theories.

For a further check of these theories one should have at one's disposal a great number of sharp fractions of polymers with widely varying degrees of stiffness. The stiffening observed on CC is probably too small to induce clear changes in the hydrodynamic properties of the chain. This would be a valuable subject of further research.

For CC(L 610) the stress-optical law is valid only at small shear stresses. At higher shear stresses appreciable deviations occur, as one could have expected for stiff macromolecules. However, a very important result may be the fact that also for stiff macromolecules the stress-optical law remains valid far into the non-linear region. In this respect the conclusion may be drawn that the stress-optical law has a more general validity than those theories which describe the hydrodynamic properties of flexible macromolecules in solution.

Literature

1. P. Munk, A. Peterlin, Rheol. Acta *9*, 294 (1970).
2. H. Janeschitz-Kriegl, Rheol. Acta *5*, 78 (1966).
3. P. Munk, A. Peterlin, Rheol. Acta *9*, 288 (1970).
4. I. Noda, J.E. Hearst, J. Chem. Phys. *54*, 2342 (1971).
5. H.A. Scheraga, J. Chem. Phys. *23*, 1526 (1955).
6. W. Kuhn, H. Kuhn, P. Buchner, Ergeb. Exakt. Naturw. *25*,1 (1951).
7. V.N. Tsvetkov, Vysokomolekul. Soedin. *7*, 1468 (1965).
8. W. Philippoff, Viskosität der Kolloide, Steinkopff Verlag, Dresden und Leipzig (1942).
9. J.T. Yang, J. Am. Chem. Soc. *80*, 1783 (1958).
10. H.A. Scheraga, J.T. Edsall, J.O. Gadd, J. Chem. Phys. *19*, 1101 (1951).
11. M. Fixmann, J. Chem. Phys. *45*, 793 (1966).
12. W. Philippoff, Nature *178*, 811 (1956); J. Appl. Phys. *27*, 984 (1956); J. Polymer Sci. C, *5*, 1 (1964).
13. H. Janeschitz-Kriegl, Adv. Polymer Sci. *6*, 170 (1969).

SUMMARY

This thesis describes an investigation into the usefulness of flow birefringence as a technique for the study of conformational transitions of polymers in solution. In the theoretical part of this work various molecular theories are discussed, which describe the hydrodynamic and optical behaviour of macromolecules in dilute solutions. On the basis of the Rouse-Zimm model the contributions of the polymer molecules to the stress tensor of the flowing solution can be calculated. The intrinsic viscosity and the reduced steady state shear compliance J_{eR} appear to be independent of the shear rate. This is a logical consequence of the use of the linear diffusion equation as a basis for these theories.

Introduction of a kind of chain stiffness into these theories, for example by the reduction of the number of subchains or by the introduction of a finite bending force constant in the Rouse-Zimm model, raises the numerical value of J_{eR}. However, even with a great stiffening of the chain the predicted changes of J_{eR} remain relatively small.

The stress-optical properties of very flexible polymers can be described by a stress-optical law. The pertinent stress-optical coefficient is independent of the molecular weight of the polymer. However, this law does not fit data for stiff polymers very well, while the stress-optical coefficient also becomes dependent on molecular weight. For those cases Gotlib and Svetlov gave a description of the molecular weight dependence of the stress-optical coefficient but only for the limiting case of zero shear rate.

The experimental part of this thesis comprises investigations into two types of conformational transitions of polymers: a coil expansion of a polyelectrolyte due to ionization of the chain and the stiffening of cellulose tricarbanilate with a change of solvent, accompanied by the formation of intramolecular hydrogen bonds.

Addition of the organic base triethylamine to a solution of a poly-(amide carboxylic acid) from pyromellitic anhydride and benzidine results in a strong increase of the stress-optical coefficient. This increase can be interpreted in terms of an expansion of the molecular coil. A decrease of the polymer concentration increases the expansion, as the mutual shielding of charges on separate macromolecules is reduced. A relation is proposed, which describes the dependence of the stress-optical coefficient on concentration with reasonable accuracy. Making use of this relation semi-quantitative conclusions can be drawn as to the degree of expansion of this polyelectrolyte in infinitely dilute solution.

With the aid of the theory of Gotlib and Svetlov the molecular weight dependence of the stress-optical coefficient for cellulose tricarbanilate

can successfully be described. The experimental results show a strong increase of the stiffness of this polymer when the solvent composition is varied from pure ester to pure ether. Moreover, the stiffness strongly depends on temperature. This increased stiffness must be ascribed to the formation of intramolecular hydrogen bonds. This results in a tremendous increase of the stress-optical coefficient, due to sterical hindrance of the free rotation of the anisotropic phenyl rings in the side-groups of the chain.

Scarcely any influence of the changing chain stiffness on the value of J_{eR} can be deduced from the behaviour of the extinction angle curves. A possible influence is nearly completely masked by the prevailing influence of the polydispersity on the measured extinction angles.

Finally, a theoretical and an experimental chapter are dedicated to the non-linear behaviour of the cellulose tricarbanilate solutions. Three subjects are considered: the non-Newtonian viscosity, the non-linear behaviour of the extinction angle curves and the deviation from the stress-optical law. Into the known molecular theories a condition must be introduced, which requires the total contour length of a macromolecule to remain constant at a deformation of the coil. This condition results in non-linear effects, which at least qualitatively agree with the experimental data. However, this correspondence does by no means say that the constant contour length may be considered to be the only reason for non-linear effects. In fact, the theoretical description of non-linear behaviour is still very obscure. In this connection it is of some interest that the stress-optical law appears to have a more general validity than the above mentioned linear theories. It remains valid experimentally at least in part of the region of shear rates, where the viscosity and extinction angle curve clearly show non-linear behaviour.

SAMENVATTING

In dit proefschrift wordt een onderzoek beschreven naar de stromings dubbele breking, als techniek voor de bestudering van conformatie-overgangen van polymeren in oplossing. In het theoretische gedeelte worden verschillende moleculaire theorieën besproken, die het hydrodynamisch en optisch gedrag van macromoleculen in verdunde oplossing beschrijven. Op basis van het Rouse-Zimm model kunnen de bijdragen worden berekend van de polymeer-moleculen aan de spanningstensor van de stromende oplossing. De intrinsieke viscositeit en de gereduceerde evenwichtscompliantie J_{eR} blijken onafhankelijk van de afschuifsnelheid. Dit is een logisch gevolg van het gebruik van de lineaire diffusievergelijking, als uitgangspunt voor deze theorieën.

Invoeren van een vorm van ketenstijfheid in deze theorieën, bijvoorbeeld door een beperken van het aantal subchains of door het invoeren van een buigingskracht-konstante in het Rouse-Zimm model, heeft tot gevolg dat de numerieke waarde van J_{eR} enigszins toeneemt. Zelfs bij grote verstijving van de keten blijven de voorspelde veranderingen van J_{eR} echter relatief gering.

De spanningsoptische eigenschappen van zeer flexibele polymeren kunnen worden beschreven door een spanningsoptische wet. De daaraan ontleende spanningsoptische coëfficiënt is onafhankelijk van het molecuulgewicht van het polymeer. Deze wet geeft echter geen goede beschrijving van experimentele resultaten voor stijve polymeren, terwijl bovendien de spanningsoptische coëfficiënt afhankelijk wordt van het molecuulgewicht. Voor die gevallen geven Gotlib en Svetlov een theoretische beschrijving van de molecuulgewichts-afhankelijkheid van de spanningsoptische coëfficiënt, echter alleen voor het limiet-geval van afschuifsnelheid nul.

Het experimentele gedeelte omvat een onderzoek naar een tweetal soorten conformatie-overgangen van polymeren: een kluwenexpansie van een polyelectrolyt ten gevolge van ionisatie van de keten en een verstijving van cellulose-tricarbanilaat bij verandering van oplosmiddel door vorming van intramoleculaire waterstofbindingen.

Toevoegen van de organische base triethylamine aan een oplossing van een poly(amid carbonzuur) uit pyromellietzuur-dianhydride en benzidine resulteert in een sterke toename van de spanningsoptische coëfficiënt. Deze toename kan worden toegeschreven aan een expansie van de moleculaire kluwen. Verlaging van de polymeerconcentratie vergroot de expansie, daar de afscherming van de ladingen op de macromoleculen onderling afneemt. Er wordt een vergelijking voorgesteld, die de concentratie-afhankelijkheid van de spanningsoptische coëfficiënt met redelijke nauwkeurigheid beschrijft. Met behulp van deze vergelijking kunnen semi-

kwantitatieve uitspraken worden gedaan over de mate van expansie van dit polyelectrolyt in oneindig verdunde oplossing.

De molecuulgewichts-afhankelijkheid van de spanningsoptische coëfficiënt voor cellulose-tricarbanilaat kan met succes worden beschreven door de theorie van Gotlib en Svetlov. De experimentele resultaten tonen aan, dat de stijfheid van dit polymeer plotseling sterk toeneemt bij verandering van de oplosmiddel-samenstelling van zuiver ester naar zuiver ether. Bovendien blijkt de stijfheid sterk afhankelijk van de temperatuur. Deze toename van de stijfheid moet worden toegeschreven aan de vorming van intramoleculaire waterstofbindingen. Dit gaat gepaard met een geweldige toename van de waarde van de spanningsoptische coëfficiënt, veroorzaakt door sterische hindering van de vrije roteerbaarheid van de sterk anisotrope fenyl-ringen in de zijgroepen van de keten.

Er kan vrijwel geen invloed van de veranderde ketenstijfheid op de waarde van J_{eR} worden afgeleid uit het gedrag van de uitdovingskrommen. Een eventuele invloed wordt vrijwel volledig gemaskeerd door de overwegende invloed van de polydispersiteit op de gemeten uitdovingshoeken.

Tot slot worden een theoretisch en een experimenteel hoofdstuk gewijd aan het niet-lineaire gedrag van de cellulose-tricarbanilaat oplossingen. Drie onderwerpen worden beschouwd: de niet-newtonse viscositeit, het niet-lineaire gedrag van de uitdovingskrommen en afwijkingen van de spanningsoptische wet. In de bekende moleculaire theorieën moet de eis worden verwerkt, dat de contourlengte van een macromolecuul konstant moet blijven bij deformatie van de kluwen. Dit resulteert in niet-lineaire effecten, die althans kwalitatief overeenkomen met hetgeen experimenteel wordt gevonden. Deze overeenstemming betekent overigens geenszins, dat de konstante contourlengte kan worden beschouwd als de enige oorzaak van niet-lineaire effecten. In feite kleven namelijk aan de hele niet-lineaire theorie nog vele bezwaren. In dit verband is het van belang dat de spanningsoptische wet een algemenere geldigheid blijkt te bezitten dan de lineaire theorieën. Deze wet blijkt experimenteel geldig te blijven tot in het gebied van afschuifspanningen, waar viscositeit en uitdovingskromme al duidelijk een niet-lineair gedrag vertonen.

STELLINGEN